# Large Array of Shape Memory Polymer Actuators for Haptics and Microfluidics

THÈSE N° 8175 (2018)

## ÉCOLE POLYTECHNIQUE FÉDÉRALE DE LAUSANNE

POUR L'OBTENTION DU GRADE DE DOCTEUR ÈS SCIENCES

PAR

## Nadine BESSE

(PFL

ÉCOLE POLYTECHNIQUE
FÉDÉRALE DE LAUSANNE

Suisse
2018

The impossible exists only until
we find a way to make it possible.
— *Mike Horn*

# Acknowledgements

I am deeply grateful to my thesis director Prof. Herbert Shea who gave the opportunity to join his laboratory, allowing me to work on this exciting topic. I would like to warmly thank him for his unlimited thrust, time and guidance throughout the four years. Collaborating and exchanging ideas with him were a pleasure. I have appreciated his great availability, productive honesty and high expectations towards me. Our discussions were always constructive and insightful, leading to clear research goals with excellent final results. I heartily thank him for being such a great advisor and mentor for my PhD thesis.

I am sincerely thankful to my thesis co-director Samuel Rosset for sharing his expertise and advanced knowledge on soft actuators with me. His advice on modeling and on fabrication was highly appreciated. I would particularity like to thank him for his dedication when reading my thesis and my papers, with valuable comments and precious suggestions. Aside work, I will be missing his sense of humor and conviviality at our coffee breaks, pub quizzes, hikes, and board game nights. Unfortunately, he had to leave for the antipodes.

I would like to thank my other thesis jury members Prof. Simon Nessim Henein, Prof. Siegfried Bauer, Prof. Alex Dommann, and Prof. Stéphanie Lacour who kindly accepted to read, review, and evaluate my thesis.

I express all my gratitude to my office mate Juan José Zárate. It has been a pleasure sharing and discussing our research together. We mutually helped and advised each other on our respective technologies in a warmly and friendly atmosphere, which surely benefited our everyday work. Also, we should be proud to have started a new field in our laboratory, which is slowly becoming one of the leaders in the haptic community for the hardware side.

I owe particular thanks to my lab mates from the LMTS for the stimulating discussions and for all the fun we had together these last four years. Specifically, my heartfelt thank are for my secretary Myriam Poliero who always helped me with administrative work. Her joviality and her sense of Swiss organization were highly appreciated. For their fruitful help and advice on my research, special mentions go to Olexandr Gudozhnik, Seun Araromi, Etienne Lemaire, Sam Schlatter, Christine de Saint-Aubin, Alexis Marette, Joanna Bitterli, Aymeric Schafflützel,

## Acknowledgements

# Abstract

My thesis advances the field of shape memory polymer (SMP) actuators by providing a versatile strategy to arbitrarily reconfigure large arrays of densely packed latching soft actuators. It exploits two key intrinsic characteristics of SMPs, which are their multistable nature and their drastic change in Young's modulus with temperature, to combine both actuation plus latching in a single actuator. The novel concept consists in individually and selectively addressing arrays of SMP actuators by synchronizing their local Joule heating with a single common air pneumatic supply. Stretchable heaters are integrated and patterned on thin SMP membranes in order to precisely define regions where the stiffness can be changed by over two orders of magnitude. By a timely synchronization of the thermal stimuli with the external air pressure, each actuator can be independently, reversibly, and rapidly latched into any positions.

The potential of coupling local Joule heating with global air pneumatic actuation for large arrays of SMP actuators is demonstrated by a 32x24 flexible haptic display and by a 4x4 microfluidic platform. The active layer of the SMP actuator is made of a commercially available SMP material for the SMP membrane and a mixture of carbon black (CB) with soft polydimethylsiloxane (PDMS) for the stretchable heating electrodes. The final SMP actuator geometry corresponds to the best trade-off between displacement and holding force for both haptic and microfluidic applications.

The 32x24 flexible haptic display is the first high resolution wearable sleeve capable to vary its surface topology. This device consists of a 40 µm thick SMP membrane, on which a matrix of 25 µm thick stretchable heaters on 4 mm pitch is integrated, interconnected by a 4-layers flexible printed circuit board (PCB) and bonded to a stretchable 3D-printed pneumatic chamber. Each tactile pixel (taxel) can be individually controlled via row/column addressing, requires 250 mW to heat up from 20 °C to 70 °C, and takes 2.5 s to latch to a different state. Each line (row or column) of taxels consumes at most 8 W and the entire haptic display is refreshed in under 1 min 30 s. The haptic display weighs only 55 g and is 2 mm thick. More than 99 % of the 768 taxels are fully functional, with a lifetime in excess of 20 000 cycles. The perception tests conducted on the 4x4 tactile tablet with 15 blindfolded sighted users resulted in 98 % correct pattern recognition in less than 10 s exploration, confirming that my SMP actuators are a promising taxel technology.

**Abstract**

The 4x4 microfluidic platform is the first latching microfluidic array where each valve is directly controlled with a common air pneumatic supply. Its active layer consists of a 50 µm thick SMP membrane, a matrix of 25 µm thick stretchable heaters, and a 37.5 µm thick styrene ethylene butylene styrene (SEBS) membrane. The actuators are electrically interconnected and mechanically bonded to a PCB. On the bottom, a polymethyl methacrylate (PMMA) pneumatic chamber is sealed and, on the top, a micromachined polystyrene (PS) microfluidic chip is bonded. The similarity in design for both normally closed (NC) and normally open (NO) valves enables to implement them in the same chip. These 3 mm in diameter valves remain closed up to 70 mbar of pressure before opening, validating that my SMP actuators are an interesting valve-unit for micropumps, mixers, and multiplexers in microfluidic large scale integration (mLSI) systems.

**Keywords:** shape memory polymer actuators, integrated stretchable heaters, local Joule heating, pneumatic actuation, scalable latching technology, flexible haptic display, microfluidic valve.

# Résumé

Ma thèse porte sur les actionneurs en polymère à mémoire de forme (SMP) et propose une stratégie permettant de reconfigurer des matrices, larges et denses, d'actionneurs mous et bistables. Elle exploite deux propriétés spécifiques aux SMPs : leur nature multistable et la forte dépendance du module de Young avec la température. Ces deux effets permettent d'actionner et de verrouiller via un seul actionneur. L'innovation consiste à déplacer sélectivement ces actionneurs en synchronisant les stimuli thermiques locaux, par effet Joule, avec une source de pression d'air externe. Des corps de chauffe étirables sont intégrés et structurés sur de fines membranes en SMP, afin de définir des zones où la rigidité variera de plus de deux ordres de grandeur. Ainsi, le verrouillage de chaque actionneur est réversible et rapide.

Le bénéfice de coupler le chauffage local avec une pression globale pour de larges matrices d'actionneurs en SMP est démontré par l'écran haptique flexible 32x24 et la plateforme microfluidique 4x4. La couche active de l'actionneur est composée d'une membrane en SMP commercial sur laquelle sont déposés des corps de chauffe étirables, un mélange de noir de carbone et de polydiméthylsiloxane (PDMS). La géométrie finale de l'actionneur est le meilleur compromis entre le déplacement et la force pour les applications haptiques et microfluidiques.

L'écran haptique flexible 32x24 est le premier brassard portable à topologie variable avec une haute résolution. Le coeur du dispositif est composé d'une membrane en SMP de 40 µm d'épaisseur et d'une matrice de corps de chauffe de 25 µm d'épaisseur, espacés de 4 mm. Il est interconnecté à un circuit imprimé (PCB) 4-couches et collé à une chambre pneumatique étirable fabriquée par impression 3D. Chaque pixel tactile (taxel) est contrôlable individuellement grâce à un adressage ligne-colonne, et requiert 250 mW pour chauffer de 20 °C à 70 °C. Une rangée consomme au maximum 8 W. Il faut 2.5 s pour verrouiller un taxel dans un nouvel état. L'écran complet est rafraîchissable en moins de 1 min 30 s. Il ne pèse que 55 g et ne fait que 2 mm d'épaisseur. Plus de 99 % des 768 taxels sont fonctionnels et leur durée de vie excède 20 000 cycles. Les tests de perception, menés sur la tablette tactile 4x4 avec 15 utilisateurs ayant les yeux bandés, ont abouti à 98 % de réponses correctes en moins de 10 s d'exploration. Ces tests confirment que mes actionneurs en SMP sont prometteurs lorsqu'ils sont utilisés comme taxels.

## Abstract

La plateforme microfluidique 4x4 est la première matrice bistable dont chaque valve est contrôlée par une source de pression commune. La couche active est composée d'une membrane en SMP de 50 µm d'épaisseur, d'une matrice de corps de chauffe étirables de 25 µm d'épaisseur et d'une membrane en styrène éthylène butylène styrène (SEBS) de 37.5 µm d'épaisseur. Les actionneurs sont interconnectés et collés à un PCB. Une chambre pneumatique en polyméthacrylate de méthyle (PMMA) est scellée dessous et une puce microfluidique en polystyrène (PS) est placée dessus. Les similitudes de conception entre les valves normalement fermées (NC) et celles normalement ouvertes (NO) permettent de les implémenter sur la même puce. Ces valves de 3 mm de diamètre fonctionnent jusqu'à une pression de 70 mbar. Ces résultats démontrent que mes actionneurs en SMP sont utilisables comme valves pour des micropompes, des mixeurs et des multiplexeurs dans des systèmes microfluidiques intégrés à grande échelle (mLSI).

**Mots clefs :** actionneurs en polymère à mémoire de forme, corps de chauffe intégrés et étirables, chauffage local par effet Joule, actionnement pneumatique, technologie modulables et bistable, écran haptique flexible, valve microfluidique.

# Contents

# Contents

# List of Figures

# List of Tables

# 1 Introduction

## 1.1 Background and motivation

The ideal reconfigurable device would change both its appearance and its mechanical function. Dividing the system motion among a plurality of densely packed actuators enables to improve the overall device performance by reshaping it with higher accuracy, precision, and resolution. These large arrays of actuators are notably required in adaptive optics, microfluidic large scale integration (mLSI) systems, soft robotics, and haptic displays. While microelectromechanical system (MEMS) mirrors are successfully implemented in purely optical products like beamers [1] and fiber switches [2], very little work has been reported on compact reconfigurable devices with hundreds of independent transducers capable to generate sufficient forces to serve a mechanical function; a key requirement for mLSI systems, soft robotics, and haptic displays. To date, MEMS technologies based on piezoelectric, electromagnetic (EM), electrostatic, thermal, or pneumatic principles have attracted most research attention for their complementarity with conventional metal-oxide-semiconductor (CMOS) industrial processes and their advanced manufacturing maturity compared to emerging technologies based on polymers and elastomers. Nonetheless, making a device highly compliant to shape any surface topology requires soft materials; an extremely demanding task given the low stiffness and thus small force generated by polymers and elastomers.

The rapidly growing field of soft robotics generally consists of systems with very small numbers of actuators [3]. While this is in part because the compliance of soft devices enables shape adaptation with a limited number of transducers [4], it also reflects the challenge in devising actuation strategies for scalable large matrices of densely packed soft actuators. For instance, most soft manipulators and grippers based on pneumatic actuation [5,6], granular jamming [7], dielectric elastomer actuators (DEAs) [8,9], DEAs coupled with electro-adhesion [10], or shape memory alloys (SMAs) [11] have either only one actuator, or several actuators all driven by the same control signal (e.g., a 3-fingers gripper driven by a common pressure supply [12]). To allow for hundreds to thousands of independent actuators, microfluidic platforms usually integrate multiplexed pneumatic systems [13], but this approach has limitations and scaling

to larger number of actuators is unsolved for portable systems. To produce haptic feedback, selective heating of a 65x65 matrix of stimuli responsive hydrogel has been reported, using an external projector to remotely heat the tactile pixels (taxels) for actuation [14]. Despite its fast response time, the system exhibited a low force and stroke. Arrays of flexible DEAs which can be wrapped around a finger have also been reported, but they could again output only very short force and stroke [15]. In this field, the most inspiring work is probably the array of 240 Braille-sized bistable soft actuators combining DEAs with shape memory polymers (SMPs) to elegantly enable latching in DEAs [16]. However, during actuation, the device had to be placed in an oven and, for addressable operation, a matrix of high-voltage (in the kilovolt range) switches was required. Independent control of all actuators coupled with selective local heating of the entire array was not reported.

Table 1.1 – Comparison table of the relevant technologies for large arrays of actuators in haptic displays. The first five principles are conventional MEMS-based technologies and the last two are emerging polymer- and elastomer-based ones. The criteria are mainly based on [17, 18] and are then completed with personal experience.

| Actuator technology | Speed | Fill factor | Force | Displacement | Complexity | Power consumption |
|---|---|---|---|---|---|---|
| Piezoelectric | + + | + | + + + | - - | - | + + |
| Electromagnetic (EM) | + + | - | + | + | + + | - - |
| Electrostatic | + + | + | + + | + | + | + + |
| Thermal | - - | + | + + | + | + | - - |
| Pneumatic | - | - | + + | + | - - | - |
| Dielectric elastomer actuator (DEA) | + | + | - - | - | + | + + |
| Shape memory polymer (SMP) | - - | + | + + | + | + | + |

Addressing large arrays of soft actuators with a simple and compact system is currently an unsolved problem. In particular, developing a high resolution haptic display is a challenging task because this application is one of the most demanding in terms of force and displacement requirements. Considering speed, power consumption, cost, reliability, comfort, array size, and ease of control further adds to the complexity. Table 1.1 compares several actuator technologies and presents their advantages plus disadvantages when implemented in a haptic display. Phase-change materials (PCMs) are particularly of interest as soft actuator since they combine programmable softness and high holding forces; specifically thermo-responsive SMPs which have attracted attention in the last decade for their controllable and reversible stiffness change in response to external thermal stimuli [19, 20]. Their Young's modulus decreases by up to 1000 times over a narrow temperature range when heated above the glass transition temperature, which is generally between 25 °C and 125 °C for commercially available materials [21]. More recently, materials exhibiting a change from 100 MPa to 0.1 MPa in less than a 10 °C temperature range were reported [22]. While SMPs have been used for reversible

shape change in medical implants [23, 24] and in large structures [25], they have not been implemented for complex shape control as they are generally globally heated, leading to the entire structure changing shape or stiffness. To avoid the use of external heaters, methods to generate the thermal stimuli directly in the SMP have been studied, notably by rendering the polymer: electrically conductive to enable direct Joule heating [26,27], magnetically permeable to allow for contactless induction heating [28, 29], or responsive to specific wavelength to enhance radiative heating [30]. However, no system implementing both the thermal stimuli and the mean of actuation has been demonstrated yet.

## 1.2 *BlindPAD* project objectives

Part of my thesis was funded by the European Union Seventh Framework Program (EU-FP7) within the project entitled *BlindPAD*, the acronym for *Personal Assistive Device for BLIND and visually impaired people* [31]. The goal of the project was to developed a dynamic tactile tablet to allow blind and visually impaired users to interact with graphical data, since coupling a refreshable haptic display with auditory information would greatly facilitate their access to information. While effective solutions for displaying text exist, such as Braille bars, displaying touchable graphical information on large surfaces in a scalable, dynamic, and portable manner is currently an unsolved technological challenge. Yet these haptic displays are much desired in the context of learning and rehabilitation. For example, equipped with such a haptic display, a visually impaired student could learn alongside his sighted friends, using his sense of fine touch to feel on this tablet what the teacher is drawing on the white board. Recent work shows that blind and visually impaired children and adolescents learn from refreshable pin arrays as efficiently as with raised line drawings, however in full autonomy [32]. For orientation and mobility, a tactile tablet could serve blind persons as Google maps serves sighted persons, with the ability to rapidly zoom in and out, pan, and highlight dangers or points of interest.

The *BlindPAD* project was a consortium involving the following partners: the Istituto Italiano di Technologia (IIT-RBCS, Italy), GeoMobile (Germany), Ateknea Solutions (Hungary), the Istituto David Chiossone Onlus (Chiossone, Italy), the Fundacja Instytut Rozwoju Regionalnego (FIRR, Poland), and the École Polytechnique Fédérale de Lausanne (EPFL-LMTS, Switzerland). The IIT-RBCS was leading the project and preparing scenarios to be tested with end-users at both rehabilitation centers Chiossone and FIRR. Both industrial partners GeoMobile and Ateknea Solutions were building up the software and the electronic drivers, respectively. At the EPFL-LMTS, we were developing and scaling up two different taxel technologies: an EM-based and a SMP-based actuation mechanism. My colleague Juan José Zárate (EPFL-LMTS, Switzerland) was in charge of the EM approach and I worked on the SMP one.

## 1.3 Research objectives

More globally, the main objective of my thesis is to demonstrate that thermo-responsive SMPs are a suitable class of materials to arbitrarily reconfigure large arrays of soft latching actuators. By developing a novel, simple, compact, and versatile concept to selectively move arrays of SMP actuators, my work opens up additional perspectives of research projects and practical applications for this emerging field. My aim is to combine local Joule heating with global air pneumatic actuation to selectively and reversibly trigger motion on the array. Correlating theoretical models with experimental data and having a good understanding of the physics involved enabled me to optimize the device parameters to reach the requirements for several applications. Specifically, it allowed me to find the best trade-off between force and displacement for any actuator size, to decrease the refresh time despite combining thermal with pneumatic principles, and to minimize the overall power consumption of the array.

In addition, to validate my strategy to reconfigure arrays of SMP actuators, I have decided to develop and demonstrate applications in the fields of haptic displays and microfluidic platforms. A high resolution flexible plus wearable haptic display has been fabricated and a smaller rigid version has been tested by end-users to demonstrate the technology potential. Since mLSI systems and haptic displays have similar actuator form factor, a microfluidic platform presenting clear open-closed valving behaviors is reported to illustrate the concept versatility and effectiveness. The final devices, shown in Figure 1.1, required the development of robust, reproducible, and reliable manufacturing processes to obtain uniform plus stable performance over time.
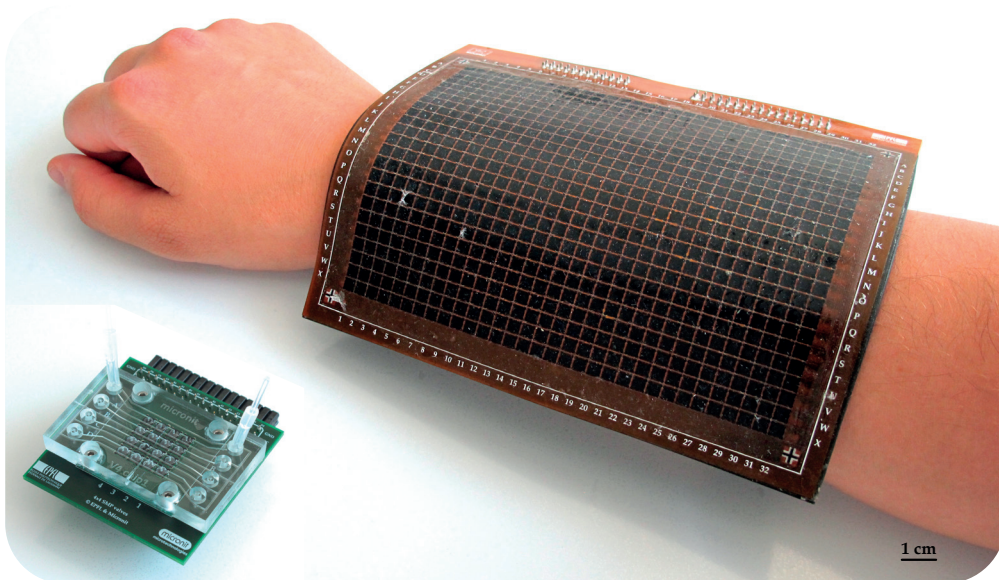


Figure 1.1 – On the bottom-left, picture of the 4x4 microfluidic platform. On the top-right, picture of the 32x24 flexible haptic display when worn as a sleeve. Both devices are on the same scale.

## 1.4 Thesis outline and contributions

My thesis advances the field of SMPs by exploiting their key instrinsic material characteristics to engineer large arrays of densely packed soft latching actuators. SMPs present the unique feature of being multistable and having a hundred- to thousand-fold change in Young's modulus with temperature, which enables to combine both actuation plus latching in a single actuator.

My work focuses on the novel actuation concept and major contribution to the SMP field, which consists in individually and selectively addressing large arrays of SMP actuators by synchronizing the local Joule heating of each actuator with a single common air pneumatic supply. Compliant heaters are patterned on thin SMP membranes in order to precisely define regions where the stiffness can be locally changed by over two orders of magnitude. The selective local Joule heating defines which actuators will be affected by the constraint generated with the common air pneumatic supply. Figure 1.2 illustrates the active layer comprising the thin SMP membrane and the stretchable heating electrodes (one per actuator).
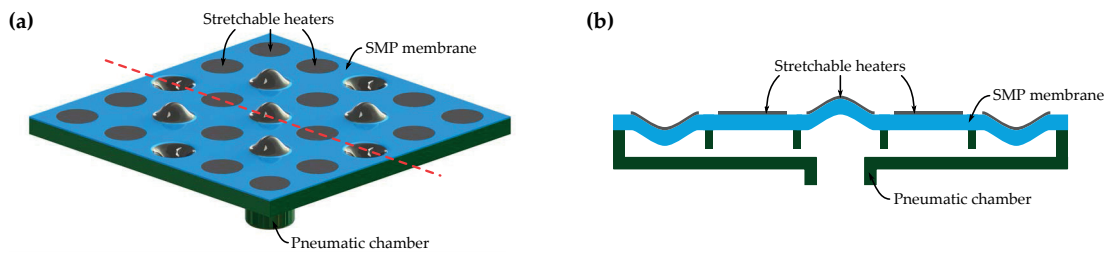


Figure 1.2 – Schematic illustration of the active layer, comprising the SMP membrane and the stretchable heaters, bonded to the pneumatic chamber. (a) Top-view of the active layer. (b) Cross-section of the active layer.
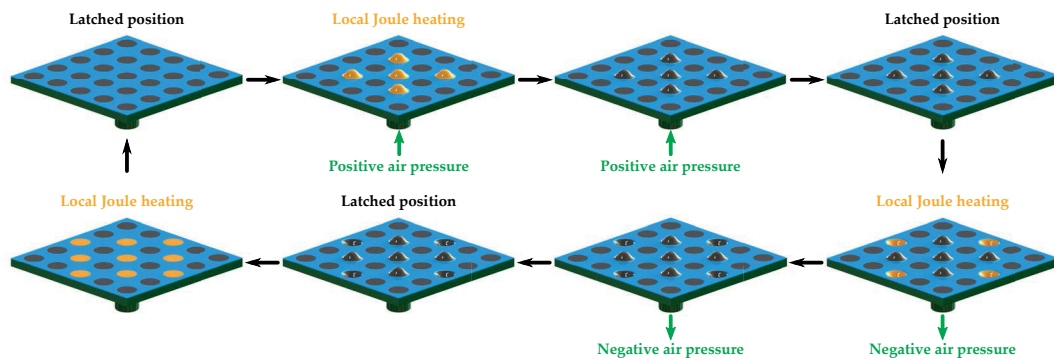


Figure 1.3 – Schematic illustration of my novel concept to arbitrarily reconfigure an array of SMP actuators. Local Joule heating and external air pressure are timely synchronized to selectively and exclusively move the desired SMP actuators. Starting from a flat array, positive and negative deformations are sequentially obtained by combining thermal and pneumatic actions.

5

## Chapter 1. Introduction

By a timely synchronization of the thermal stimuli and the external air pressure, each actuator can be independently, reversibly, and rapidly latched into several positions. This innovative actuation strategy is shown in Figure 1.3, where positive and negative motions are obtained. This matrix of latching actuators is highly versatile: in the mechanical domain, it can exert high forces, needed for instance for haptic displays, arrays of microfluidic valves, or soft robotic grippers. The deformable surface also controls how electromagnetic waves are reflected, leading to applications in camouflage, adaptive optics, and reconfigurable radio-frequency (RF) or millimeter-wave surfaces. In particular, my approach using arrays of SMP actuators is validated by both the 32x24 flexible haptic display and the 4x4 microfluidic platform shown in Figure 1.1.

My thesis is organized as following:

**Chapter 1** introduces the thesis by summarizing its objectives and its contributions.

**Chapter 2** presents the key characteristics of SMP actuators, and discusses the material and actuation choices through selected state-of-the-art devices.

**Chapter 3** presents the operating principle which combines local Joule heating and global air pneumatic actuation. It also details the design, modeling, and fabrication of the large array of SMP actuators. The reported size and thickness for the active layer, comprising the thin SMP membrane and the matrix of compliant heaters, correspond to the optimal trade-off between displacement and holding force for haptic displays and microfluidic platforms.

**Chapter 4** presents the performance of SMP actuators as taxels in a 32x24 flexible haptic display, which is the first high resolution wearable sleeve capable to vary its surface topology and thus its appearance. It reports measurements of displacement, holding force, power consumption, and lifetime. The perception test conducted with blindfolded sighted users on a 4x4 SMP tactile tablet resulted in 98 % correct pattern recognition in less than 10 s exploration, confirming that SMP actuators are a promising taxels technology.

**Chapter 5** presents the performance of SMP actuators as microfludic valves in a 4x4 microfluidic platform, which is the first latching microfluidic array where each valve is directly controlled with a common air pneumatic supply. It reports cyclic valving measurements with respect to heating power, air pressure, and water pressure, validating that our SMP actuators are an interesting valve-unit for micropumps, mixers and multiplexers in mLSI systems. Both normally closed (NC) and normally open (NO) type of SMP valves have similarities in design and performance.

**Chapter 6** concludes the thesis by summarizing its main outcomes, by discussing a promising application coupling fluidics with haptics, and by proposing a technique to render the active layer optically transparent.

# 2 Fundamentals of shape memory polymer (SMP) actuators

## 2.1 Summary

In this chapter, I introduce the concept of SMP actuator, a type of soft actuator exhibiting large stiffness change with temperature and intrinsic latching capabilities. I first summarize the theory behind this unique combination of properties. I then discuss the available materials and explain the choices I made for the SMP membrane and the stretchable electrodes forming the active layer of SMP actuators I have developed. In the last section, I present relevant examples of SMP applications.

## 2.2 Introduction to shape memory polymers

Shape memory polymers (SMPs) are programmable phase-change materials (PCMs) which can memorize a permanent shape, can be deformed and fixed to a temporary shape under specific conditions, and then later can relax to their original permanent shape upon external command; with their relaxation being associated to the storage of elastic energy during the actuation cycle. There exist four main activation and recovery methods: thermal [33–36], solvent [37], light [38], and mechanical [39]; with the amorphous thermosets and thermoplastics SMPs being the most widely studied in literature. As reproduced in Figure 2.1a, the shape memory effect (SME) is associated to the dual-domains system of the polymer, with one being always elastic and the other one being transitionable (hard below the glass transition and soft above) [40]. Below the glass transition (in the glassy state), both the elastic and the transition domains are hard and, above it (in the rubbery state), the transition domain becomes soft while the elastic domain remains hard. Consequently, under external constraint, the elastic domain is forced to deform to a temporary shape, inducing elastic energy in the system. If this temporary shape is held during cooling, the elastic energy will be largely locked and stored in the system even after removal of the constraint. Indeed, the transition domain is hard below the glass transition and thus prevents the elastic recovery of the elastic domain. Upon reheating above the glass transition and removal of the constraint, the transition domain

softens back and thus loses its ability to hold the elastic domain in place. Accordingly, the SMP returns to its original permanent stress-free shape. During the heating + cooling cycle, the SMP exhibits a Young's modulus change of at least two orders of magnitude, with a characteristic similar to Figure 2.1b in the case of amorphous thermosets and thermoplastics [41].

When selecting the appropriate SMP, two main figures of merit should be considered [43]: the shape-recovery ratio $R_r$ (the ratio of recovered strain to programmed strain) and the shape-fixity ratio $R_f$ (the ratio of fixed strain to applied strain). As illustrated in Figure 2.1c [42], the stress-strain curve obtained during $N$ shape memory cycles is characterized by several important quantities: the programmed strain $\varepsilon_m$, the fixed strain $\varepsilon_f$, the recovered strain $\varepsilon_r$, and the permanent strain $\varepsilon_p$. Both figures of merit $R_r$ and $R_f$ evaluating the best the SMP performance are defined by Equation 2.1 and Equation 2.2 [43].

$$R_r(N) = \frac{\varepsilon_m - \varepsilon_p(N)}{\varepsilon_m} = \frac{\varepsilon_r(N)}{\varepsilon_m}, \qquad \varepsilon_r(N) = \varepsilon_m - \varepsilon_p(N) \tag{2.1}$$

$$R_f(N) = \frac{\varepsilon_f(N)}{\varepsilon_m} \tag{2.2}$$

Ideally, both figures of merit should be equal to 100 %, indicating no strain losses within the actuation cycle. These ratios can be brought close to 100 % by optimizing the actuation cycle timings and conditions; notably by insuring proper heating + cooling rates and by avoiding large deformations leading to irrecoverable plastic deformations.

In addition to SMP performance, important parameters to consider when designing applications using SMP actuators are: the Young's modulus of the plateau in the glassy state $Y_C$ with its corresponding cold temperature $T_C$, the Young's modulus of the plateau in the rubbery state $Y_H$ with its corresponding hot temperature $T_H$, and the glass transition temperature $T_G$ with the temperature range of this transition region. These variables define the temperature and the constraint which should be used to program plus store the temporary state, and then to recover the permanent state. The larger the stiffness drop from the cold to the hot state, the more efficient the array of SMP actuators, since it implies higher motion difference among activated and unactivated actuators. Also, the closer the glass transition temperature to room temperature and the narrower the transition region, the less power required to heat one actuator. Nevertheless, to prevent undesired motion due to thermal cross-talk or ambient condition variation, margins of 10 °C to 20 °C with respect to the transition region are commonly taken as working temperatures $T_C$ and $T_H$.
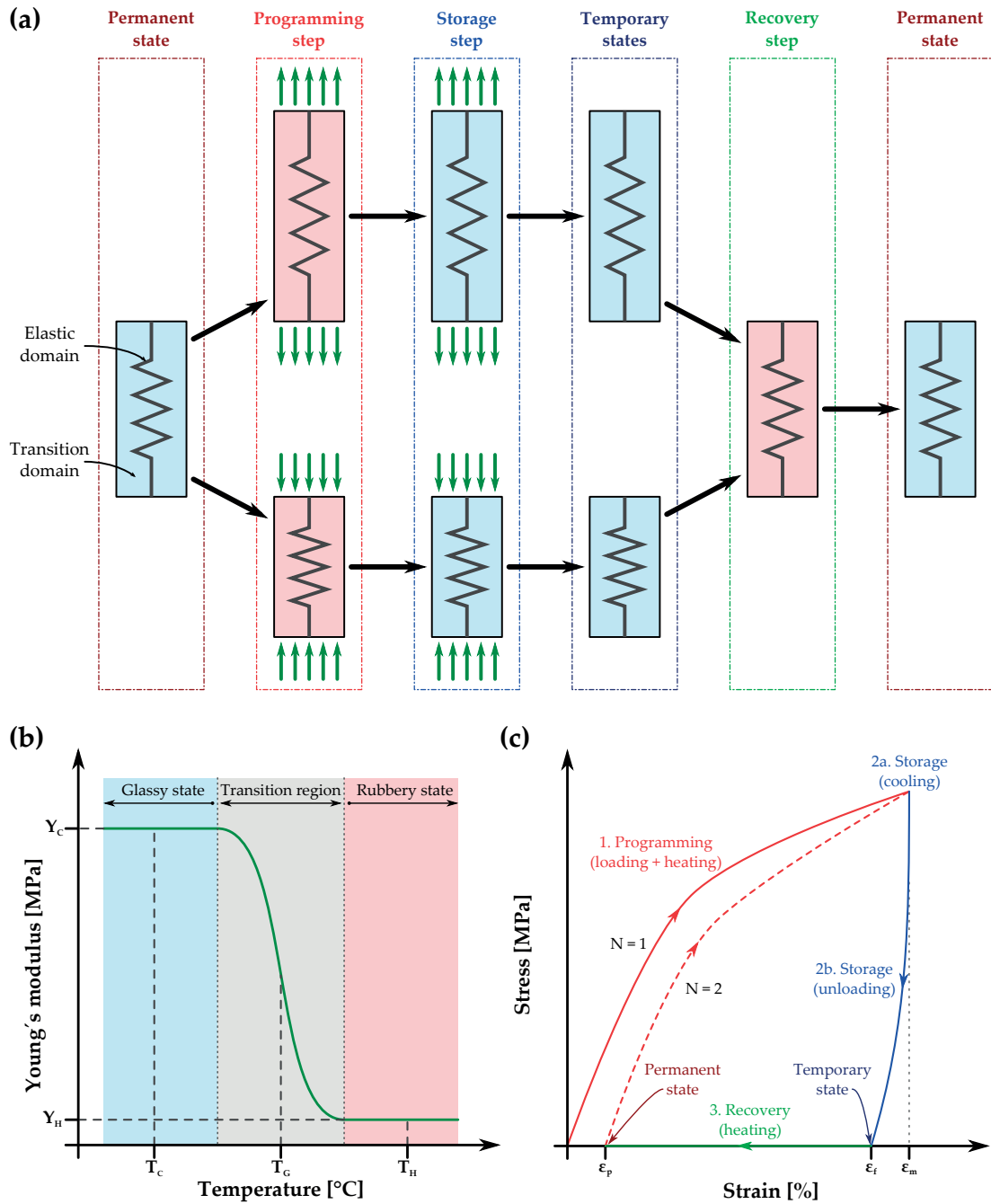
Figure 2.1 – SME associated to the dual-domains system of the polymer. (a) Schematic illustration of a typical actuation cycle to program plus store any temporary shape, and then recover the permanent shape (Adapted from [40]). (b) Schematic representation of a typical Young's modulus versus temperature curve for thermoset and thermoplastic SMPs (Adapted from [41]). (c) Schematic representation of the stress versus strain curve illustrating the SME (Adapted from [42]).

## 2.3   Selected materials

In this section, I briefly review commercially available SMPs and stretchable heating electrodes. I also present which materials I have selected for the array of SMP actuators.

### 2.3.1   Commercially available shape memory polymers

Current SMP research is mainly focused on tailoring the material characteristics and properties by tuning the SMP molecular structure to meet specific application requirements, by finding alternative stimulation mechanisms that are relevant for the intended application, or by creating new molecular designs beyond the simplest SMP system of chemically or physically crosslinking amorphous and crystalline polymers [21,44,45]. My thesis is focused on validating the innovative strategy to selectively move a large array of SMP actuators, rather than on developing new SMP materials. Consequently, only commercially available SMPs have been considered. There exist three main companies selling SMPs:

- *SMP Technologies* which is selling thermoplastic and thermoset polyurethane-based SMPs under the trade names *Diary* and *DiAPLEX* [46].

- *Cornerstone Research Group* which is selling styrene- and epoxy-based SMPs under the trade name *Veriflex* [47].

- *Composite Technology Development* which is selling epoxy-based SMPs under the trade name *TEMBO* [48].

In particular, the shape memory polyurethanes (SMPUs) are of great interest for a wide range of applications. They are polymerized from bifunctional diisocyanate, polyol, and chain extender [49]. By selecting a proper diisocyanate and polyol combination, one can easily tailor the elastic-to-transition domains ratio and thus modify material properties such as elasticity, crystallization temperature range, and glass transition or melting point [50]. More specifically, *SMP Technologies* offers the thermoplastic polyurethanes in pellet form (MM) or dispersed in a solvent (MS), and the thermoset polyurethanes in a two-part resin-hardener system (MP). All types have the following interesting properties [46,51,52]:

1. shape-recovery and shape-fixity ratios higher than 90 %.

2. board selections of glass transition temperatures ranging from 25 °C to 90 °C.

3. various processing possibilities including notably extrusion, injection or blow molding, foaming, and solution casting.

4. stiffness variations by 2 to 3 order of magnitudes.

5. biocompatibility.

On the one hand, thermoplastic SMPs offer easier processability and, on the other hand, thermoset SMPs offer better performance due to their inherent lower creep compared to thermoplastics; while both present similar glassy and rubbery stiffness properties.

In this thesis, I use the *MM4520* pellets from *SMP Technologies* [46]. This material was selected for its ductility at room temperature (to ease the manufacturing), its high shape-recovery and shape-fixity (to extend the operating lifetime), and its glass transition temperature of 45 °C (to allow latching in ambient conditions, while requiring only minimal heating to trigger motion). I dissolve it in dimethylformamide (DMF) to obtain a castable solution. In Chapter 3, I present more in detail the measured SMP membrane characteristics. Similar results would probably have been obtained with the thermoset *MP4510* resin-hardener and the thermoplastic *MS4520* solution from *SMP Technologies*, since they all present close mechanical properties [51].

### 2.3.2 Stretchable heating electrodes

Several strategies can be adopted to locally and rapidly heat the SMP membrane. Methods to intrinsically generate the thermal stimuli by adding fillers have been reported; notably by rendering the polymer electrically conductive (to enable direct Joule heating) [26, 27], magnetically permeable (to allow for contactless induction heating) [28, 29], or responsive to specific wavelength (to enhance radiation heating) [30]. While being probably the most efficient approach, changing the SMP membrane composition affects its mechanical properties and no method using fillers to precisely defining active zones was reported to date. The path studied in this work is to integrated stretchable heating electrodes directly on the SMP membrane surface. Ideally, they should be highly compliant not to affect the overall motion and highly conductive to homogeneously spread the heat; both properties being usually incompatible. Indeed, on the one hand, soft materials are intrinsically insulators and, on the other hand, good conductors can be stretched only to few percents. Stretchable heating electrodes based on carbon black [53, 54], metallic nanowires [55–57], liquid metals [58], and metallic nanoparticles [59, 60] embedded or bonded to soft materials have notably been reported for flexible and stretchable transducers.

In this thesis, building on the laboratory expertise, I use a mixture of carbon black (CB) and soft polydimethylsiloxane (PDMS). This carbon-silicone (CB/PDMS) composite was selected for its good bonding to the SMP membrane, its ease of patterning on a large area [61, 62], its high resistance stability within few tens of percent of strain [63], its low stiffness compared to the SMP membrane [63], and its reliable operation as a heater to over 100 °C [54]. In Chapter 3, I present more in detail the CB/PDMS electrode properties. Thin-film gold evaporation [64, 65] has also been investigated, but the microcracks inherent to the fabrication process lead to local hot spots, resulting in the device failure. An interesting alternative to the carbon-silicone composite are the silver nanowires (AgNWs), since nanowires networks were proven to be stretchable, highly conductive, and even in certain conditions transparent [55]. Their usual fabrication involved for years complex processing not compatible with large

scale manufacturing. Recently, a simple technique has been proposed [66], rendering them potentially attractive as stretchable heaters in the future.

## 2.4 Examples of SMP applications

In this section, I highlight promising and inspiring applications benefiting from the specific use of SMPs. I summarize their operation principle and compare them when relevant to my own strategy of selectively integrating compliant heaters on the SMP membrane and of suitably synchronizing the local Joule heating with the global pneumatic air supply.

### 2.4.1 Classical thermo-responsive SMPs

Thermo-responsive SMPs are the most studied in the field. To demonstrate the SME of their newly developed material, most chemists first temporarily preshape the SMP structure by applying important deformation and then heat it up externally to recover the permanent shape. The classical example shown in Figure 2.2a was presented by Behl et al. [19]. Recently, Zarek et al. reported on a three-dimensional (3D) printable SMP material [67], an interesting concept to design complex SMP structures; notably the cardiovascular stent, the Eiffel tower, and the bird presented in Figure 2.2b. Combining this approach with other conventional additive manufacturing materials is of great interest to simultaneously fabricate hard, soft, and adjustable parts [68]. A compact mean of actuation and heating still needs to be design to make this technology fully functional.
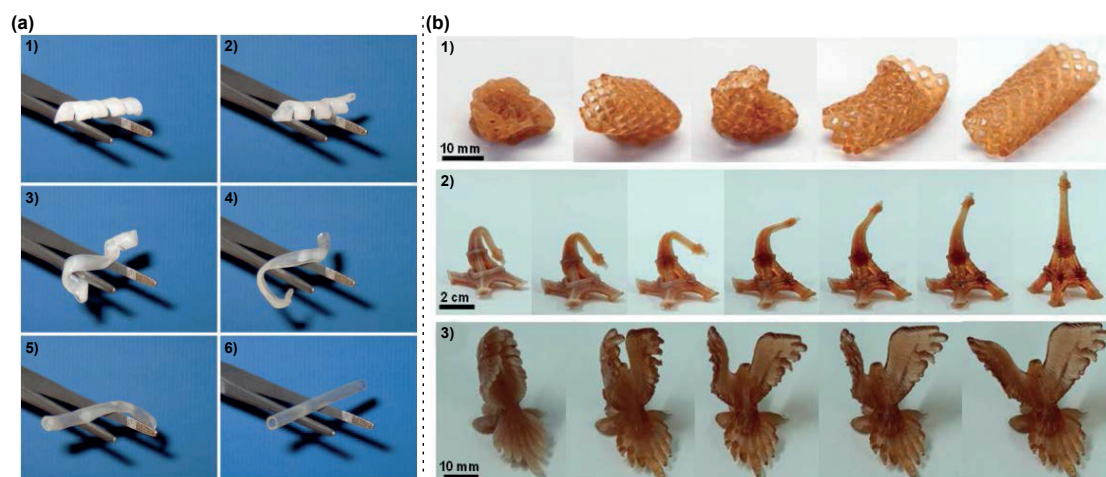


Figure 2.2 – Examples of classical thermo-responsive SMPs illustrating the SME [19, 67]. (a) From 1 to 6, shape recovery in 10 s of a SMP tube upon heating at 50 °C (Reprinted from [19]). (b) 3D-printed SMP structures (a cardiovascular stent, an Eiffel Tower, and a bird) recovering their original shape upon heating at 70 °C (Reprinted from [67]).

### 2.4.2 SMP actuators for adaptive optics

Most SMPs are optically transparent, rendering them highly attractive for adaptive optics. Xu et al. [69] demonstrated that via compression molding and further deformation via hot pressing, they can fabricate micro-optical components. Their microprism arrays, microlens arrays, surface relief gratings, and holograms are shown in Figure 2.3. Furthermore, by incorporating an array of transparent indium tin oxide (ITO) resistive microheaters below the SMP block, they can selectively trigger the shape of the micro-optical device. Their elegant system enables to locally change the optical property by switching between the as-fabricated and the programmed configuration, but still requires a bulky external system to deform the device. Alternative methods to preshape SMP micro-optical components like thermal exposure nanoimprint lithography (TE-NIL) [70], and laser exposure [71] have also been reported.
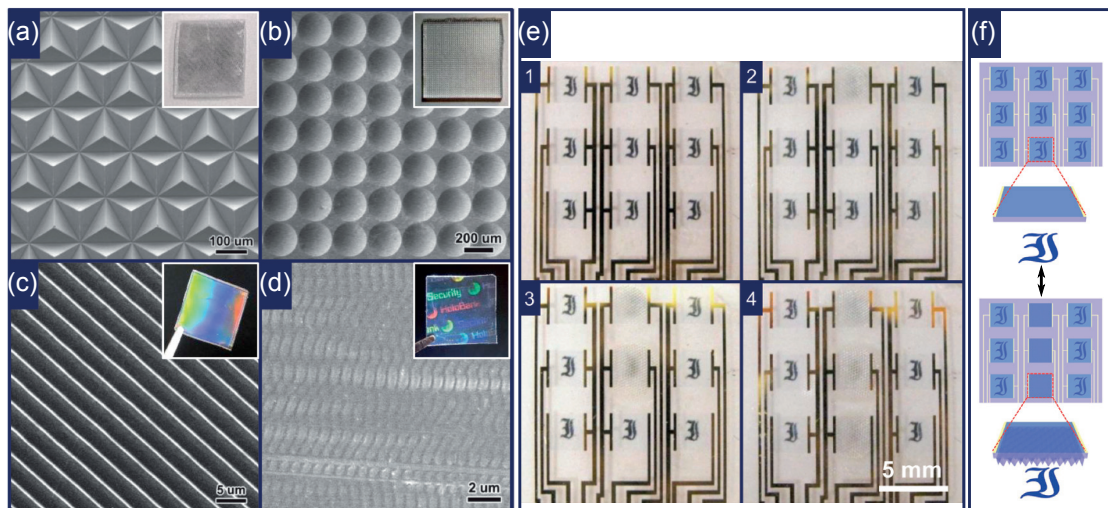


Figure 2.3 – Examples of deformable and programmable SMP micro-optical components [69]. Scanning electron microscope (SEM) images of several molded micro-optical components with in the inset the macroscopic picture: (a) a microprism array, (b) a microlens array, (c) a transmission grating, and (d) a white-light hologram. (e) Deformed microprism array attached to a 3x3 transparent indium tin oxide (ITO) heater array to selectively recover the microprism array. From 1 to 4, the center column is heated and recovered in sequence from top to bottom. (f) Schematic illustration of the programmable device before and after recovery via selective heating (Reprinted from [69]).

### 2.4.3 SMP actuators for microfluidics

Several microfluidic examples using SMPs exploit both their compatibility with molding plus hot embossing techniques to pre-shape the device and their SME to drive fluid through the chip. The very first example, shown in Figure 2.4a, was reported by Gall et al. [72]. First, the surface of a SMP circular section was locally machined using a laser to temporary create a fluid reservoir connected to a microfluidic channel. After embossing and filling the channel with fluid, a glass slide was placed atop the device, enclosing the channel and the reservoir.

Upon heating, the reservoir gradually recovered its flat state, displacing the fluid along the microfluidic channel. A similar fabrication approach was used by Takehara et al. [73] to design the one-shot normally closed (NC) and normally open (NO) valves illustrated in Figure 2.4b-d. The valves were first molded to define their original shape and then hot embossed via nanoimprinting to form their temporary shape. Upon heating, with the microheater located below the SMP material, the valve recovers its original shape. Despite benefiting from the high holding force of the SMP in its cold state compared to standard PDMS technology, these SMP valves are lacking in cyclic operation.
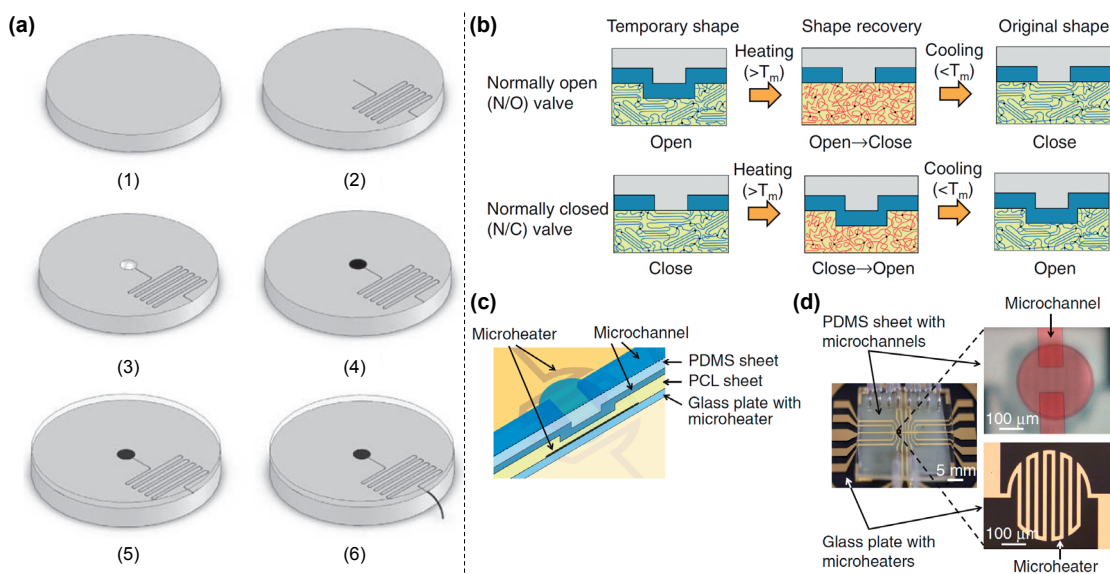


Figure 2.4 – Examples of one-shot SMP microfluidic reservoirs [72] and valves [73]. (a) From 1 to 6, schematic illustration of the fabrication and operation of a SMP microfludic reservoir. The reservoir is first pre-shaped, then filled with fluid plus sealed to a glass plate, and finally, upon heating, fluid flows along the channel (Reprinted from [72]). (b) Schematic illustration of the operating principle for one-shot NC and NO valves. The valves were first molded to define their original shape and then hot embossed via nanoimprinting to form their temporary shape. (c) Schematic structure of the SMP one-shot valve. (d) Picture of the SMP one-shot valve (Reprinted from [73]).

As described in detail in Chapter 5, by integrating both the heating system and the actuation mechanism, I have developed the first reversible NC and NO valves in collaboration with my colleague Bekir Aksoy (EPFL-LMTS, Switzerland) and my partners Robert Jan Boom plus Bas-Jan Hoogenberg (Micronit Microtechnologies, Netherlands). Our approach differs from the one of Takehara et al. since no device preshaping is involved and our valves can be repeatedly opened and closed.

### 2.4.4 SMP actuators for soft robotics

Two key aspects of SMPs are their drastic change in Young's modulus with temperature and their latching property. These features have notably been exploited in soft robotics, since they enable both to couple high compliance with significant holding force when grasping objects and to freeze the shape when lifting them. Several robotic origamis incorporate SMPs and stretchable metallic heaters at their finger joints to facilitate miniaturization and integration of desired functions in a gripper by locally adapting their stiffness [74–76]. In particular, Firouzeh et al. [75] showed that multiple degree of freedoms (DoFs) can be achieved using a continuous tendon coupled with adaptive stiffness SMP joints, as depicted in Figure 2.5.
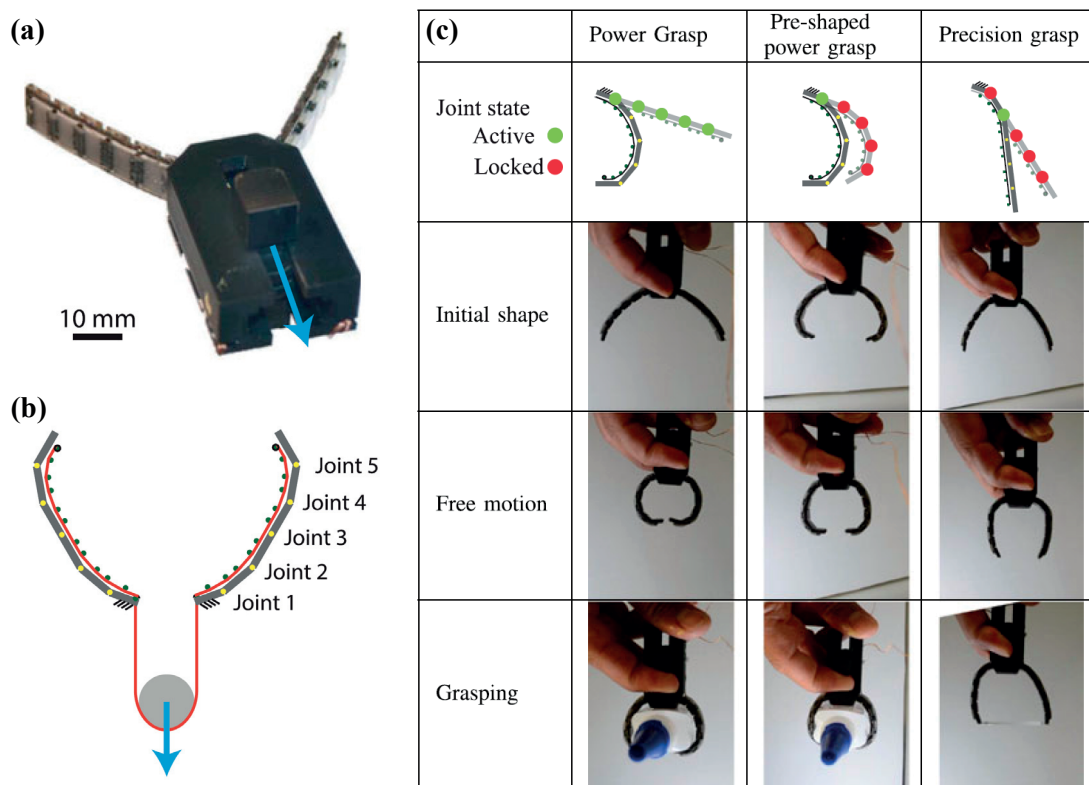


Figure 2.5 – Example of a robotic origami using SMP joints [75]. (a) Picture of the adjustable gripper with each adaptive stiffness joint. The gripper has two fingers, each with five joints. The stiffness of each joint can be adjusted independently. (b) Schematic illustration of the gripper highlighting the tendon route and the joint positions. (c) Picture of several possible grasping modes, resulting from different sets of joints activation (Reprinted from [75]).

A more lightweight approach, which I helped design, was reported by McCoul et al [54]. We developed the shape memory dielectric elastomer minimum energy structure (DEMES) gripper shown in Figure 2.6. Conventional DEMES consist of a soft prestretched DEA membrane bonded to a flexible frame. Upon release of the prestretch, they find their equilibrium in bending and then, when the actuation voltage is applied, present out-of-plane motion. One of their main drawback is the small holding force they can provide. Hence, we replaced the conventional CB/PDMS ground electrode by a CB/SMP heating electrode to double the holding force. The 4.1 kV actuation voltage being much higher than the 300 V heating voltage required to soften the SMP electrode, we could selectively address, heat, and move each segment. Figure 2.6 illustrate the actuation cycle and demonstrate that our gripper can hold and lift a 30 g container in its hard state, but not in its soft state.
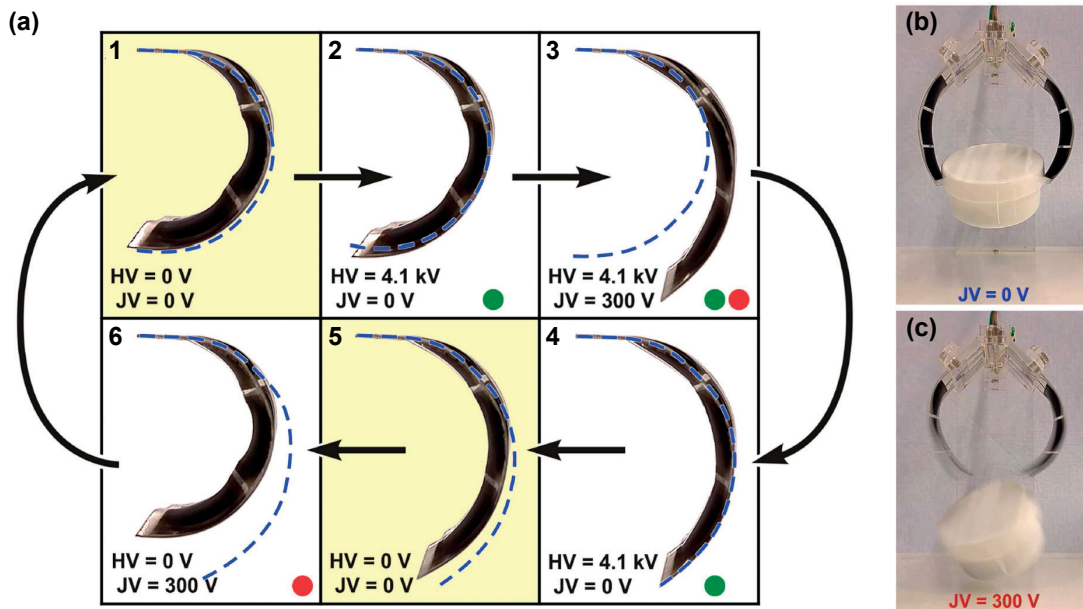


Figure 2.6 – Example of a soft gripper with variable stiffness segments [54]. (a) From 1 to 6, schematic illustration of the actuation cycle of a shape memory DEMES gripper finger, for the case where all three segments are simultaneously heated or cooled. The outline of the previous state is shown as a blue dashed line to aid in visualizing the deflection. The high voltage (HV) applied across the PDMS of all three segments is denoted by the green dot; the Joule voltage (JV) applied along all the SMP electrodes is denoted by a red dot. (b) Picture of the gripper holding a 30 g container in its cold state (JV = 0 V). (c) Picture of the gripper dropping the container in its hot state (JV = 300 V on all segments). No high voltage is applied, but it could be to open the gripper digits and assist with dropping, picking up, and conforming to objects of different shapes. (Reprinted from [54]).

### 2.4.5 SMP actuators for haptics

SMPs have attracted attention in haptics for their interesting SME property, including their programmable, storage, and recovery steps. Actually, this field is one of the most demanding in terms of force, displacement, speed, resolution, and power consumption requirements. Leng et al. [71] proposed to replace the standard Braille paper with thermoplastic SMP sheets to allow for both infinite reprinting using a laser printer and erasing minor errors using a hot pen. More recently, Niu et al. [16] combined DEAs and SMPs to create the array of Braille-sized bistable actuators shown in Figure 2.7. Their approach of using the SMP as the elastomer in the DEA elegantly enables latching in DEAs and significantly enhanced the holding force. However, their approach requires high voltage switches (in the kilovolt range) and lacks of an efficient and compact heating strategy to independently address each actuator. They either reported one actuator with an integrated heater significantly bigger than the actuator [77], or an array of actuators globally heated and driven cell-by-cell with a matrix of high voltage switches [16].
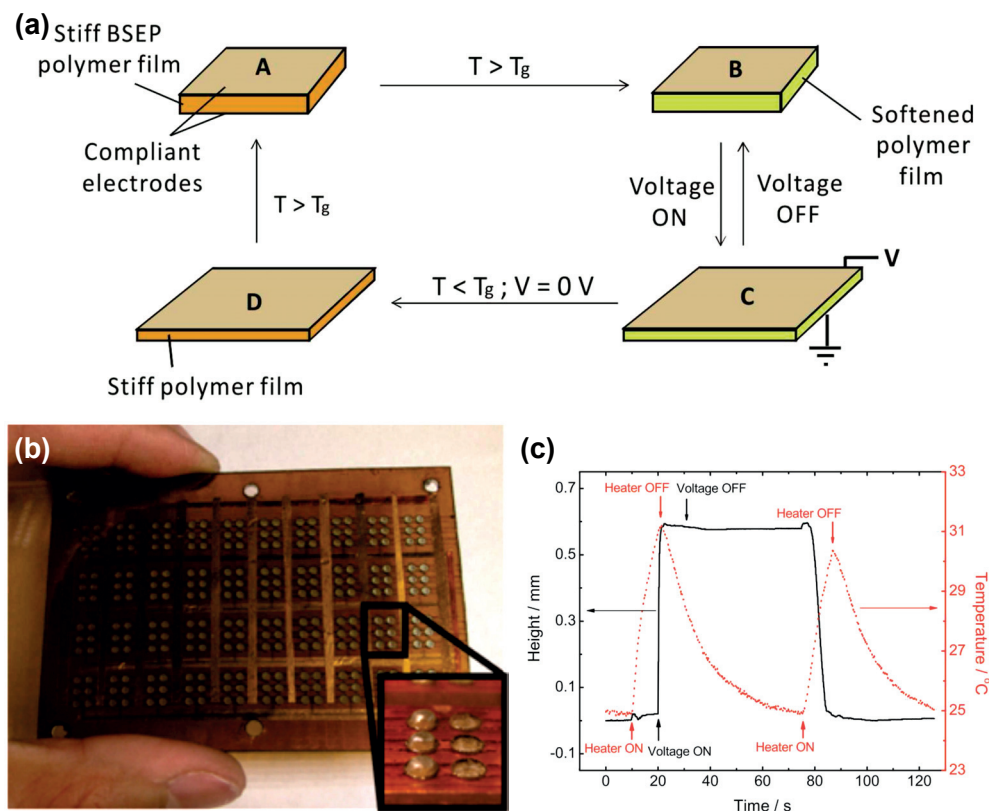
Figure 2.7 – Example of an array of Braille-sized bistable SMP actuators [16]. (a) Schematic illustratio of the actuation mechanism using the bistable electroactive polymer (BSEP) material. (b) Picture of a refreshable Braille tablet with in the inset a zoom-in on a cell displaying the Braille letter $L$ .(c) Measured displacement and temperature for a Braille dot as a function of time. An external heater is incorporated below each cell driven by a matrix of 2x3 high voltage switches. (Reprinted from [16]).

17

As described in detail in Chapter 4, by integrating both the heating system and the actuation mechanism, I have developed the first haptic display with a large array of individually addressable SMP actuators. My approach differs from the one of Niu et al. since the pneumatic actuation is preferable over the electrostatic one and the local Joule heating enables selective actuator motion. Moreover, my device is demonstrated to be operating when flexed and worn as a sleeve.

## 2.5 Conclusion

In this chapter, I introduced the concept of SMP actuator, I discussed the key properties of SMP materials, and I presented a selection of state-of-the-art SMP devices. I first summarized the SME and described the general actuation cycle to program plus store any temporary shape, and then recover the permanent shape. I then compared several available materials interesting to form both an efficient SMP membrane and compliant patternable heating electrodes. Keeping in mind that I want to demonstrate a novel concept by locally integrating heaters on thin SMP membrane to selectively actuate an array, the major criteria were material accessibility, ease of manufacturing, and overall performance. I finally reviewed relevant applications using SMP actuators and explained how by implementing my innovative strategy, their performance could be improved with additionally a simpler and more compact system.

# 3 Design and fabrication of arrays of SMP actuators

## 3.1 Summary

In this chapter, I detail the design and fabrication steps I have developed for large arrays of SMP actuators. I first highlight my novel strategy to selectively reconfigure this device by suitably synchronizing the local Joule heating with the global pneumatic air supply. I then justify the design choices made to meet the targeted requirements for haptic displays and microfluidic platforms by optimizing the actuators size, geometry, and thickness using experimentally validated finite element analysis (FEA) models. I finally present the fabrication and assembly processes specifically developed during my thesis.

The potential of coupling local Joule heating with global pneumatic air actuation for driving large arrays of SMP actuators is demonstrated by the 32x24 flexible haptic display and by the 4x4 microfluidic platform. Both devices rely on the same SMP actuator design, demonstrating the high versatility of my innovative concept. The heart of the technology, illustrated in Figure 3.1, is a thin ($10\,\mu m$ to $100\,\mu m$ thick) SMP membrane, on which a matrix of individually addressable compliant CB/PDMS heaters is patterned. This active layer is electrically and mechanically bonded to a printed circuit board (PCB) to route the Joule heating currents, and then sealed to the microchanneled chamber to distribute a controlled air pressure to the entire device. In the microfluidic platform, an additional styrene ethylene butylene styrene (SEBS) membrane acting as an impermeable barrier is placed atop the active layer to protect it from the fluid. Figure 3.1 highlights that the SMP actuator can be latched in any arbitrary *down*, *flat*, or *up* position. Despite working only with bistable positions in both reported haptic and microfluidic applications, the SMP actuator can actually latch in any intermediate position, which would permit for a true 3D surface on the haptic display or for tuning the fluidic impedance of the microfluidic platform.

Part of the sections on the operating principle, the material properties and the manufacturing processes have already been published in *Advanced Material Technologies* [78] and presented at the *Transducers 2017 Conference* [79]. Additional information on the design methodology are provided in this chapter.
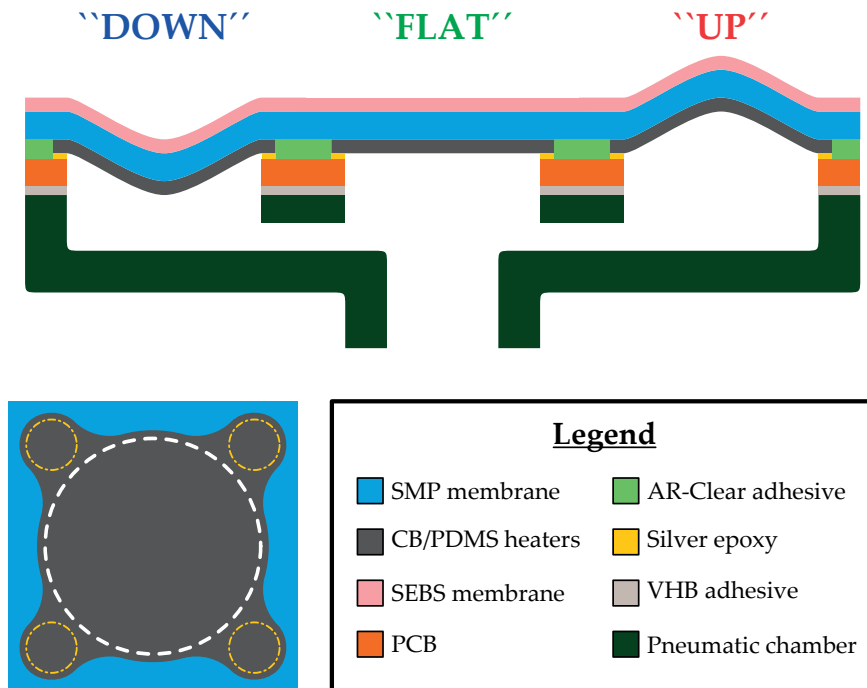
Figure 3.1 – On the top, schematic illustration of the device highlighting the main layers composing the array of SMP actuators I have developed. Any arbitrary *down*, *flat*, or *up* positions can be obtained. On the bottom-left, schematic illustration of the heater geometry. Atop the active layer (SMP membrane + CB/PDMS heaters for haptics and SMP membrane + CB/PDMS heaters + SEBS membrane for microfluidics) either a pin interface for the haptic display or a microfluidic chip for the microfluidic platform is placed.

## 3.2 Operating principle

My novel strategy, for which I filed a US Patent with my colleagues Juan José Zárate, Samuel Rosset, and Herbert Shea (EPFL-LMTS, Switzerland) [80], is a simple method to independently, efficiently, rapidly, and reversibly control plus operate a large array of latching SMP actuators. Passing current through the individually addressable local heating elements selectively changes the stiffness of the SMP actuators. The common pneumatic air supply triggers motion of only the actuators that have been heated, leaving undisplaced the unheated elements. By turning off the heating current, each actuator can be latched into its current position, enabling holding any array configuration with zero power consumption. To lock the actuator shape, it is important to keep the pneumatic air supply turned on longer than the Joule heating current. It enables to store the elastic energy in the system while cooling the actuator. Each actuator starts in the as-fabricated permanent flat position. Then, as illustrated in Figure 3.2, it can be deformed into an infinite number of stable positions: deflated (negative pressure), flat (no pressure) or inflated (positive pressure). To minimize the power consumption, Joule heating is restricted to the actuators that need to be reconfigured when switching between two arbitrary stable positions.
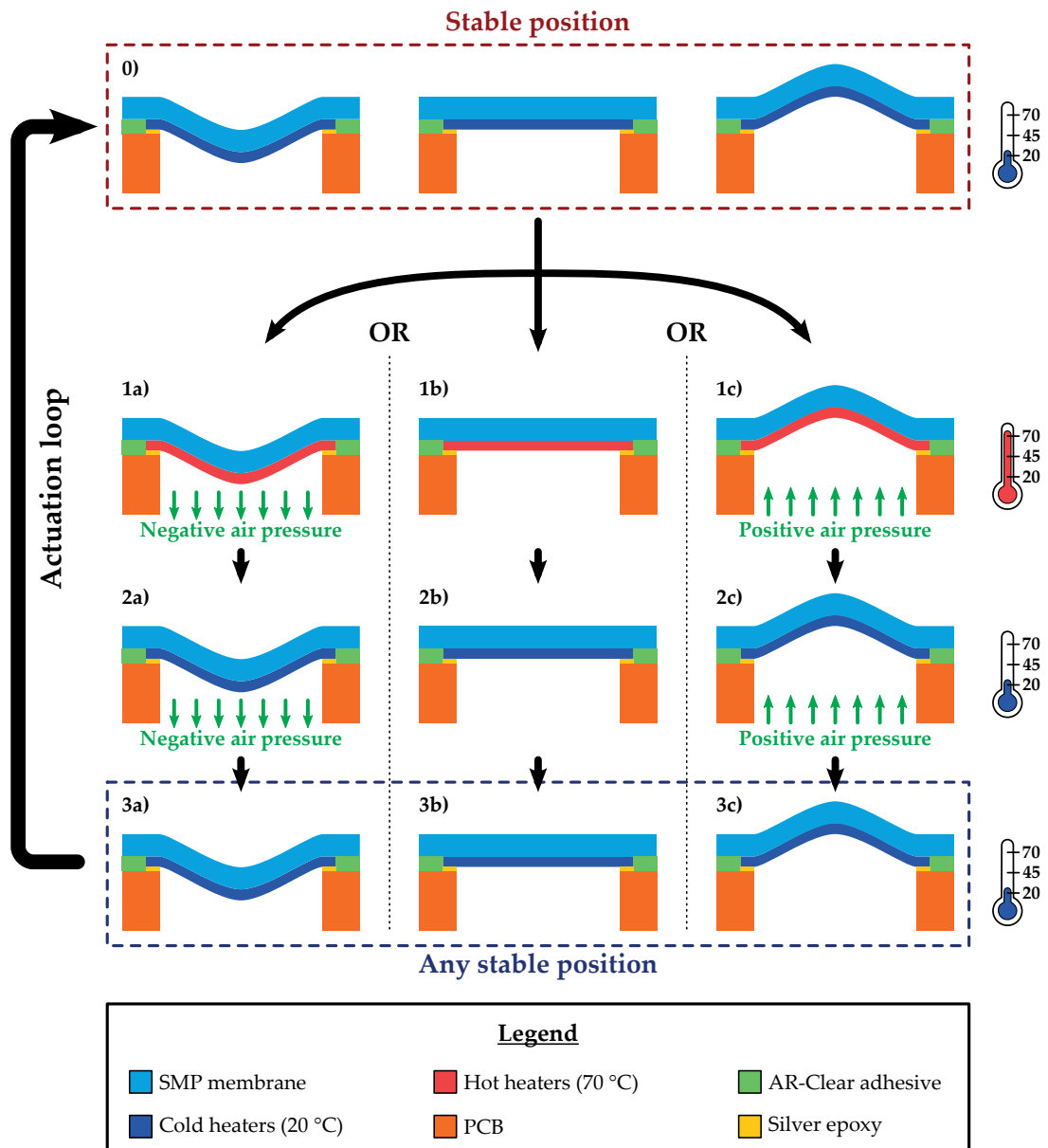
Figure 3.2 – Schematic illustration of the operating principle to reconfigure an array of SMP actuators. The heater is shown in red when hot (70 °C) and in blue when cold (20 °C). First, pressure (positive, none, or negative) is applied and the actuators to be moved are heated using their integrated addressable heaters, reducing their stiffness by two orders of magnitude. Those actuators thus deform. Second, the local heating is turned off and the pressure is kept on to latch the actuator in place as it cools. Finally, the pressure is switched off; resulting in a new stable position. The sequence on the left is to raise an actuator, on the middle to recover the permanent flat state, and on the right to pull down an actuator. All actuators can be arbitrarily, selectively, and repeatedly reshaped. The actuators which are not heated remain rigid, and hence do not change position regardless of applied pressure.

## 3.3   Actuator design and modeling

In this section, I discuss the SMP actuator design, in particular its thickness and geometry optimization to reach the targeted requirements for haptic displays and microfluidic platforms. Haptic displays are actually more demanding than microfluidic platforms, because they require simultaneously large displacement and high holding force on a small pitch. Stroke and pitch requirements in microfluidics are more adaptable, since the shape and location of the valve in the microfluidic chip can be adjusted to match the displacement reached by the SMP actuator. Hence, most of the requirements are set by the haptic display application.

### 3.3.1   Key requirements for haptic displays and microfluidic platforms

Most of my work was developed in the framework of the *BlindPAD* project, whose key requirements are reported in Table 3.1. Hence, I based my design of the large array of latching SMP actuators on these requirements. For sake of information, they are compared to the ideal requirements for developing a Braille tablet covering a Letter-size paper with tactile pixels (taxels) on a 2.54 mm pitch. My thesis goes well beyond a simple graphical tactile tablet for blind and visually impaired persons, since it also adds flexibility to the display, opening opportunities in virtual reality (VR) or augmented reality (AR) scenarios and in novel human-machine interfaces (HMIs). For sighted people, a pitch of 5 mm to 10 mm is sufficient to discriminate between two nearby taxels when coupled to visual information [81]; whereas for blind and visually impaired people the ideal target should be the Braille standard of 2.54 mm to combine graphical and textual information on the same tablet [18].

Table 3.1 – Summary table of the key requirements for the array of SMP actuators as set by the *BlindPAD* project. For information, these objectives are compared to ideal requirements for developing a Letter-size Braille tablet.

| Parameter | *BlindPAD* requirement | Braille tablet requirement |
|:---:|:---:|:---:|
| Actuator pitch | 4 mm | 2.54 mm |
| Displacement | >200 µm | >500 µm |
| Holding force | >60 mN | >1000 mN |
| Array refresh time | >0.1 Hz | >1 Hz |
| Average power consumption | <10 mW/actuator | <1 mW/actuator |
| Array size | 64 x 48 | 110 x 85 (Letter-size paper) |
| Lifetime | >10 000 cycles | >1 000 000 cycles |
| Latching mechanism | Essential | Essential |
| Portability | Essential | Essential |

Additionally, for the microfluidic platform, to operate with no performance degradation when in contact with fluid, the active layer should be impermeable and optionally biocompatible. Since the form factor in microfluidics is similar than in haptics, the same force and

displacement requirements have been considered for the SMP valves.

### 3.3.2 Characterized material properties

Given that no information is available on the properties of the SMP membrane when processed as a thin film, and in order to obtain the materials parameters needed to design the active layer (SMP thickness, heater shape and thickness, device dimensions, and applied pressure) for different applications, the mechanical, electrical, and thermal properties of the active layer were characterized in-house. They were obtained with the help of my colleague Juan José Zárate (EPFL-LMTS, Switzerland) and of Cédric Plesse (University of Cergy-Pontoise, France). Specifically, the SMP glass transition temperature, as well as the heat capacity, heater resistance, and real plus imaginary parts of the Young's modulus as a function of temperature were measured. The SMP membrane used for characterizing these properties was 42.7 μm thick and the CB/PDMS electrode was 23.9 μm thick. Dynamic mechanical analysis (DMA) was performed on the SMP membrane with and without the CB/PDMS electrode; the temperature dependence of the Young's modulus is reported in Figure 3.3. In the cold state (at 20 °C), a Young's modulus of 1.7 GPa for the bare SMP membrane and of 1.1 GPa for the SMP membrane with the CB/PDMS electrode were measured. In the hot state (at 70 °C), 13.8 MPa for the bare SMP membrane and 12.7 MPa for the SMP membrane with CB/PDMS electrode were obtained. The datasheet values for the SMP pellets are a Young's modulus of 2.15 GPa for the glassy state and of 1.4 MPa for the rubbery state. The difference between the datasheet and the measured values probably originates from the thickness of the membrane, as the datasheet is for bulk material. Another potential source of variation in elastic modulus compared to the datasheet are the two heating steps introduced in the fabrication process to ease the dilution and to cure the membrane, since temperature can directly affect the cross-links [50, 82].
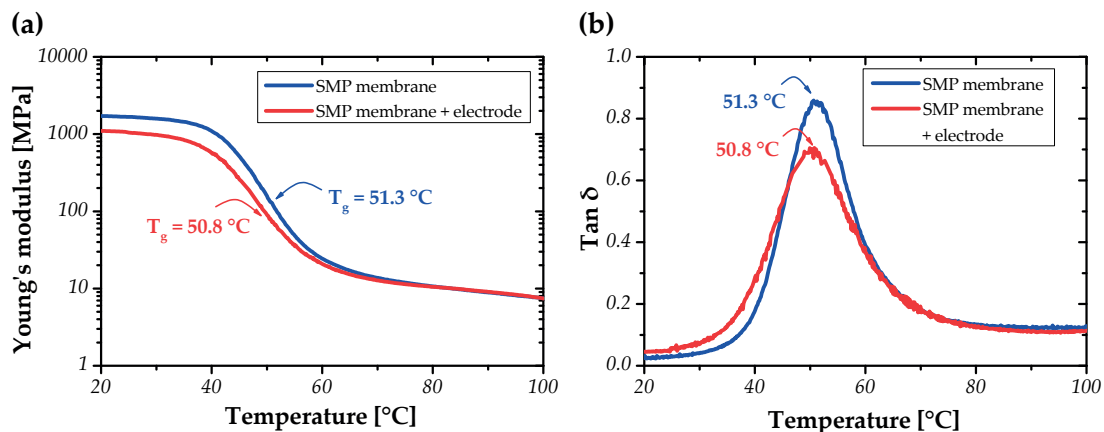


Figure 3.3 – Mechanical properties of the SMP membrane and the CB/PDMS heater obtained from the DMA measurement. (a) Measured Young's modulus versus temperature for the bare SMP membrane and the SMP membrane with CB/PDMS electrodes. (b) Dissipation factor (tangent delta) for the bare SMP membrane and the SMP membrane with CB/PDMS electrodes showing high losses at the glass transition temperature.

23

The CB/PDMS electrode has a resistivity of $0.054\,\Omega\,m$, a typical Young's modulus of 2 MPa and a negative thermal coefficient of resistance (TCR) of $-0.0013\,1/°C$, as reported in Figure 3.4a. Differential scanning calorimetry (DSC) was performed to measure the thermal capacity of the materials and to confirm the glass transition temperature obtained with the DMA. The calculated heat capacity curve is reported in Figure 3.4b. The thermal capacity is $1.2\,J/(g°C)$ in its cold state and $1.9\,J/(g°C)$ in its hot state. For the bare SMP membrane, the glass transition temperature measured with the DMA and the DSC are $51\,°C$ and $47\,°C$, respectively; a value close to the $45\,°C$ expected from the datasheet. It indicates that moisture was low throughout the entire fabrication process [49]. In the future, to ensure reproducible actuator performance, additional storage precaution will be taken to avoid any humidity content in the SMP+DMF solution.

**(a)**

**(b)**
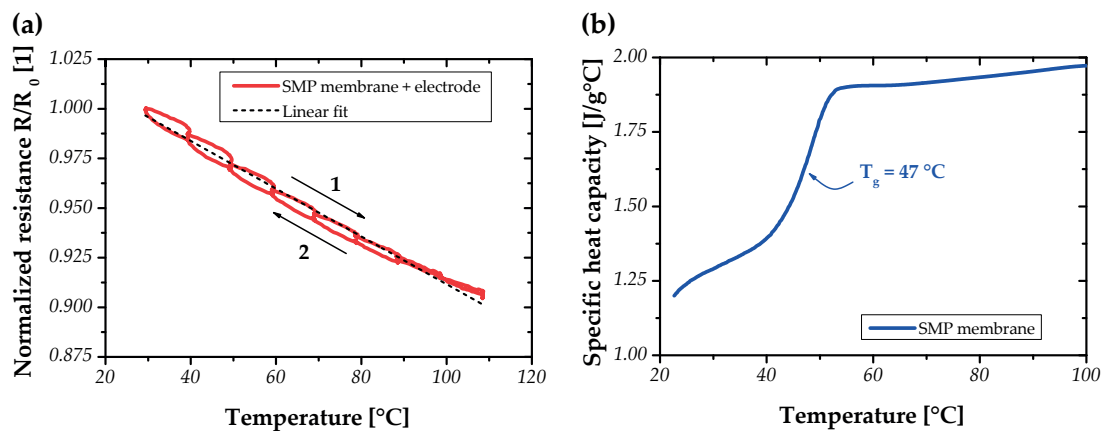


Figure 3.4 – Electrical and thermal properties of the SMP membrane and the CB/PDMS heater. (a) Measured TCR on a SMP membrane with CB/PDMS electrode strip of 1 cm x 4 cm. The normalized resistance corresponds to the measured resistance value divided by the initial resistance value at $30\,°C$. (b) Measured heat capacity of the SMP membrane. The glass transition temperature measured with the DSC agrees with the one obtained with the DMA.

### 3.3.3 Membrane and heater thickness optimization

The material characterization enabled me to build a *COMSOL Multiphysics* FEA model of one actuator in order to optimize its geometry. An interpolation curve of the measured Young's modulus as a function of temperature is used as an input parameter for the FEA simulations. As reported in Figure 3.5, the FEA simulations match the experiment extremely well in terms of force as a function of displacement in the cold state ($20\,°C$) and displacement as a function of applied pressure in the hot state ($80\,°C$) for actuator diameters ranging from 2 mm to 10 mm. A non-linear hyperelastic Neo-Hookean model was implemented in *COMSOL Multiphysics* to account for large mechanical deformations. The FEA models were validated using experimental measurement performed in a highly controlled environment: in an oven with an external pressure supply for the displacement versus applied pressure measurement and with a precision motorized stage setup for the force versus displacement measurement, respectively. In

practice, the thermal heat distribution over the heater is not perfectly homogeneous and the pressure supplied by portable pumps can fluctuate, resulting in slightly smaller displacements. Nonetheless, my models provide a good estimation of the actuator performance.
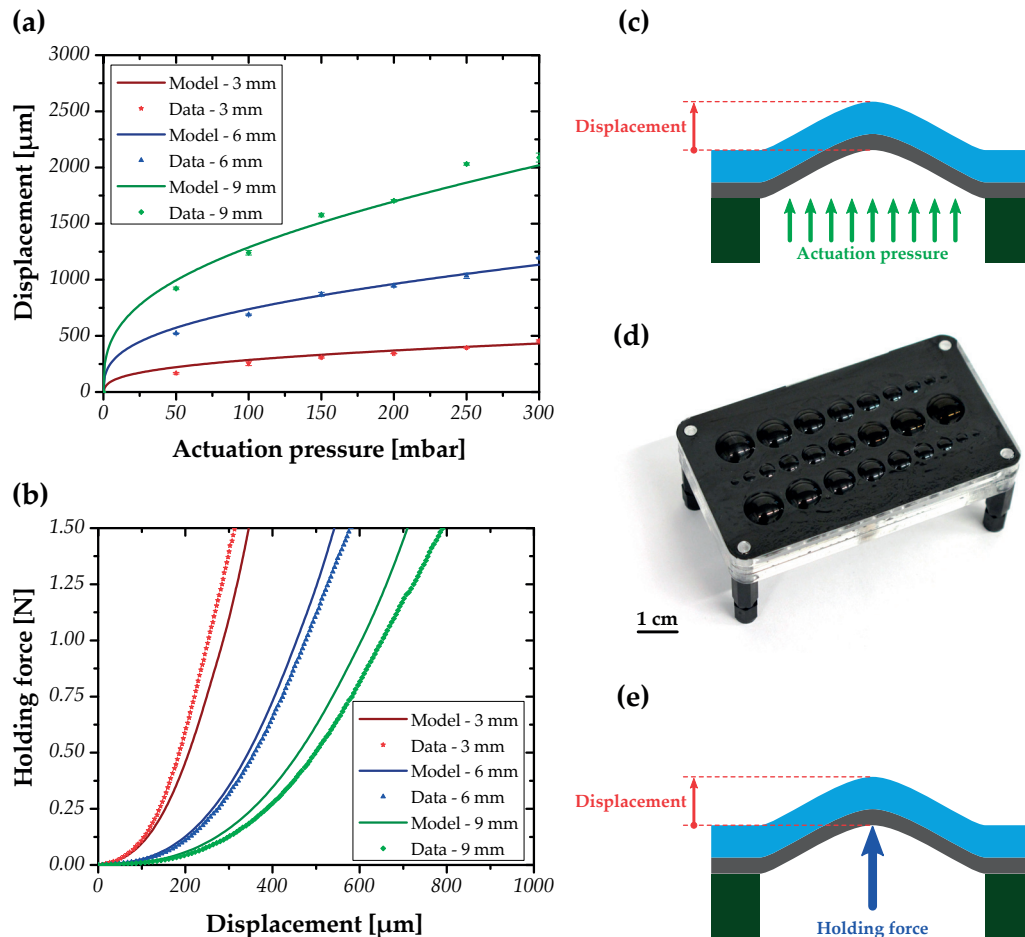


Figure 3.5 – Simulated and measured displacements and holding forces for SMP actuators with diameters ranging from 3 mm to 9 mm, showing excellent agreement between model and measured data. (a) Vertical displacement versus applied positive pressure at 80 °C. (b) Holding force versus displacement at 20 °C, starting from a flat state. (c) Schematic illustration of the measured vertical displacement versus applied positive pressure at 80 °C. (d) Picture of the device used to compare different SMP actuator diameters, with 3 actuators of each size (ranging from 2 mm to 10 mm diameter). In this picture, all taxels are latched in the up state. (e) Schematic illustration of the measured holding force versus displacement at 20 °C, starting from a flat state.

For the haptic displays, a pitch of 4 mm was chosen, because it is smaller than a fingerprint, it is close to be the Braille standard of 2.54 mm, and it already permits for high resolution in graphical information. The actuator performance is then maximized by designing circular taxels of 3 mm in diameter; a size and shape which avoids stress concentration at the anchor and allows for space to electrically plus mechanically bond the densely packed array. Dis-

placements over 300 µm and holding forces over 100 mN were proven to be perceivable by end-users [18]. Hence, the SMP membrane thickness was set to 40 µm, a good compromise between force and displacement for a 3 mm diameter actuator as shown in Figure 3.6. The FEA simulations predict 400 µm displacement when 300 mbar is applied at 70 °C and forces over 1 N to move an initially flat membrane down by more than 400 µm at room temperature. Determining the optimal membrane thickness is not trivial since the taxel should present both sufficient stroke and force to be perceived. On the one hand, the thinner the membrane, the larger the displacement and the lower the holding force. On the other hand, the thicker the membrane, the smallest the displacement and the higher the holding force. The thickness of the CB/PDMS compliant heater was chosen to be 25 µm in order to have a resistance value between 1 kΩ and 2 kΩ. This ensures that less than 24 V are needed to generate the 200 mW to 300 mW required to heat, according to FEA simulations, the taxel from 20 °C to 80 °C in 1.25 s.
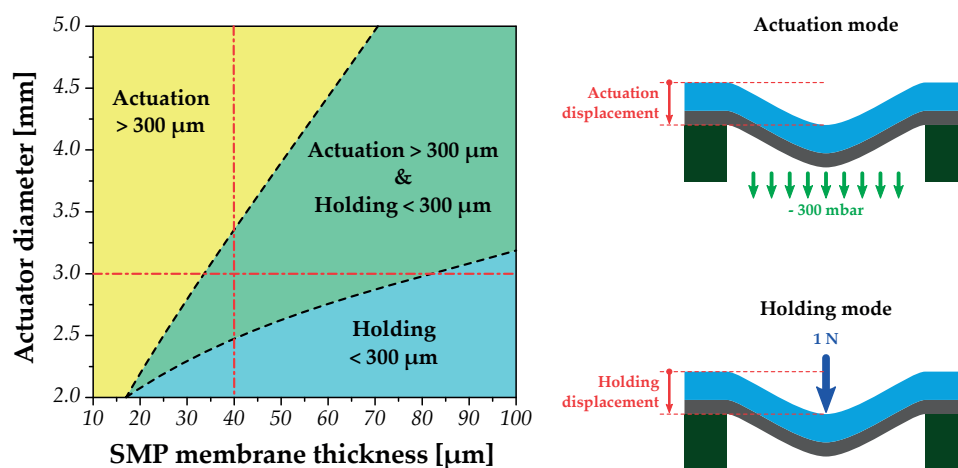


Figure 3.6 – Actuator thickness and diameter optimization to meet the requirements in terms of force and displacement for a 3 mm in diameter actuator. The SMP membrane thickness was set to 40 µm, a good compromise enabling to move down by more than 300 µm when −300 mbar of air pressure is applied and to hold more than 1 N. The green area represents the targeted design, the yellow area the acceptable one for actuation, and the blue area the acceptable one for holding. The yellow zone presents enough displacement, but a force lower than the requirement, whereas the reverse is true for the blue zone.

For the microfludic platform, the same actuator size and heater thickness is used. The SEBS membrane protecting the SMP actuator from the fluid is 37.5 µm thick with a Young's modulus of 1.5 MPa. The valves in the microfluidic chip were manufactured by Robert Jan Boom and Bas-Jan Hoogenberg (Micronit Microtechnologies, Netherlands) with depth smaller than 300 µm to ensure that the shallowest one could be closed using 300 mbar of air pressure. Further optimization can be performed to tailor the valve behavior to the application, by either increasing the SMP membrane thickness to enhance the holding force or decreasing it to speed up the heating + cooling rate plus reduce the power consumption. The 4x4 microfluidic platform is actually mainly a proof-of-concept device, validating the high versatility of my

concept and allowing to quickly test plus compare several valve designs. In the future, the plan is to incorporate these SMP latching valves in a color mixer with 16 latching SMP valves.

### 3.3.4 Heater geometry optimization

Thermal simulations using *COMSOL Multiphysics* were used to define the optimal heater geometry, which is the *4-pads* circular electrode with both opposite pads short-circuited together reported in Figure 3.7. This design was selected because it is the most efficient heater capable to provide an homogeneous heat distribution over the 3 mm in diameter actuator with an acceptable heating voltage. Two envisioned alternatives (the *spiral* and *butterfly* designs) are shown in Figure 3.7, with their heat distribution compared to the optimal *4-pads* heater design. Two cases have been investigated: with and without a metal heat sink atop the array of SMP actuators. The aluminum heat sink enables to keep the background at room temperature, but more power is consumed to reach the same peak temperature. The FEA simulations results to reach 80 °C in 1.25 s at the actuator center are summarized in Table 3.2. Despite their overall lower power consumption, both *spiral* and *butterfly* alternatives present the disadvantage of heating less the borders than the selected *4-pads* heater design, a key criteria to obtain large displacements. Indeed, most of the displacement is triggered by the actuator motion close to the anchor. Moreover, due to a high resistance, the *spiral* heater requires voltages close to 100 V, a value incompatible with standard electronics. In the FEA simulations, the convection parameter was set to $10 \, \text{W}/(\text{m}^2 \, \text{K})$ and the thermal conductivity of the CB/PDMS electrode was estimated to be 5 W/(m K). This last value was obtained by comparing experimental images with simulations and validated by correlating electrical conductivity with thermal conductivity for carbon-silicone (CB/PDMS) composites reported by [83] and [84], respectively. Since the studied system seems to be dominated more by conduction than by convection, the higher the heater thermal conductivity, the faster and the more efficient the heating.

Table 3.2 – Summary table of the simulated resistance, voltage, and power results for the *4-pads, spiral,* and *butterfly* heater design to reach 80 °C in 1.25 s at the actuator center. Two cases are evaluated: with and without a metal heat sink atop the SMP actuator. Despite its higher power consumption, the *4-pads* heater design was selected for its lower resistance and for its higher plus more homogeneous heat distribution at the anchor, a key criteria to obtain large displacements.

| | Without the metal heat sink | | | With the metal heat sink | | |
| --- | --- | --- | --- | --- | --- | --- |
| | 4-pads heater | Spiral heater | Butterfly heater | 4-pads heater | Spiral heater | Butterfly heater |
| Resistance [kΩ] | 1.24 | 122 | 1.90 | 1.24 | 122 | 1.90 |
| Voltage [V] | 15.6 | 97 | 15.5 | 17.8 | 100 | 16.8 |
| Power [mW] | 196 | 77 | 126 | 256 | 82 | 149 |

**(a)**



**(b)**
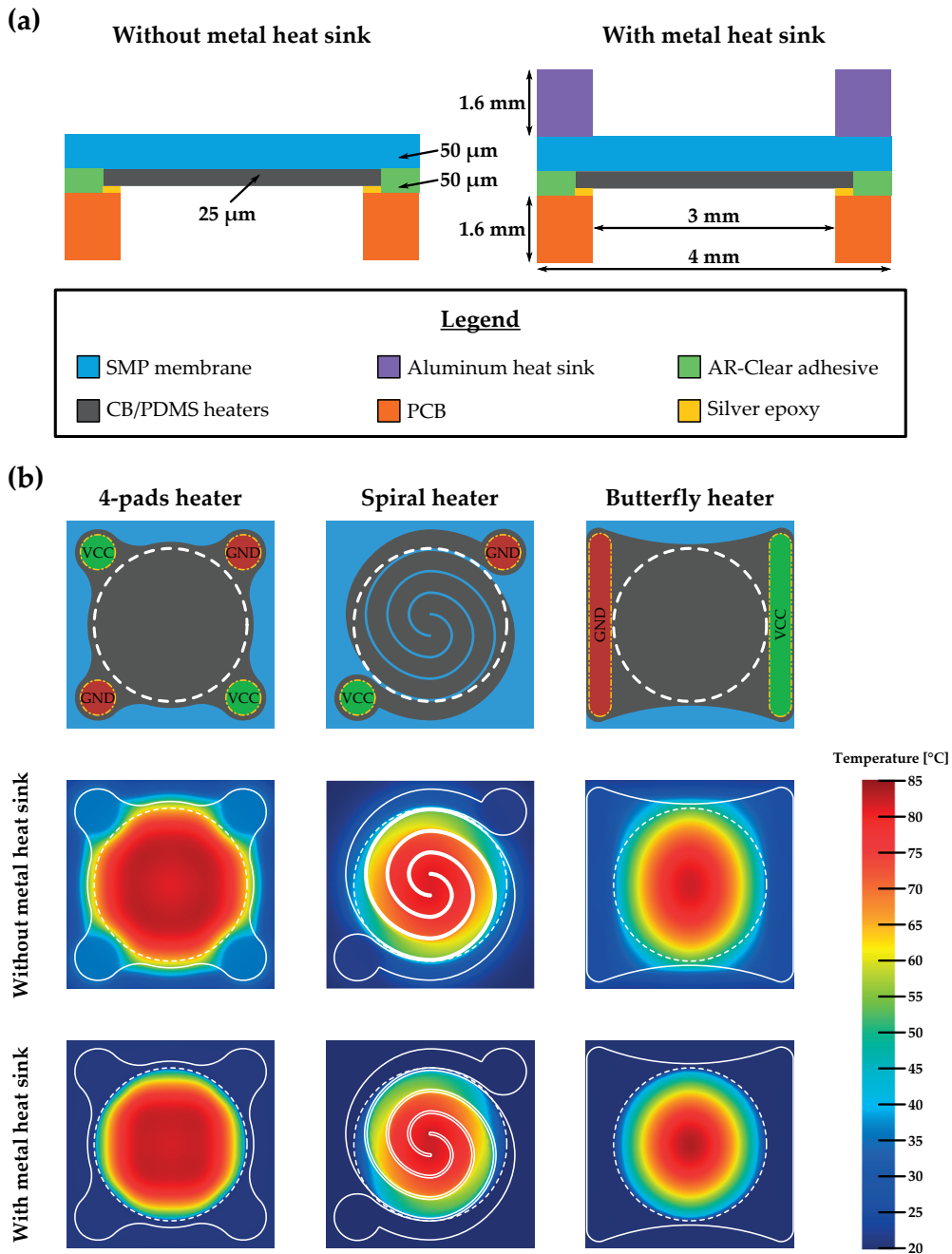


Figure 3.7 – Heater design comparison using *COMSOL Multiphysics* FEA simulations. (a) Simulated dimensions and materials. (b) FEA simulation results comparing the *4-pads*, the *spiral*, and the *butterfly* heater designs. The *4-pads* heater design was selected as the optimal electrode geometry because its heat distribution is more homogeneous over the SMP actuator than the *spiral* and the *butterfly* heater designs. For each simulation, the temperature of 80 °C at the actuator center is reached in 1.25 s.

Additional FEA simulations have been performed to estimate the heating and cooling time constants of the SMP actuator. The results for the *4-pads* heater are shown in Figure 3.8. For the heating phase, a constant voltage is applied during 2.5 s. For the cooling phase, the last result of the heating phase is taken as input and no voltage is applied to passively cool the device for 7.5 s to observe the complete cooling. Since some actuator have to move up and some down during the actuation cycle, 5 s is actually the maximum heating+cooling time to have a total refresh time faster than 10 s for the entire array. It can either be equally shared between the heating and cooling phases or the heating phase can be shorten by applying a higher voltage to allow for a longer cooling phase, while ensuring an homogeneous heat distribution during the heating phase.

**(a)**

**(b)**
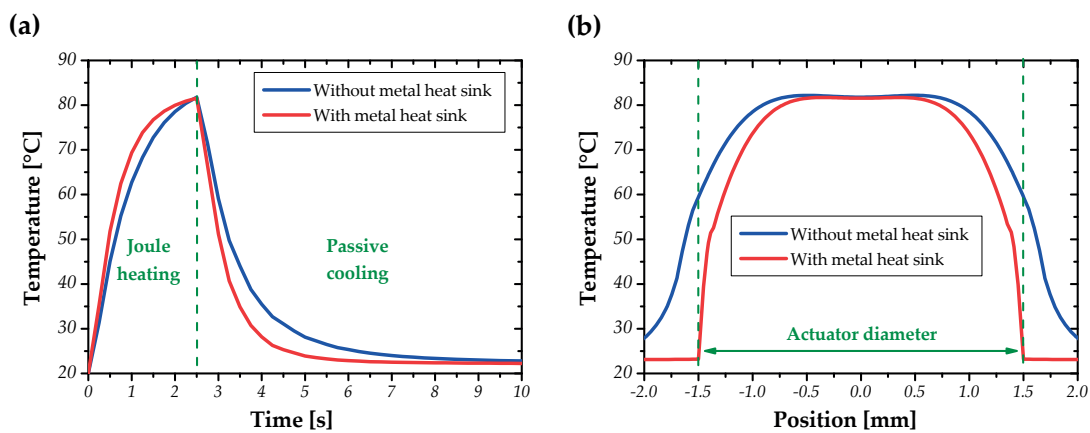


Figure 3.8 – Heating and cooling time constants of the SMP actuator with and without the metal heat sink. (a) FEA simulations with a Joule heating of 2.5 s followed by a passive cooling of 7.5 s. With the metal heat sink, the time necessary to go back to room temperature is roughly 2.5 s and without it roughly 5 s. (b) FEA simulations of the heat distribution over the SMP actuator. With the metal heat sink, the background remains at room temperature and hence the temperature close to the anchor is lower.

## 3.4 Fabrication and assembly processes

In this section, I present the fabrication and assembly processes developed during my thesis. I first detail the final optimized process to manufacture the large array of SMP actuators. I then discuss the most challenging steps, in particular the laser engraving and the alignment parts.

### 3.4.1 Final optimized process

The complete fabrication of the active layer for the haptic displays is schematically illustrated in Figure 3.9. *MM4520* SMP pellets from *SMP Technologies* [46] are first dissolved in DMF at a weight ratio of 1:5 and then mixed overnight at 80 °C with a magnetic stirrer. Each layer is fabricated by blade-casting using a *Zehntner ZUA2000* variable gap applicator and a *Zehntner ZAA2300* film applicator coater [62], with the heater geometry defined by laser ablation using a *Trotec Speedy 300* [61]. Each casting step is preceded by an oxygen plasma exposure to activate the surface of the substrate. First, a thin sacrificial *Teflon AF* layer (<100 nm thick) from *Chemours Company* [85] is coated on the polyethylene terephthalate (PET) sheet to ease the active layer release. Next, the SMP+DMF solution is blade-casted on the PET sheet with the *Teflon AF* sacrificial layer. The SMP membrane is then cured for 2 h at 80 °C on a hotplate. The same process is used to blade-cast the CB/PDMS electrode directly on the SMP membrane. The carbon-silicone composite is a mixture of *Ketjenblack EC-600JD* from *Akzo Nobel* [86] and *Silbione 4305* from *Bluestar Silicone* [87] at a weight ratio of 1:10 [62]. The CB/PDMS electrode is cured for 4 h at 80 °C in an oven. The final layer thickness depends on the applicator gap and the material-to-solvent ratio. For my thesis, 40 µm to 50 µm for the SMP membrane and 25 µm for the CB/PDMS electrode are targeted. Finally, the heater pattern is defined via laser ablation [61]. For the active layer of the microfluidic platform, a thin SEBS layer composed of *Dryflex 500040* from *Hexpol TPE* [88] is casted on the *Teflon AF* layer prior to cast the SMP membrane. The subsequent steps described above are then unchanged.



**1)** A4-size PET sheet  **2)** Cast the Teflon sacrificial layer  **3)** Cast the SMP membrane

**6)** Release the active layer  **5)** Laser ablate the heaters  **4)** Cast the CB+PDMS electrode
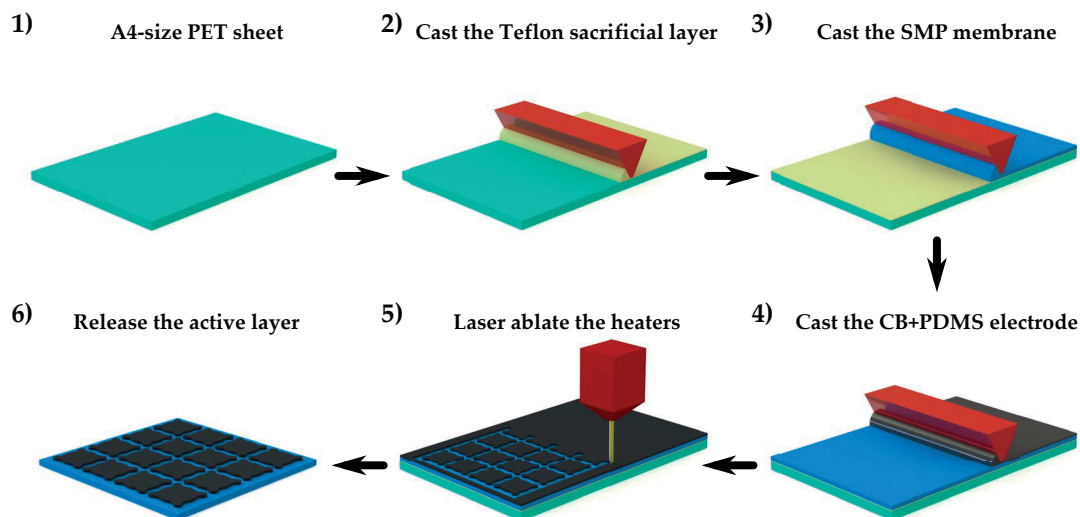
Figure 3.9 – Schematic illustration of the fabrication process of the active layer. On an A4-size PET sheet, the *Teflon AF* sacrificial layer, the SMP membrane, and the CB/PDMS electrodes are successively blade-casted. Between each step, the solvent is evaporated and prior each casting the surface is treated by oxygen plasma. Next, the heaters are patterned using laser ablation. Finally, the active layer is released form the PET sheet.

The assembly sequence is schematically illustrated in Figure 3.10, with the three main layers composing the device highlighted. The active layer is first mechanically and electrically bonded plus aligned to the 4-layers PCB using an *AR-Clear 8932EE* adhesive foil from *Adhesives Research* [89]. Vias are pre-patterned in this foil and filled by stencil lithography with *ECCOBOND CE3103WLV* silver epoxy from *Henkel* [90] to robustly interconnect the heaters to the PCB. Four alignment marks, one at each corner of the active layer and of the PCB, allow for precise and accurate alignment using portable universal serial bus (USB) microscopes. A high precision motorized x-y-z stage coupled with vacuum was used to ensure a successful assembly. This step is crucial as 100 μm transversal and 1° rotational misalignments lead to heater short-circuits and hence non-functional actuators. Both the active layer and the PCB are then sealed to the pneumatic chamber using a 500 μm thick *VHB 4905* adhesive from *3M* [91].
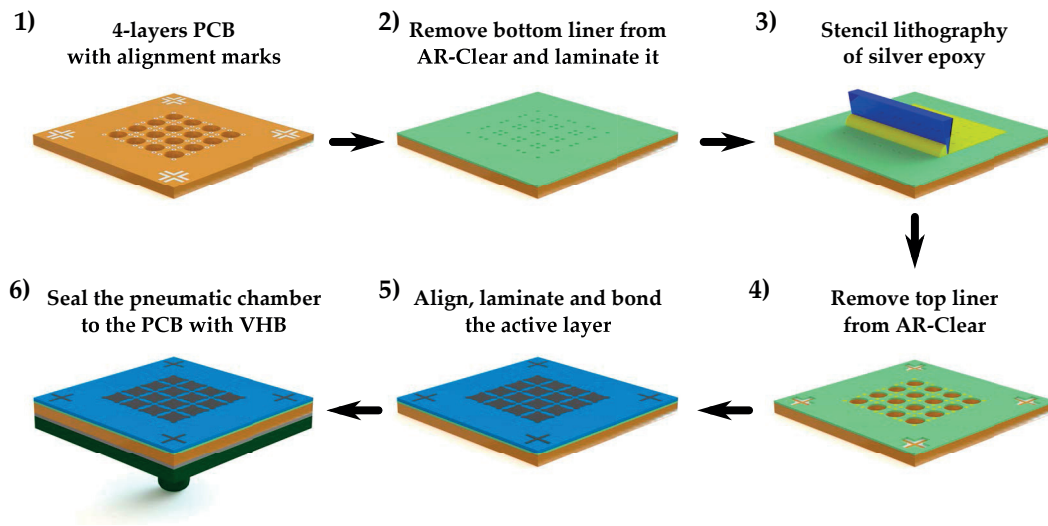


Figure 3.10 – Schematic illustration of the assembly process to first bond the active layer to the 4-layers PCB and then seal both to the pneumatic chamber. The *AR-Clear* foil is used as both adhesive and mask for the stencil lithography step.

Pictures of the 32x24 flexible haptic display before and after its assembly are reported in Figure 3.11, with an emphasis on the three main layers which are the active layer, the flexible PCB, and the pneumatic chamber. This optimized fabrication and assembly process enabled me to obtain an actuator fabrication yield of 99 % and only 10 % variation in heater resistance over the array.
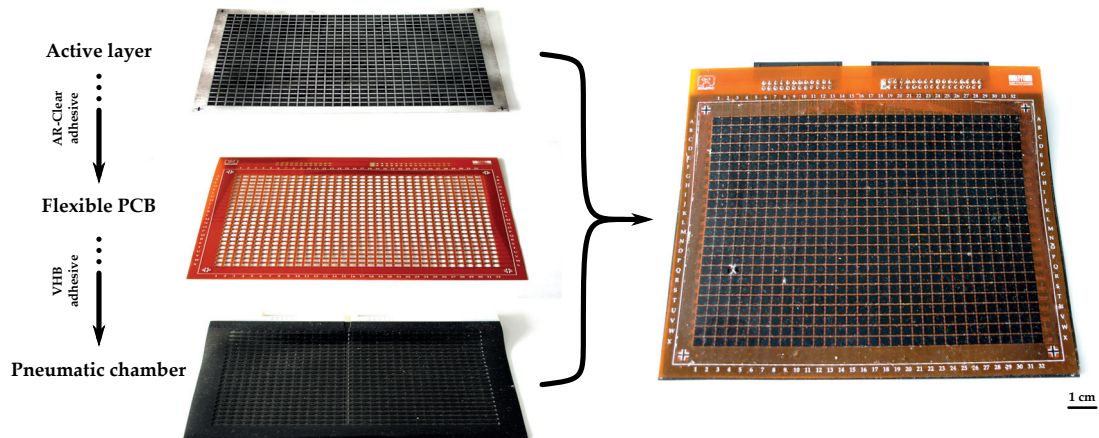
Figure 3.11 – On the left, picture of the three main layers illustrating the assembly procedure of the 32x24 flexible haptic display. On the right, picture of the assembled device with 99 % of the 768 actuators fully functional.

### 3.4.2 Challenging steps

Two main steps remain critical when assembling large arrays because they can lead to non-functional devices: the laser ablation to define the heater pattern and the final alignment between the PCB and the active layer.

The engraving step necessitate to keep the laser in focus within few microns over a large surface to obtain an adequate result similar to the one in Figure 3.12a. As reported in Figure 3.12b for an extreme case, when the laser is out-of-focus, the active layer can be either over-engraved leading to holes and air-leaks in the thin SMP membrane or under-engraved resulting in short-circuits between the neighboring heaters. This step is very sensitive to the cleanliness of the laser lens, to the flatness of the laser plateau, and to the vacuum obtained when sucking the active layer. The tendency is to slightly over-engrave the active layer to ensure no short-circuits by multiplying the number of passes at low engraving power. To solve this problem now that the heater design is optimized, the best option is to replace this laser ablation step by a commonly used printing technique like screen, flexure, or gravure printing. Actually, laser ablation is convenient to quickly test and compare heater designs, but not suited for production since it can damage the membrane underneath. In my thesis, the moving part of each SMP actuator is unaffected by the engraving, which hence prevents from performance degradation.

**(a)**                                    <u>Good engraving</u>
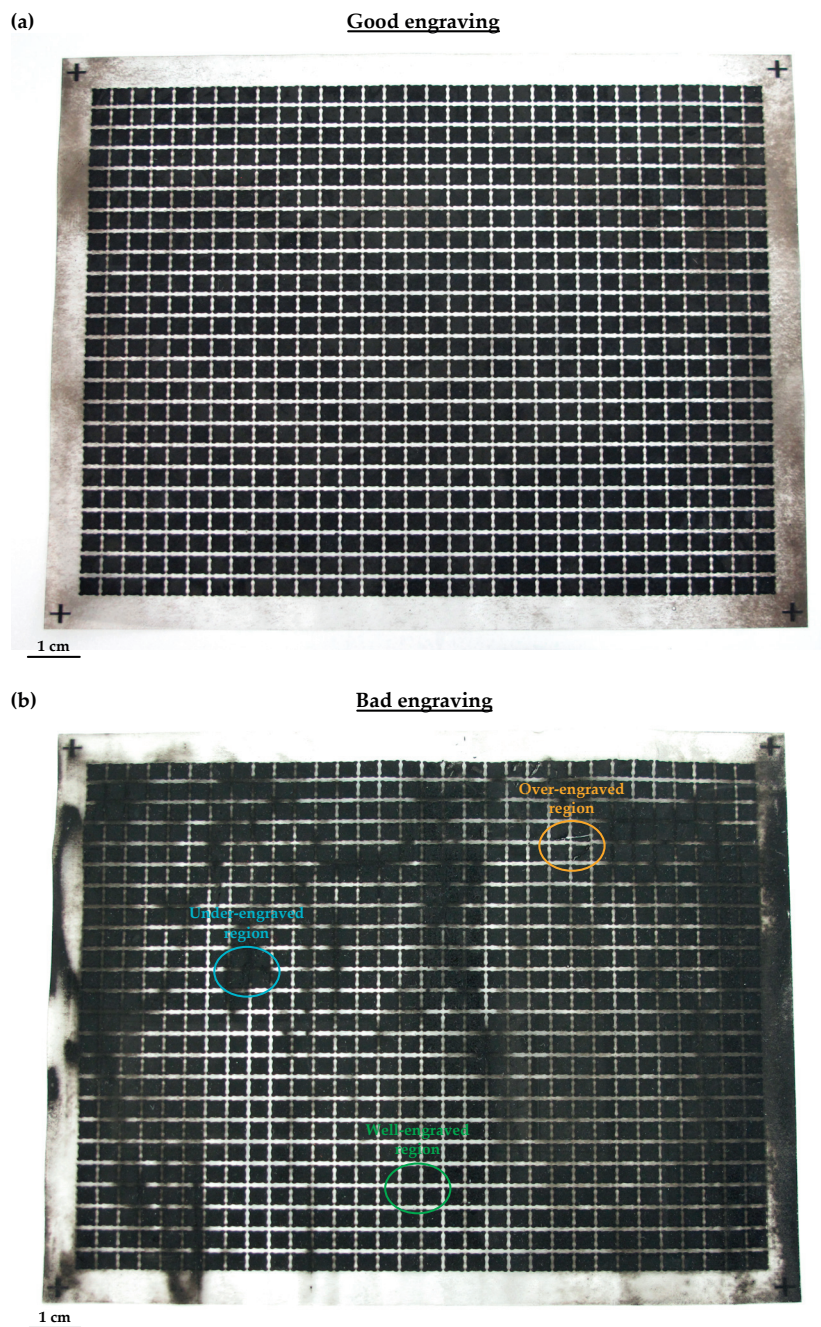


**(b)**                                    <u>Bad engraving</u>



Figure 3.12 – Pictures of the active layer after the engraving step for: (a) a successful laser ablation process and (b) a missed laser ablation process. The inhomogeneous engraving is due to the poor flatness of the active layer during the laser ablation step.

The dedicated alignment rig shown in Figure 3.13 was developed, combining a high precision motorized x-y-z stage with more than 100 µm precision coupled with vacuum to suck the active layer and with manual rotation of the PCB with roughly 1° precision. While assembling, two portable USB microscopes enable to see the alignment marks on the active layer and the PCB, respectively. Figure 3.14 compares a functional and a non-functional device, showing that 100 µm transversal and 1° rotational misalignments can lead to heater short-circuits and hence non-functional actuators.
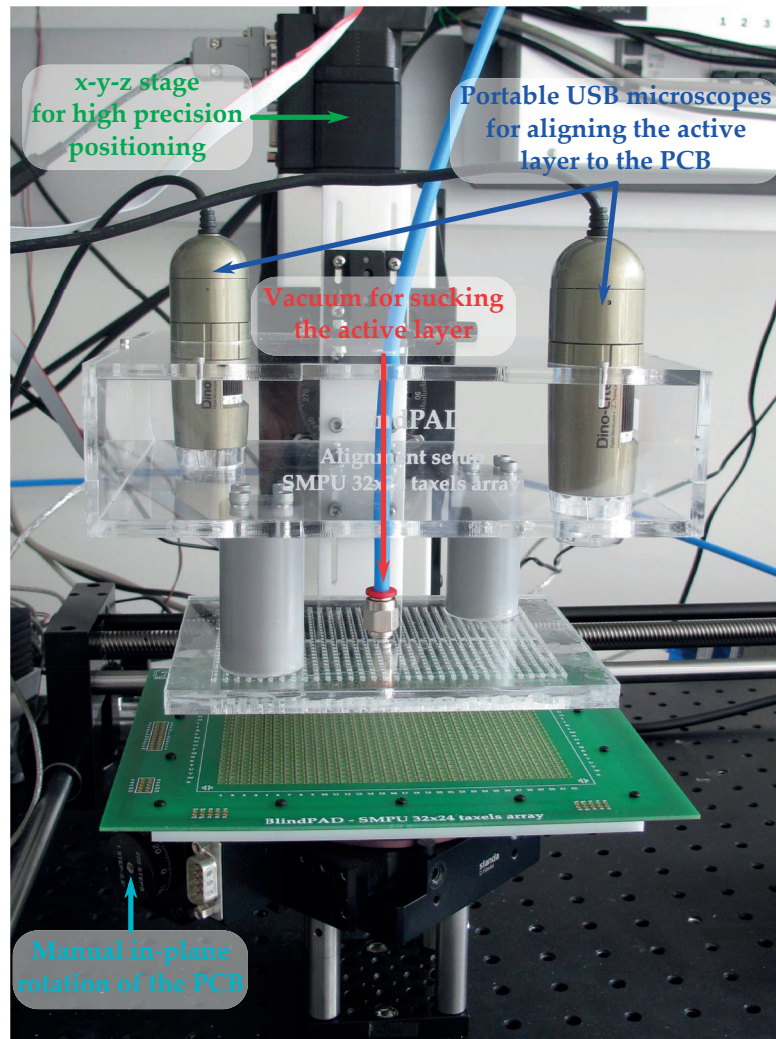


Figure 3.13 – Picture of the alignment rig consisting in a high precision motorized x-y-z stage with more than 100 µm precision coupled with vacuum to suck the active layer and with manual rotation of the PCB with roughly 1° precision.
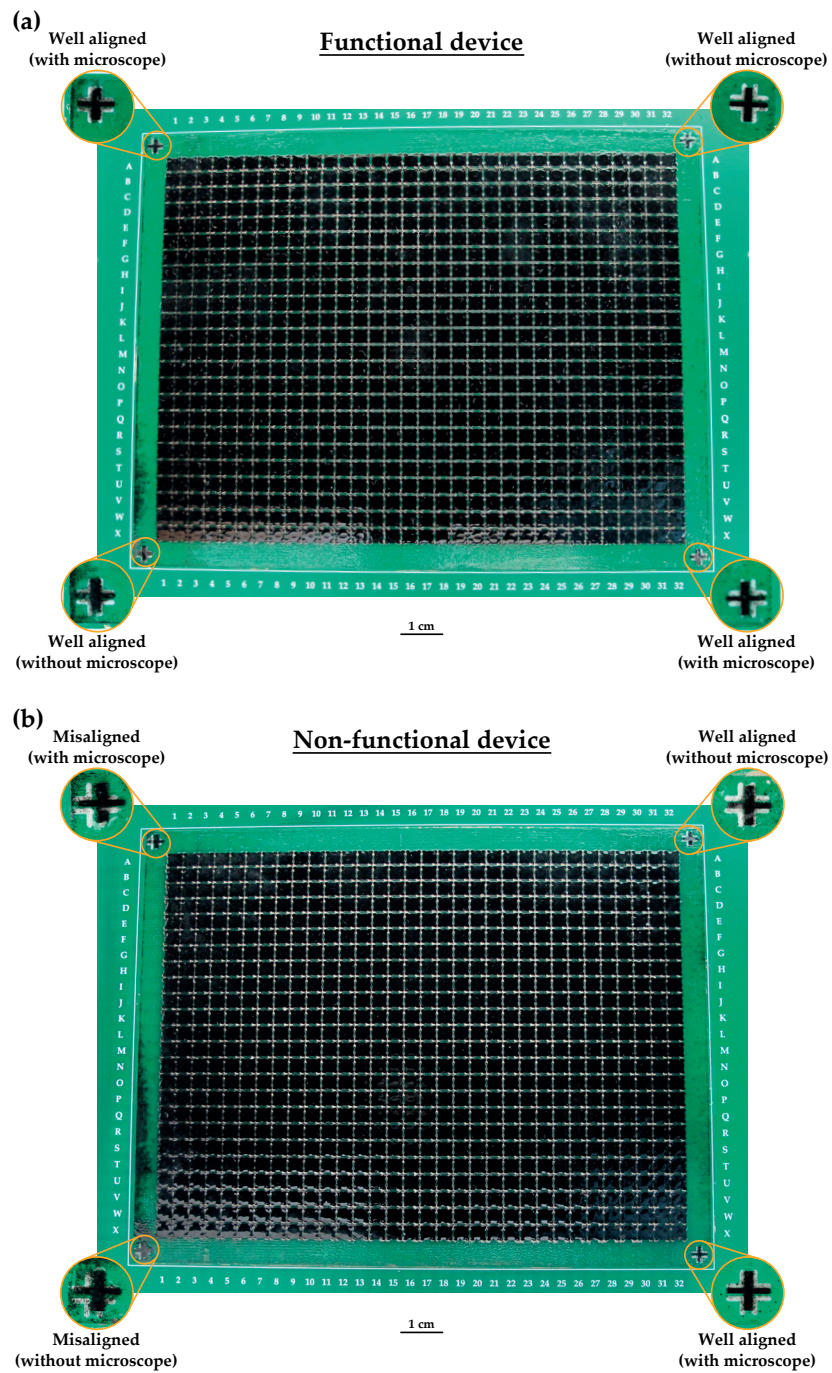
Figure 3.14 – Pictures of the device after the alignment step for: (a) a functional device and (b) a non-functional device. A tiny transversal plus rotational misalignment results in short-circuited neighboring heaters.

## 3.5   Conclusion

In this chapter, I introduced my concept to selectively reconfigure large arrays of SMP actuators, I discussed the actuator optimization phase, and I described the fabrication plus assembly processes. I first explained the operating principle consisting of a timely synchronization of the local Joule heating with the global pneumatic air supply. Benefiting from the large stiffness change with temperature of SMPs, the pneumatic air supply triggers motion of only the Joule heated actuators. Any arbitrary array configuration can be obtained, since each actuator position depends only on the air pressure applied during its reshaping phase. I then detailed the actuator design steps to reach the targeted requirements for haptic displays and microfluidic platforms. Experimentally validated FEA simulations were used to optimize each parameter. The selected SMP actuator geometry, dimension and thickness are reported in Figure 3.15. I finally summarized the fabrication processes and assembly tools specifically developed during my thesis, which had to be large scale compatible and to present high actuator yield with good performance reproducibility.
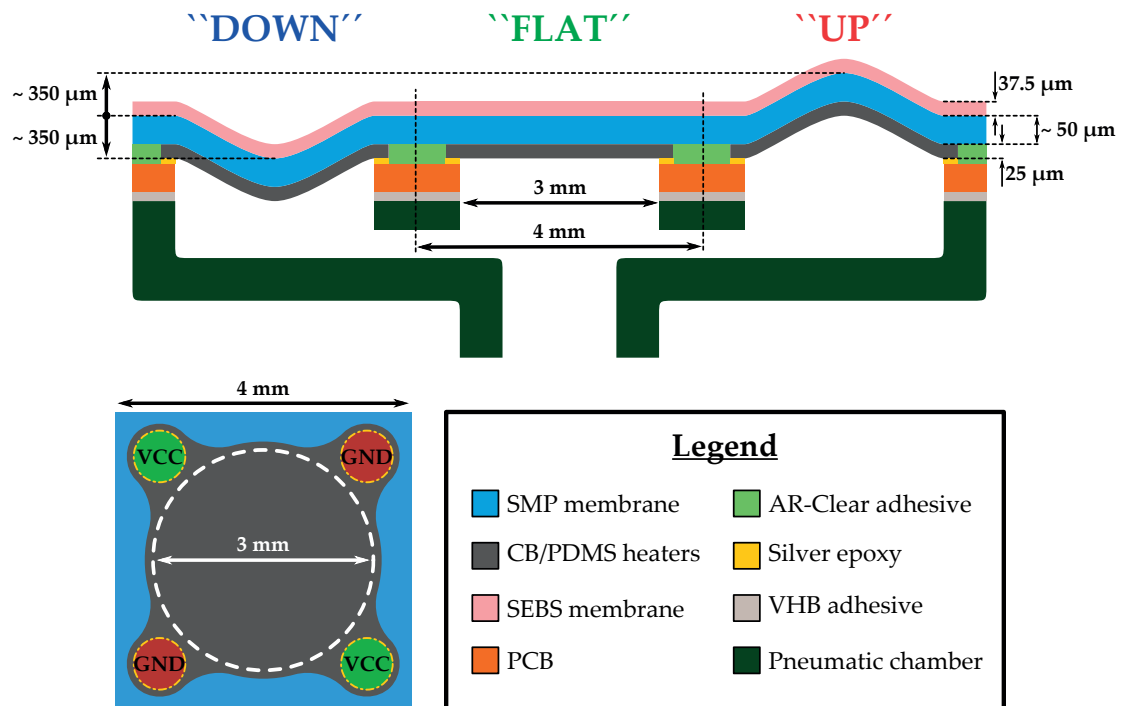


Figure 3.15 – On the same figure than Figure 3.1, the selected SMP actuator geometry, dimension, and thickness are reported. On the top, schematic illustration of the device highlighting the thickness of the main layers composing the array of SMP actuators and the actuator size plus pitch. Any arbitrary *down*, *flat*, or *up* positions can be obtained, with the typical displacement reported. On the bottom-left, schematic illustration of the heater geometry showing the electrical connection and the actuator dimensions.

# 4 Haptic displays using arrays of SMP actuators as taxels

## 4.1 Summary

In this chapter, I demonstrate that arrays of SMP actuators are a suitable taxel technology for haptic displays. I first present a selection of state-of-the-art high resolution haptic displays. I then detail the design and operating principle of my devices. I follow with an analysis on the actuator performance in terms of displacement, force, and lifetime. I finally validate my approach by describing the perception tests conducted with sighted, blind, and visually impaired people. My concept is highly scalable as demonstrated by the array size evolution shown in Figure 4.1, corresponding to the progress of my thesis from a 2x2 rigid tactile tablet on a 8 mm pitch to a 32x24 flexible haptic display on a 4 mm pitch. Throughout the process, the core of the technology remained unchanged, with significant improvements on the actuator performance, on the fabrication plus assembly steps, and on the understanding of the physics involved.

The results presented in this chapter are part of two manuscripts, specifically the SMP actuator performance has been described in *Advanced Materials Technologies* [78] and the perception tests have been reported in *Transactions on Haptics* [92]. The 32x24 flexible haptic display has been fabricated and assembled with the help of my colleagues Juan José Zárate, Olexandr Gudozhnik, and Samuel Rosset (EPFL-LMTS, Switzerland). Perception tests on the 4x4 rigid tactile tablet were performed in collaboration with Elisabetta Ferrari and Luca Brayda (IIT-RBCS, Italy). Tamás Csielka and László Jakab (Ateknea Solutions, Hungary) provided me with the electronic drivers for the 4x4 rigid tactile tablet. Claudio Lorini, Giorgio Zini, Franco Bertora, and Diego Torazza (IIT-RBCS, Italy) developed the electronic drivers plus the pin interface for the 32x24 rigid tactile tablet. Jochen Meis and Henning Kettler (GeoMobile, Germany) created the software for both rigid tactile tablets. The 4x4 rigid tactile tablet was demonstrated operating for several hours at both the *SPIE-EAPAD 2016 Conference* and the *Haptics Symposium 2016 Conference*, with a finalist award at the latter one.

**Rigid 2x2**

**Rigid 4x4**

**Rigid 32x24**
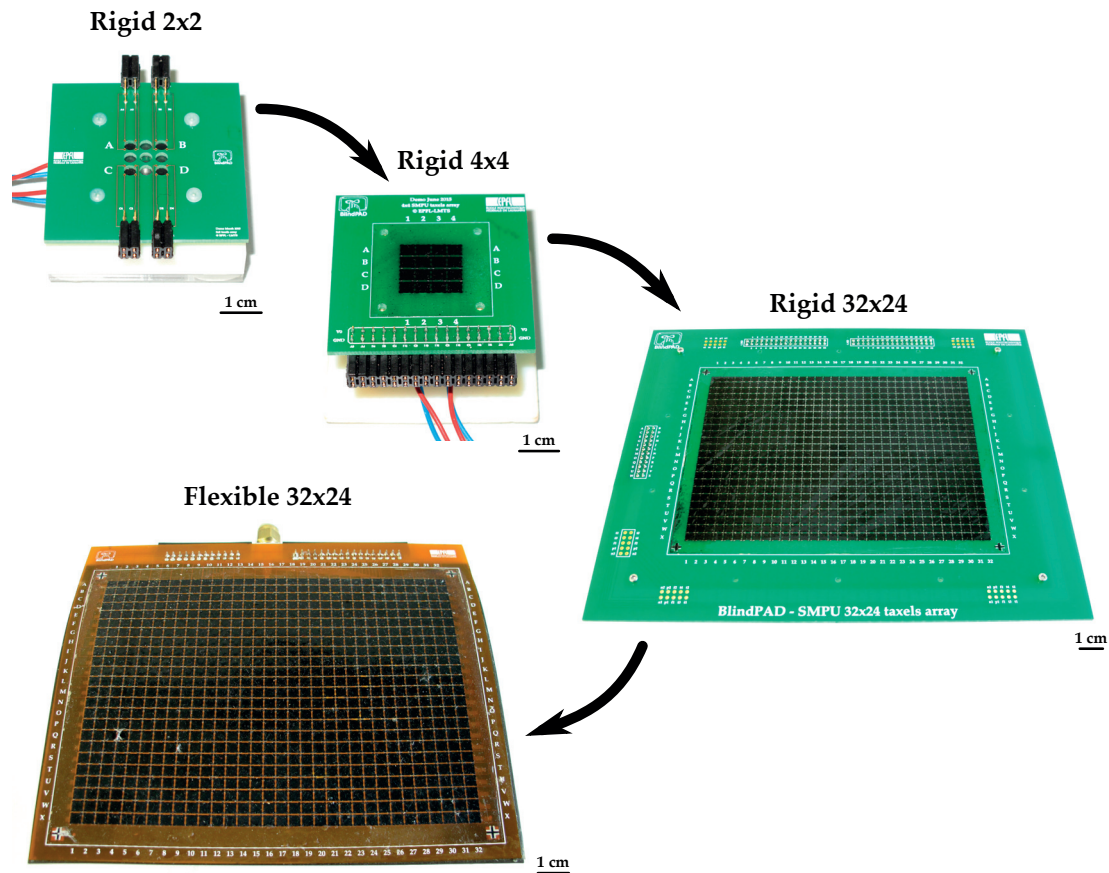
**Flexible 32x24**

Figure 4.1 – Pictures of the SMP haptic displays I have developed within my thesis from a 2x2 rigid tactile tablet on a 8 mm pitch to a 32x24 flexible haptic display on a 4 mm pitch.

## 4.2 Introduction to haptic displays

Coupling haptic feedback with visual and auditory information on displays could remarkably improve the user experience because it would enrich the interaction among people, machine, and data. The sense of touch is extremely developed in humans, yet surprisingly underexploited due to the demanding force, displacement, and resolution requirements. Indeed, while conveying visual information with high spatio-temporal resolution is now widely commercially available, only few techniques have been reported to render haptic feedback with good fidelity by reconfiguring the display shape and surface structure. The Tangible Media Group from the Massachusetts Institute of Technology (MIT, USA) developed a true 30x30 3D haptic display of $0.15\,\mathrm{m}^2$, but it requires approximately $1\,\mathrm{m}^3$ of actuators and linkages under the table to operate [93]. The only commercially available high resolution Braille tablet is the *HyperBraille* from *Metec* [94], a device based on bimorph piezoelectric bending actuators which costs 10 000 to 50 000 dollars. Attempts to develop more cost-effective taxel technologies have been reviewed in [17]; yet remaining a major challenge to assemble them in a simple, low-cost, large-scale, densely packed, pleasant to touch, reliable, and robust architecture.

The most relevant high resolution haptic displays are presented in Figure 4.2. Piezoelectric solutions [95–97] are particularly attractive for their large force and low power consumption, but, due to their small displacement, they require complex manufacturing processes to be assembled in a compact form factor. Electromagnetic (EM) approaches [98–100] are mainly appealing in view of their speed, however they had never been implemented in arrays larger than 8x8 before the work of my colleague Juan José Zárate (EPFL-LMTS, Switzerland) within the *BlindPAD* project [101]. The high power consumption and strong magnet-to-magnet interactions were the major challenges for implementing them in large arrays. Moreover, the generated forces significantly weakens with scaling down the actuator sizes, limiting their scope of applications to pitches bigger than 5 mm. Pneumatic systems are commonly used in soft robotics and microfluidics, but rarely in haptics [102] because the size of the valving system required to switch each taxel makes them neither portable nor scalable. Recently, the interest in haptics shifted towards variables stiffness materials due to their intrinsic latching capabilities coupled with interesting performance in terms of force and displacement. Prototypes based on SMAs [103, 104], phase-change wax [105], and SMPs [16] have notably been reported.
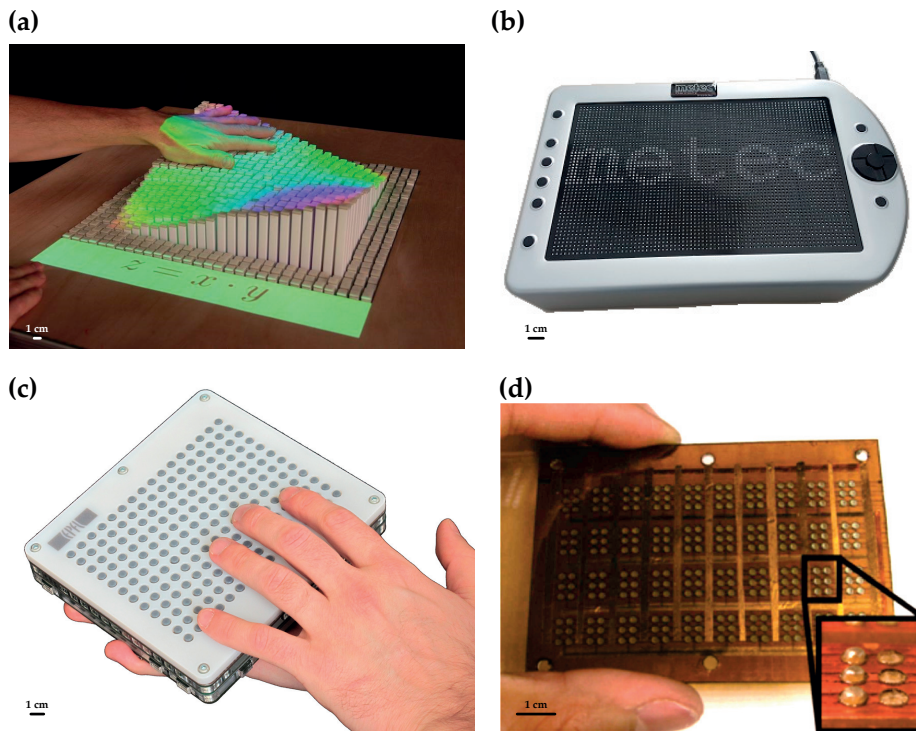


Figure 4.2 – Selected examples of high resolution haptic displays. (a) Picture of the true 30x30 3D haptic display developed by the Tangible Media Group. Each actuator is driven by servomotors (Reprinted from [93]). (b) Picture of the 76x48 *HyperBraille*, the only commercially available Braille tactile tablet. The display is based on piezoelectric bimorphs beams (Reprinted from [94]). (c) Picture of the 16x12 EM haptic display developed by my colleague Juan José Zárate within the *BlindPAD* project (Reprinted from [101]). (d) Picture of the first reported SMP haptic display with 240 actuators (Reprinted from [16]).

Making flexible and wearable haptic displays further adds to the task complexity, as soft materials generally exert only limited forces. Attempts to exploit DEAs have been proposed by staking them [15], coupling them with fluids [106], or combining them with SMPs [16]. Nonetheless, no perception tests with users have been reported and DEAs require driving voltages in the kilovolt range to switch each taxel, a solution incompatible with portable large array devices. Actually, the only soft materials enabling simultaneously high force and large displacement are SMPs thanks to their drastic change in Young's modulus.

## 4.3 Haptic displays design and operation

In this section, I detail the operating cycle of my SMP haptic displays and their overall design. In particular, I discuss the switching sequence and timing to display new symbols with an example taken from the 4x4 rigid tactile tablet used during the perception tests. The main components present in the rigid tactile tablets and the flexible haptic display are highlighted.

### 4.3.1 Operating cycle of SMP haptic displays

For all displays, the heart of my technology is a $40\,\mu m$ to $50\,\mu m$ thick SMP membrane with on top a matrix of individually addressable compliant carbon-silicone composite heaters patterned on a 4 mm pitch. This active layer is electrically and mechanically bonded to a 4-layers PCB to route the Joule heating currents, and then sealed to the 3D-printed microchanneled chamber to distribute a controlled air pressure to the membrane. Having one compliant heater per actuator on a thin SMP membrane enables independent, efficient, rapid, and reversible stiffness change of each taxel. By synchronizing the global pneumatic air supply and the local Joule heating, selective out-of-plane motion of the active layer is achieved. Each actuator starts in the as-fabricated flat state, and can then be deformed into a multitude of temporary inflated or deflated stable shapes, depending on the pressure applied during the actuation cycle. Heating is needed only to switch between stable positions and only the actuators that need to be reconfigured are heated. Heating an actuator without applying any pressure brings it back to its initial flat state. As illustrated in Figure 4.3 and shown in the online video [107] for the 4x4 rigid tactile tablet, the switching sequence to refresh any haptic display necessitate 7 steps. First, after having explored the initial pattern, the end-user removes his finger. Second, the positive pressure is applied and only the taxels that have to move up are locally heated. Third, the heating power is removed, while keeping the positive pressure turned on to latch the inflated taxels in the upward position. Fourth, the positive pressure is turned off, resulting in an intermediate pattern. Fifth, the negative pressure is turned on and the taxels that will move down are locally heated. Sixth, the heating power is switched off, while keeping the negative pressure turned on to latch the down taxels. Seventh, the negative pressure is turned off and the end-user can explore the final pattern.
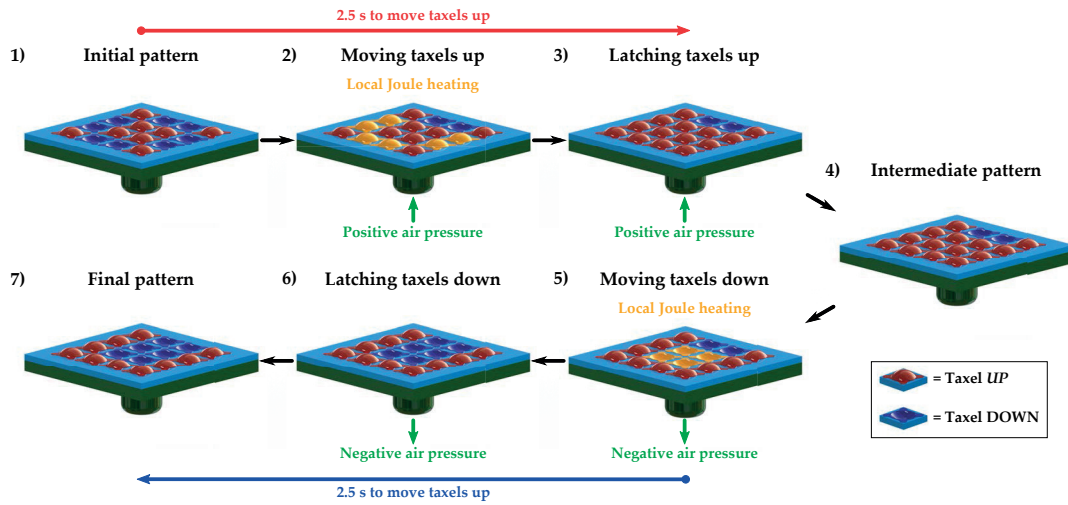
Figure 4.3 – Schematic illustration of the sequence procedure to change the displayed pattern from a X-shaped symbol to a U-shaped one. Taxels latched up are shown in red, taxels latched down are in blue, and heated taxels are in orange.

Even so only two discrete states have been implemented in my haptic displays (*down* + *up*, *flat* + *up*, or *down* + *flat*), any arbitrary pressure can be applied during this cycle. In the 4x4 rigid tactile tablet, both positive and negative pressures were used to enhance the overall displacement. Unfortunately, parasitic motion was observed on the 32x24 devices when generating both positive and negative pressures. Hence, either positive or negative was applied in the chamber, with positive motion being easier to feel on a 4 mm pitch and negative motion more robust over time. When using a pin interface, *down* + *flat* states can be easily transferred into apparent *flat* + *up* states by offsetting the interface. Indeed, the maximum negative state of the SMP becomes the flat state from the user's perspective and the flat SMP taxel corresponds to a raised pin. The 32x24 flexible haptic display operates without such an interface and the 4x4 rigid tactile tablet has a pin interface to allow for more effective haptic sensation. One actuation cycle lasts 5 s: 2.5 s for the moving phase (Joule heating + applied pressure) and 2.5 s for latching in position (pressure only + passively cooling). The time scale is given by the heating and cooling time constants of each actuator, and thus depends on taxel size and thickness. The heating and cooling time constants can easily be seen in the online videos [108, 109] where real-time thermal imaging of the line-by-line heating is shown alongside visible light imaging reporting taxel displacement.

### 4.3.2  Rigid tactile tablets design

The 4x4 rigid tactile tablet used for the perception tests is reported in Figure 4.4. This device consists of an active layer, an interface to a single common pneumatic system comprising two miniature pumps assembled back-to-back, a 4-layers PCB, an aluminum plate, and a 3D-printed pin interface. The aluminum plate and the 3D-printed pin interface are used to improve the system passive cooling and to avoid direct contact by the user fingertip with the active layer, respectively. Due to the low thermal conductivity of the pin interface, and to the distance separating the top surface from the active layer, the temperature of the interface is expected to be at room temperature.
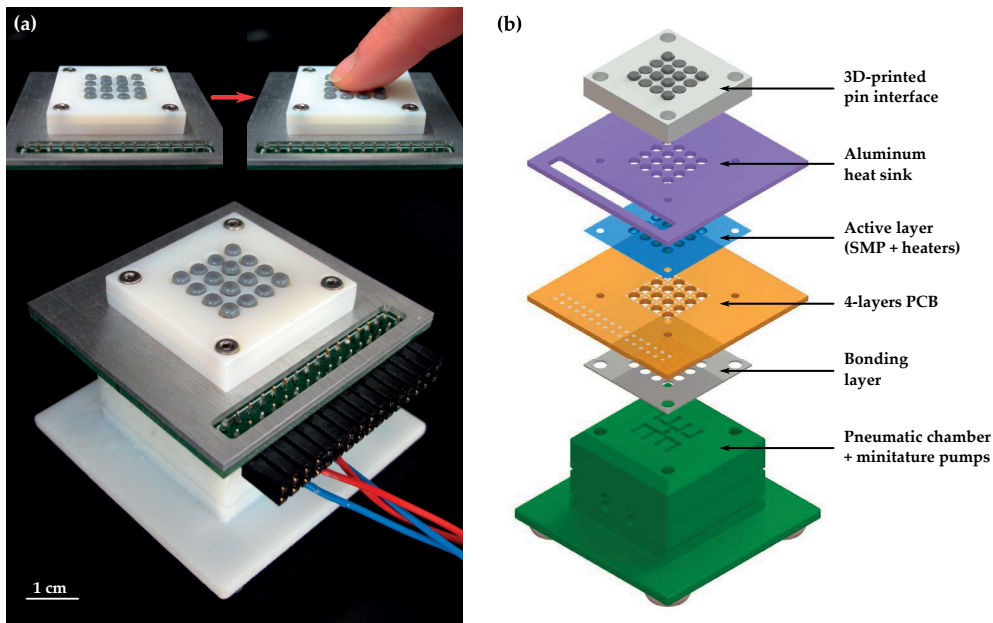


Figure 4.4 – Design of the 4x4 rigid tactile tablet. (a) Picture of the 4x4 rigid tactile tablet. The two top smaller images show how a user explores the X-shaped pattern. (b) Exploded view of the device, which consists of a pneumatic chamber with two miniature pumps assembled back-to-back, a bonding layer for sealing purposes, a 4-layers PCB to route the heating currents, an active layer comprising the SMP membrane plus the patterned CB/PDMS heaters, an aluminum plate acting as heat sink, and finally a 3D-printed pin interface.

This technology was scaled up to the 32x24 rigid tactile tablet shown in Figure 4.5. The core of the actuator technology remains the active layer, which is obtained using the same fabrication processes as for the 4x4 device.  In the 32x24 rigid tactile tablet, the pneumatic supply is external to the device, the driving electronics uses a row-column addressing scheme to reduce the number of tracks on the PCB, the pins are in metal to reduce friction with the plastic interface, and the metallic sink is in copper to speed up the heat dissipation.

Unlike with the 4x4 rigid tactile tablet, the 32x24 device has not been tested by end-users because positive and negative pressures could not be alternatively generated in the chamber due to unavoidable parasitic buckling motion on such a large area due to higher variations

in the active layer thickness (SMP membrane plus CB/PDMS heaters). Hence, by working with only one direction pressure (preferably negative pressure) only half of the displacement (~300 µm) was obtained, rendering the pattern discrimination tedious. On the one hand, without the pin interface, this 300 µm indent is hard to feel since it is smaller than a finger-print when gently scanning over a surface. On the other hand, 300 µm displacement is not sufficient to accommodate for the pin interface and PCB non-uniformity. Moreover, despite the same fabrication process for both tactile tablets, manufacturing the large scale array is more challenging because higher accuracy in alignment and homogeneity in layer thickness is required. Misalignments (in translation or rotation) and inhomogeneity (defects or irregular surfaces) generate variation in resistance and displacement values. The most critical step being the laser ablation process to define the heater design, since it necessitate to keep the laser in focus within few microns over a large surface. I have faced the issue that either the active layer was over-engraved leading to holes and air-leaks in the thin SMP membrane or it was under-engraved resulting in short-circuits between the neighboring heaters. To solve this problem now that the heater design is optimized, the best option would be to replace this laser ablation step by a commonly used printing technique like screen, flexure or gravure printing.

**(a)**



1 cm

**(b)**



1 cm
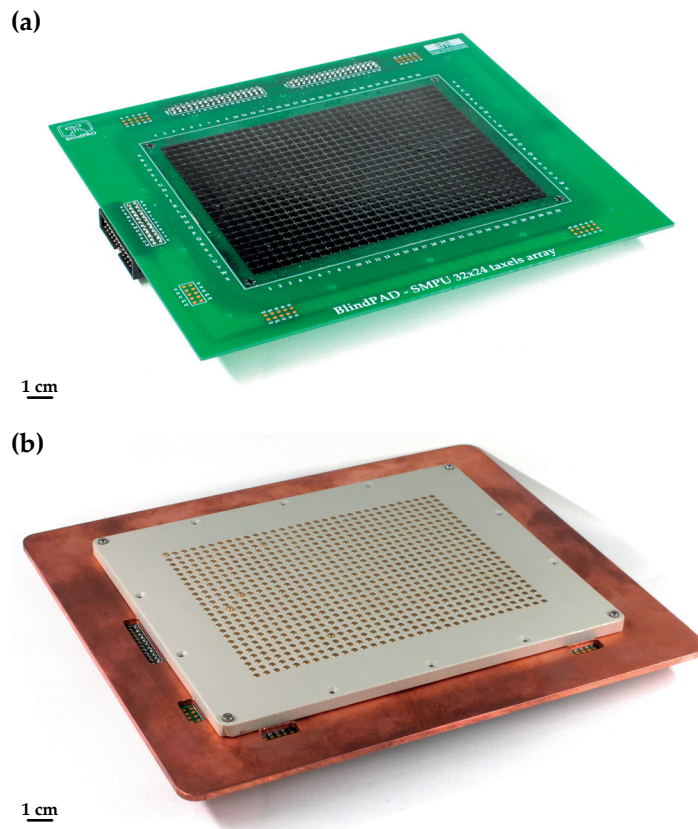
Figure 4.5 – Pictures of the 32x24 rigid tactile tablet: (a) without the copper sink and the pin interface to emphasis on the active layer, (b) complete device ready to be tested by end-users.

### 4.3.3 Flexible haptic display design

The 32x24 flexible haptic display shown in Figure 4.6 was fabricated to demonstrate the ability to locally reshape a flexible surface into any arbitrary topography using only low-voltage signals in a simple row/column architecture, since generating patterns on bended displays is an extremely challenging task. The device integrates a thin active layer, a flexible 4-layers PCB, a 3D-printed stretchable pneumatic chamber, and two adhesive layers. It weighs 55 g and its active part is only 2 mm thick. 757 of the 768 taxels are fully functional in the fabricated flexible haptic display, meaning that an actuator fabrication yield of 99 % was obtained. The heater resistance was measured to be $(0.97 \pm 0.11)$ kΩ, enabling good performance homogeneity and driving voltages lower than 24 V. This device can be worn as a haptic sleeve with immediate applications in virtual reality (VR) or augmented reality (AR) scenarios, and for novel human-machine interfaces (HMIs).
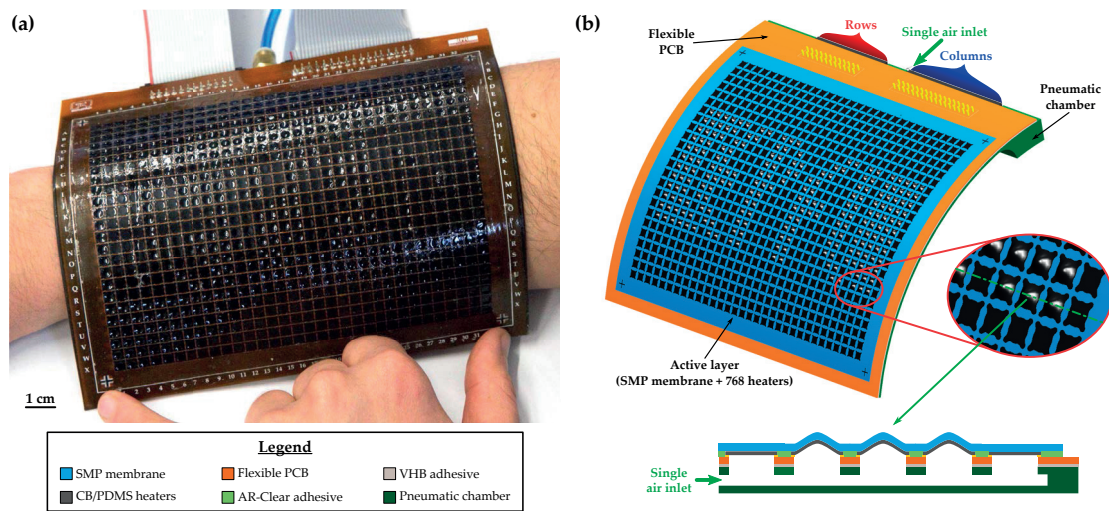


Figure 4.6 – Design of the 32x24 flexible haptic display. (a) Picture of the 32x24 flexible haptic display when worn as a sleeve. (b) Schematic illustration of the display, which main components are the pneumatic chamber, the flexible PCB, and the active layer comprising the SMP membrane plus the 768 patterned CB/PDMS heaters.

## 4.4 Technology validation for haptic displays

In this section, I present the results on actuator performance and perception tests. Several high resolution patterns are reported to demonstrate that any arbitrary images can be generated on my displays. I also discuss the actuator performance in terms of force, displacement, and lifetime. Finally, I validate the use of SMP actuators as taxel technology with perception tests on sighted, blind, and visually impaired people.

### 4.4.1 Displaying high resolution patterns

Figure 4.7 and Figure 4.8 demonstrate that my SMP membrane plus CB/PDMS heaters concept allows to display any high resolution logos or camouflage patterns on the 32x24 rigid tactile tablet and the 32x24 flexible haptic diplay, respectively. The taxel states implemented in these devices are either *down* (negative pressure) or *flat* (no pressure) to prevent from debonding the active layer when no pin interface is placed atop the actuators. Real-time videos including thermal images to illustrate how patterns are displayed can be found online [108, 109]. One actuator requires 250 mW and 2.5 s to heat from 20 °C to 70 °C, meaning that each row or column of taxels consumes at most 8 W. To speed-up the refresh rate on the 32x24 rigid tactile tablet, two lines are addressed simultaneously, enabling to change the displayed pattern in under 30 s.
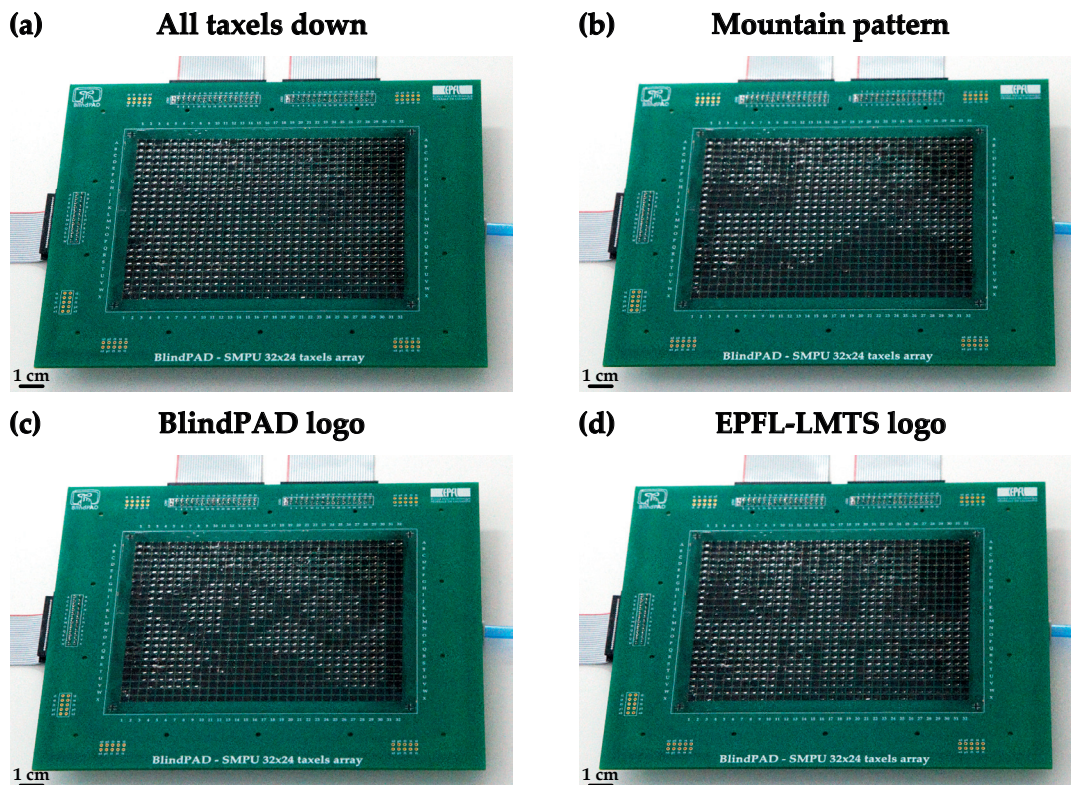


Figure 4.7 – Pictures of several patterns displayed on the 32x24 rigid tactile tablet: (a) all taxels down, (b) a mountain pattern, (c) the BlindPAD logo, and (d) the EPFL-LMTS logo.

If placed on an autonomous robot, the 32x24 flexible haptic display would allow dynamically adapting the robot appearance to the background. The online video [108] shows the flexible haptic display refreshing in real time while the device is wrapped around an arm, as well as its high bendability.

45

**(a)**        **All taxels flat**

**(b)**        **All taxels down**

**(c)**        **EPFL logo**

**(d)**        **Map of Switzerland**

**(e)**        **Giraffe camouflage**
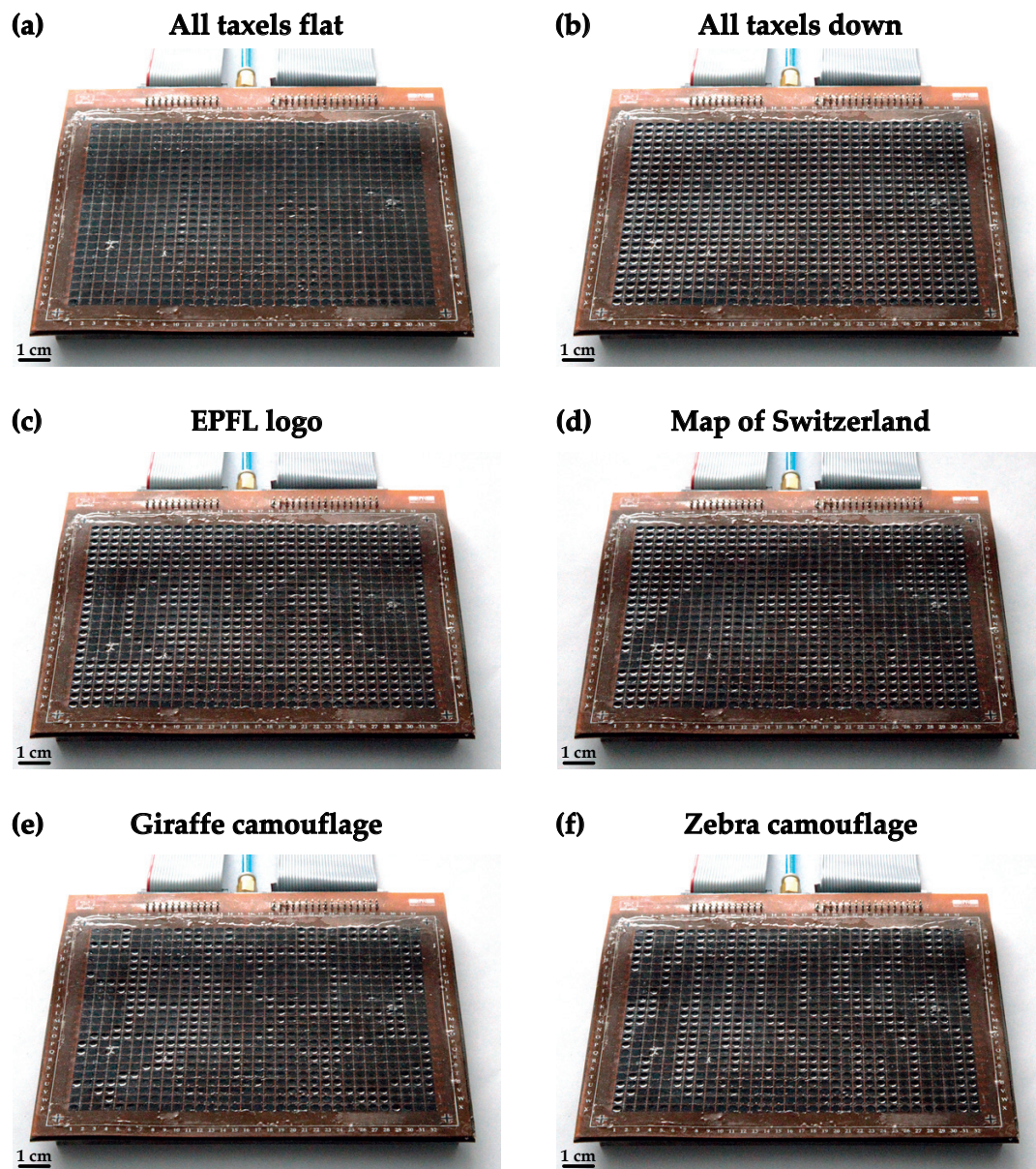
**(f)**        **Zebra camouflage**

Figure 4.8 – Pictures of several patterns displayed on the 32x24 flexible haptic display: (a) all taxels flat, (b) all taxels down, (c) the EPFL logo, (d) the map of Switzerland, (e) a giraffe camouflage, and (f) a zebra camouflage.

### 4.4.2 Actuator force and displacement performance

Since either positive or negative pressure can be applied in the pneumatic chamber, the holding force as a function of displacement for both raised and flat taxels have been measured. Without an interface between the active layer and the finger, positive pressure is better because it is far easier to feel taxels when they are inflated (*up*) than when they are deflated (*down*). For long-term reliability reasons, negative pressure is preferred since it avoids to mechanically debond the active layer from the PCB and to electrically damage the interconnects. Hence, to transfer these *down* + *flat* states into *flat* + *up* ones, an intermediate soft buffer layer would need to be added for future VR and AR wearable applications using the flexible haptic display. For the rigid display, this motion transfer is ensured by the pin interface. As compared in Figure 4.9, both flat and raised taxels behave differently. On the one hand, a flat taxel acts as a spring and hence is easy to displace with a gentle touch, but tends to return back to its flat state when the constraint is removed. On the other hand, a raised taxel presents a bistable motion and thus will return to its up stable state for small displacements only, but snaps to its other down stable state if pushed too hard. The reported measurements are performed on the same 4x4 rigid tactile tablet, which has a 50 μm thick SMP membrane and 20 μm thick heaters.
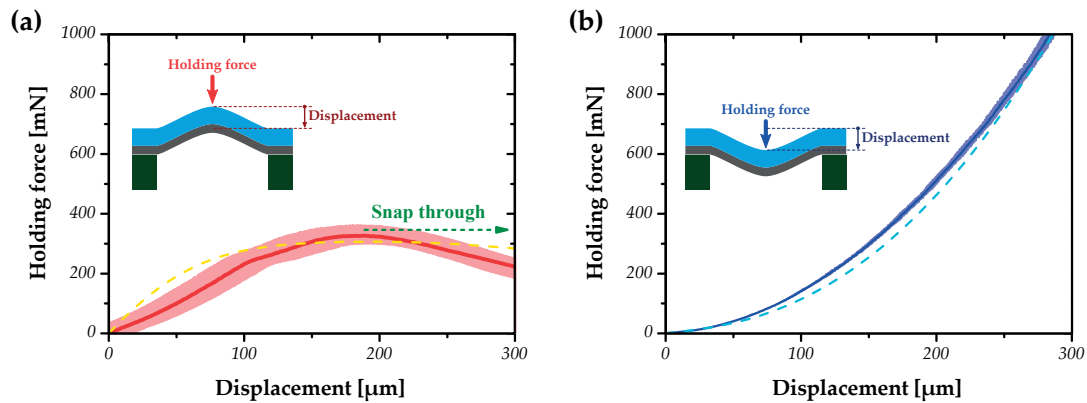


Figure 4.9 – Comparison of the holding force versus displacement for flat and raised taxels. (a) Measured holding force versus displacement for a flat taxel. (b) Measured holding force versus displacement for a raised taxel. The solid line represents the measured mean value over the 4x4 rigid tactile tablet, the filled area the measured standard deviation and the dashed line the simulated data. The flat taxel acts as a spring and hence comes back flat, while the raised taxel presents a bistable motion and thus remains dented.

When compared to FEA simulations, both flat and raised taxels behave as predicted. The only small difference is the initial shape of the raised taxel, which height is measured to be $(300 \pm 19)$ μm, whereas a height of 312 μm to 362 μm is expected when 200 mbar to 300 mbar is applied to a 70 °C homogeneously heated actuator. In this measurement, neither the achieved temperature distribution over the taxel, nor the exact supplied air pressure were measured; two parameters which actually have a direct influence on the motion achieved during the actuation phase. Figure 4.9 reports only the latching phase, with the experimentally measured height considered in the FEA simulations for the raised taxels.

### 4.4.3 Actuator lifetime performance

Commonly, polymer-based actuators are facing significant degradation over time [82, 110]. Hence, aging measurements on a single taxel mounted on a 4x4 rigid tactile tablet were performed. As reported in Figure 4.10, stable and robust operation was observed when the device was operated continuously for one week, which corresponds to 20 160 cycles. For this test, a cycle lasts 30 s, with 2.5 s to inflate the taxel, 12.5 s latched in the *up* position, 2.5 s to deflate the taxel, and 12.5 s latched in the *down* position. The timing corresponds to a typical tactile tablet *serious game* scenario where the user requires in the order of 10 s to explore and understand the pattern [32]. The experiment was stopped after 20 525 cycles, and the taxel was still operating normally. The small overshoot in displacement at the beginning of each switching cycle corresponds to the removal of the drive air pressure coupled to the thermal expansion and relaxation of the actuator due to the Joule heating. The present lifetime confirms the robustness of the active layer and could be further improved with active thermal control.
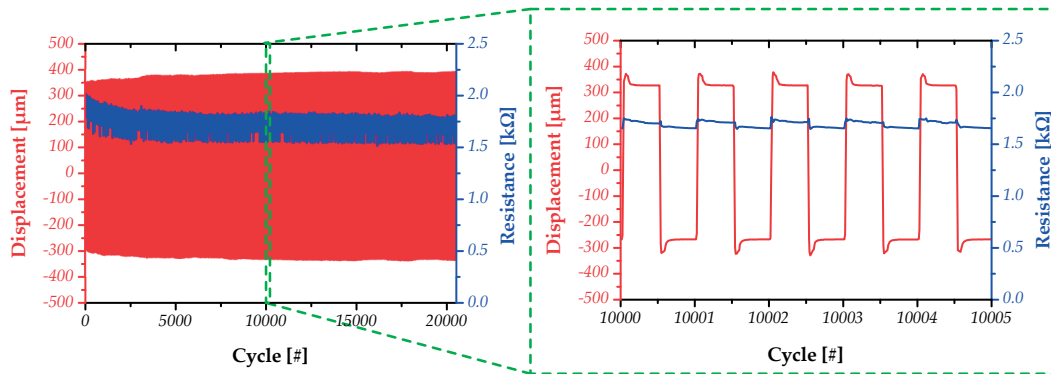


Figure 4.10 – Lifetime measurement on a single taxel, with a continuous operation for more than one week (20 160 cycles). The displacement and the resistance values are very stable over time. The small initial displacement overshoot at each cycle corresponds to the removal of the pressure coupled to the thermal expansion and relaxation of the material.

### 4.4.4 Perception tests with sighted people

To validate the use of SMP actuators for haptic display applications, perception tests with 15 sighted users (4 females and 11 males with age ranging from 22 to 44 years old) were performed to investigate their ability to distinguish graphical information through their sense of touch. The 4x4 rigid tactile tablet was hidden from their view in a box. The results obtained are reported in Figure 4.11b. The experiment consisted in discriminating among the 10 symbols shown in Figure 4.11a by scanning their finger on the pin interface. Each perception test includes 50 trials, with each symbol displayed randomly. Over 98 % correct pattern recognition was observed in less than 10 s exploration. The experiment was automated since the participant was pressing the corresponding symbol number on a keyboard. Auditory signals were used to indicate when to start exploring the tactile tablet.

**(a)**

**(b)**
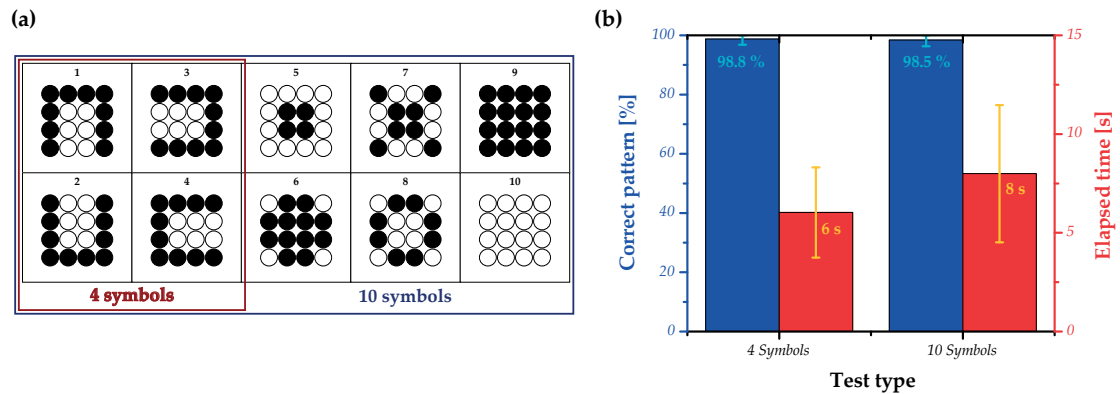


Figure 4.11 – Perception tests conducted with blindfolded sighted people. (a) Alphabet with 4 and 10 symbols used during the experiments. (b) Results of the perception tests with nearly 100 % of the symbols which are correctly identified even when using the full 10-symbol alphabet. The chance level is of 2 % for these experiments.

### 4.4.5   Perception tests with blind and visually impaired people

Finally, within the *BlindPAD* project, my partners Elisabetta Ferrari and Luca Brayda (IIT-RBCS, Italy) conducted perception tests on the 4x4 rigid tactile tablet with 24 blind and severely visually impaired (SVI) participants (10 females and 14 males with age ranging from 17 to 61 years old) at both the Rehabilitation Institute for Blind People Istituto David Chiossone Onlus (Genoa, Italy) and the special school Fundacja Instytut Rozwoju Regionalnego (Cracow, Poland). A summary of the results is shown in Figure 4.12b, demonstrating that both groups (blind versus SVI persons) could understand graphical information using the 4x4 rigid tactile tablet. The test consisted in first discriminating among the 12-symbol alphabet shown in Figure 4.12a by scanning their finger on the tactile tablet, and then in indicating to the experimenter the corresponding felt symbol on a raised paper dictionary. A total of 288 trials was recorded. Over 65 % correct pattern recognition was observed for both groups in less than 25 s and 45 s exploration for blind and SVI participants, respectively. The reaction times are significantly higher than for sighted users because both the dictionary was more complex and the blind plus SVI participants had to search for the corresponding symbol on a raised paper. With practice, the exploration time is expected to significantly decrease.

The confusion matrices reported in Figure 4.13 were computed revealing that symbols with diagonals and symmetric symbols were the most confused. These observations are confirming previous statements from [111] and [112], respectively. Blind users performed better than SVI participants, possibly because of long-term exposure to tactile information on maps and Braille reading [113]. This study prove that the latching property of SMPs is crucial as it does not set any time restriction to explore the display. Indeed, it enabled to have a maximum peak power consumption of 4 W during 2.5 s for the 4x4 rigid tactile tablet no matter how long the experiments with blind and SVI people lasted.
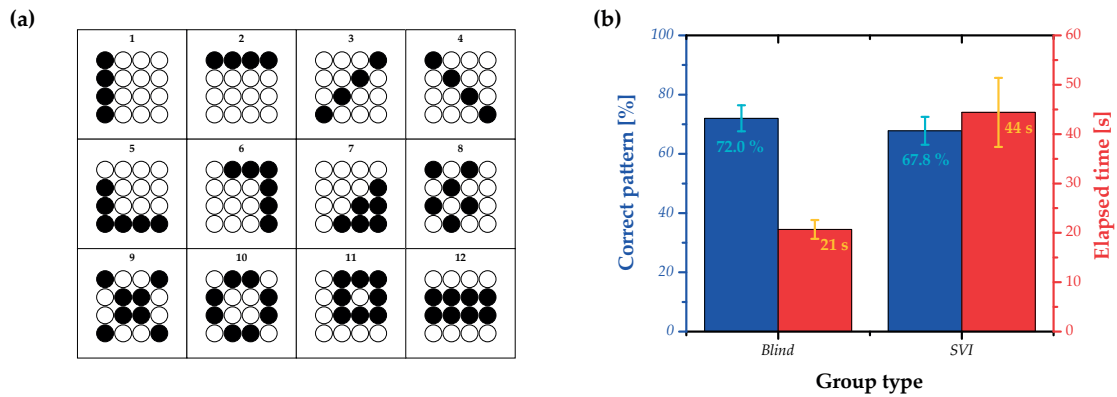
Figure 4.12 – Perception tests conducted with blind and SVI people. (a) Alphabet with 12 symbols used during the experiment. (b) Results of the perception test with over 65 % of the symbols which are correctly identified even when using the complex 12 symbols alphabet. The chance level is of 8.3 % for this experiment. Blind participants are twice faster than SVI users for the same accuracy, probably originating from their longer experience with Braille reading.
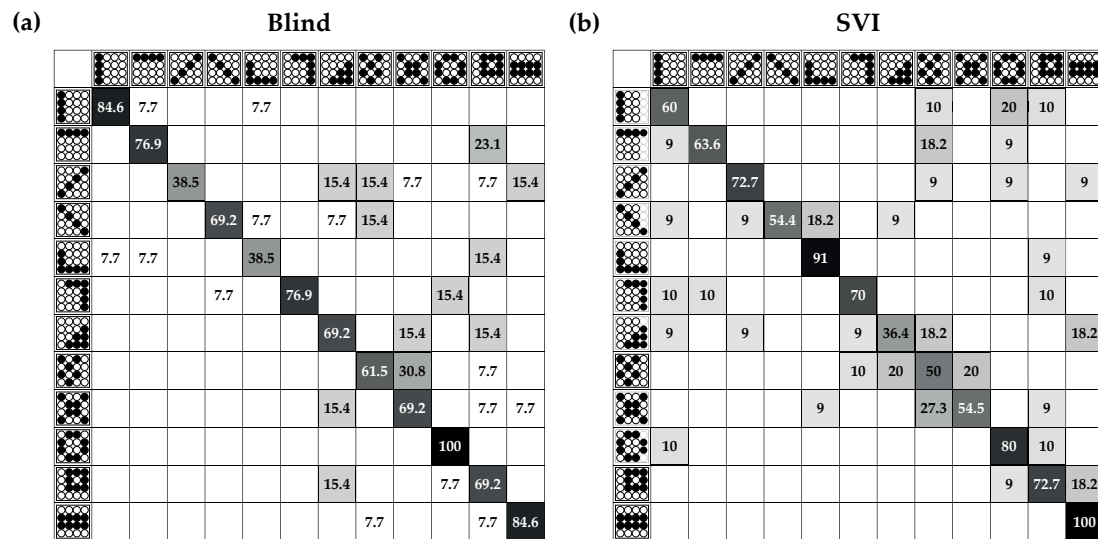


Figure 4.13 – Confusion matrices from tests with (a) blind and (b) SVI participants. The rows are indicating the presented symbols and the columns are indicating the user reply. The numbers in the diagonal report correct answers in percent. Cell shading is proportional to answer correctness. Values lower than chance are not shaded since they are considered as noise. A successful recognition task presents a confusion matrix which is mainly diagonal, as it is the case in this experiment.

## 4.5 Conclusion

In this chapter, I described my haptic displays and I reported on actuator performance to validate the use of SMP actuators as taxels. The heart of all the devices is the same, specifically a 40 µm thick SMP membrane, on which a matrix of 25 µm thick CB/PDMS stretchable heaters on 4 mm pitch is integrated, interconnected by a 4-layers PCB and bonded plus sealed to a 3D-printed microchanneled pneumatic chamber. Each taxel can be individually controlled, requires in average 250 mW to heat up from 20 °C to 70 °C, and takes 2.5 s to latch to a different state. The 4x4 rigid tactile tablet demonstrates that SMP actuators are perceivable by any users and the 32x24 flexible haptic display opens opportunities for HMIs needed in VR and AR applications. Any array configuration can be independently and reversibly obtained with a simple, highly reproducible, and compact system architecture running at low voltage (below 24 V). In the large array devices, each line (row or column) of taxels consumes at most 8 W, and the entire flexible haptic display is refreshed in under 1 min 30 s. This latter device weighs only 55 g and is 2 mm thick. More than 99 % of its 768 taxels are fully functional, with an actuator lifetime in excess of 20 000 cycles. Similar actuator yield was obtained with the 32x24 rigid tactile tablet. The perception tests conducted with 15 blindfolded sighted users on a 4x4 rigid tactile tablet resulted in 98 % correct pattern recognition in less than 10 s exploration. Additional experiments with 24 blind and SVI participants demonstrated that SMP-based tactile tablets are promising devices to help them understand graphics in full autonomy.

As reported in Table 4.1, despite meeting most of initial requirements and objectives for the *BlindPAD* project, the 32x24 rigid tactile tablet still needs improvements in terms of stroke to be easily felt by end-users. The obtained force and displacement are sufficient to discriminate each taxel independently, but distinguishing the displayed pattern with high fidelity remains a challenge. To obtain a better stroke reproducibility, the heaters could be driven at a constant power rather than at a constant voltage. A more sophisticated electronic driver board able to continuously measure the heater resistance would then be required. Ideally, with a pin interface atop the large array of SMP actuators, displacements over 500 µm should be targeted to accommodate for the pin interface and PCB non-uniformity. A suggested approach to amplify the motion using fluids will be discussed in Chapter 6. Moreover, since the heater design is now optimized, printing techniques like screen, flexure or gravure printing would be preferable to avoid damaging the SMP membrane during the laser ablation step. Finally, to speed up the refresh time, active thermal control of both the heating and the cooling phases is needed. At the cost of more power consumption, higher voltage can be implemented to improve plus accelerate the Joule heating and effective fans or Peltier elements can be added to the device to accelerate the cooling.

Table 4.1 – Summary table of the performance of my haptic displays compared to the initial requirement as set by the *BlindPAD* project.

| Parameter | *BlindPAD* requirement | SMP haptic displays |
|---|---|---|
| Actuator pitch | 4 mm | 4 mm |
| Displacement | >200 μm | >300 μm |
| Holding force | >60 mN | >300 mN |
| Array refresh time | >0.1 Hz | >0.01 Hz |
| Average power consumption | <10 mW/actuator | 250 mW/actuator (for 2.5 s only) |
| Array size | 64 x 48 | 32 x 24 |
| Lifetime | >10 000 cycles | >20 000 cycles (for one actuator only) |
| Latching mechanism | Essential | Intrinsic to SMPs |
| Portability | Essential | Partially |

# 5 Microfluidic platforms using arrays of SMP actuators as valves

## 5.1 Summary

In this chapter, I demonstrate that arrays of SMP actuators are a promising valve-unit for microfluidic platforms. I first present a selection of state-of-the-art valve technologies implemented in microfluidic large scale integration (mLSI) systems including micropumps, mixers, and multiplexers. I then detail the design and operating principle of my normally closed (NC) and normally open (NO) valves. I finally conclude with an analysis on their performance showing a clear stable cyclic opening and closing behavior with the system consuming power exclusively during the state switching phase.

The results reported in this chapter have been presented at the *MicroTAS 2017 Conference* [114]. They are the fruit of a recent collaboration involving my partners Robert Jan Boom, Bas-Jan Hoogenberg plus Marko Blom (Micronit Microtechnologies, Netherlands), my colleagues Bekir Aksoy plus Herbert Shea (EPFL-LMTS, Switzerland), and myself. Our collaborators have an advanced expertise in microfluidics and we brought our knowledge on SMP actuators to develop the first latching SMP valves which can be repeatedly open and closed. The conceptual SMP valves idea followed a presentation on the SMP haptic display and originated from a discussion at a conference among their chief Marko Blom and my professor Herbert Shea. The electronic driver to individually address each valve was developed by my colleague Olexandr Gudozhnik (EPFL-LMTS, Switzerland). The similarity in form factor between haptic displays and microfludic platforms plus the high versatility of my concept enabled us to quickly obtain compelling results. They demonstrate that my SMP actuators are a promising valve-unit for mLSI systems, although no parameter has been optimized for any real microfluidic application yet. A manuscript is planned upon testing and characterizing a color mixer with 16 latching SMP valves. Our objective is to prove that this matrix can be directly controlled with a single pneumatic air supply while accomplishing complex functions. Our approach significantly simplifies microfluidic platforms by both avoiding sophisticated microfluidic logical structures and replacing the standard bulky pneumatic tubing controls with electronic drivers coupled to a single pneumatic air supply.

## 5.2 Introduction to microfluidic platforms

A microfluidic platform implementing large arrays of valves based on a soft membrane placed between the microfluidic chip and the pneumatic chamber, as shown in Figure 5.1a, is called a mLSI system. Each valve is either open or closed depending on the air pressure applied to the corresponding control channel [115, 116]. By combining hundreds to thousands of valves, complex functions like micropumps, mixers, or multiplexers can be successfully integrated on a single chip. In this field, multilayer soft lithography processes are commonly used to hermetically bond together several PDMS layers, resulting in a monolithic structure with densely packed functional microfluidic elements. Compared to other microfluidic platform concepts, mLSI systems based on PDMS valves are highly versatile and scalable. Their main drawback remaining the cumbersomeness and size of the external control equipment. To simplify the device, valves are usually multiplexed in large arrays, allowing for operating $n$ fluid channels with only $\log_2\left(n^2\right)$ control channels. The largest reported array to date is a microfluidic memory storage device with 1000 independent compartments, 3574 on-chip valves and 22 off-chip control channels [13]. A method implementing a latching valves structure has also been reported [117], enabling to reduce the number of control channels to drive $n$ fluid channels to only $\log_2\left(2n\right)$. Two latching valve structures consisting of three- and four-valves circuits have been demonstrated and they latch in 120 ms. Hence, a 10-bit demultiplexer with 1000 independent compartments might be set in 2 min using 4046 on-chip valves and 11 off-chip control channels.

More recently, phase-change materials (PCMs) including waxes and SMPs have been investigated because they allow for direct valve control with additionally latching properties. The most relevant phase-change valves are shown in Figure 5.2. Several latching paraffin valves have been reported [118–121], with only [121] avoiding direct paraffin-to-fluid contact to prevent from fluid contamination. The design integrates a heater below the fluid channel to reversibly open and close the valve, although integrating the heater onto the PDMS membrane would be more efficient. An array of carbon-loaded wax-based latching valves with selective light illumination addressing has also been demonstrated [122]. Either a computer-controlled digital projector or a battery-operated high power laser pointer aligned manually were used to generate reconfigurable virtual heaters. Convex lenses were used to focus the light on the actuators layer. Light illumination is an interesting alternative to heat arrays of phase-change actuators from a distance. To convert light resolution into spatial resolution, substrates with low thermal conductivity are required to achieve high array density due to the lateral heat diffusion over the microfluidic chip. While using liquid-to-solid PCMs, this concept presents many similarities with my approach. Liquid-to-solid PCMs are less convenient than solid-to-solid PCMs because of the need for encapsulation. Moreover, SMPs present a wide range of glass transition, enable a good control on the membrane thickness, and ease the integration of the heating elements. Hence, despite only one-shot SMP valves having been successfully demonstrated to date [73], they are expected to be a simple, compact, and cost-effective solution for microfluidic platforms.
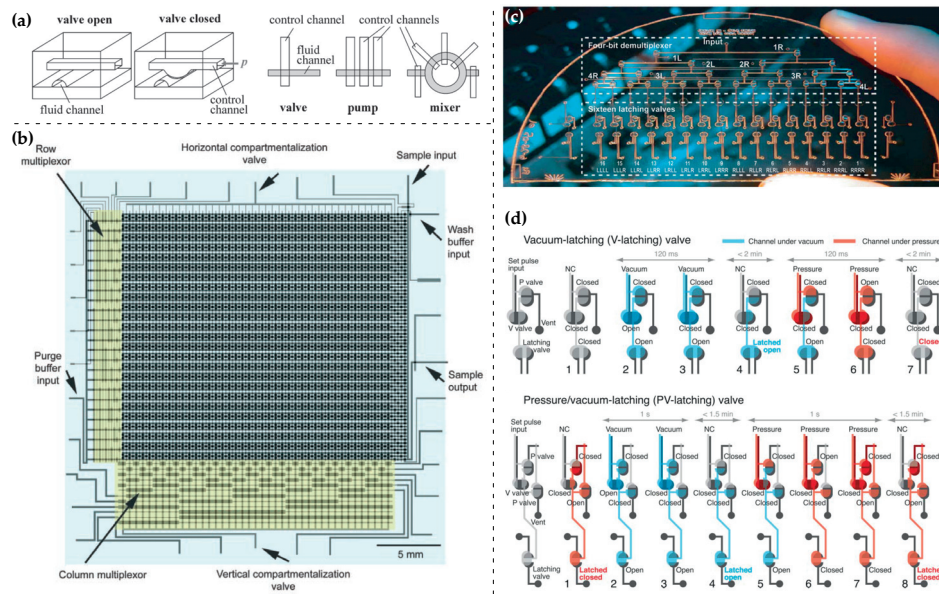
Figure 5.1 – Selected examples of large array microfluidic platforms. (a) Schematic illustration of classical valves implemented in mLSI systems (Reprinted from [115]). (b) Mask design of the 40x25 microfluidic memory storage device (Reprinted from [13]). (c) Picture of the multiplexed latching valves device, with a 4-bit demultiplexer for routing pressure and vacuum pulses to each of the 16 latching valves. (d) Schematic illustration of the design and operating principle for both types of latching valve structures (Reprinted from [117]).
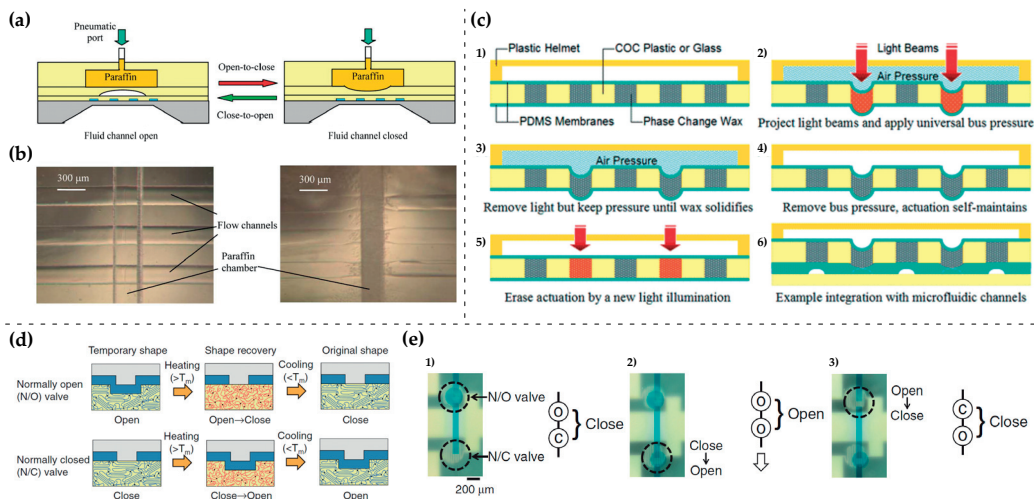


Figure 5.2 – Selected examples of phase-change microfluidic valves. (a) Schematic illustration of the design and operating principle of a paraffin wax latching valve. (b) Pictures of the fluid channels upon filling the chamber with paraffin (Reprinted from [121]). (c) From 1 to 6, schematic illustration of the structure and operating principle of carbon-loaded phase-change wax valves with their motion selectively triggered via light illumination (Reprinted from [122]). (d) Schematic illustration of the operating principle of one-shot NC and NO SMP valves. (e) From 1 to 3, actuation cycle to close–open–close a circuit using tandemly coupled one-shot NC and NO valves (Reprinted from [73]).

My approach is to combine local Joule heating with a single global pneumatic air supply to selectively trigger motion of SMP valves. The target is to demonstrate that an array of SMP valves can be repeatedly open and closed in a compact and simple form factor. Eliminating the need for multiplexing and replacing the external pressure sources by electronic drivers coupled to a single pneumatic inlet significantly downscales the device footprint. In comparison to my microfluidic platform where a single pneumatic air supply can trigger 16 valves, both multiplexing methods shown in Figure 5.1b-d would require 8 control channels [13] and 5 control channels [117] to independently drive these 16 valves, respectively. In my thesis, only preliminary results validating the concept are presented. My colleague Bekir Aksoy (EPFL-LMTS, Switzerland) is currently pursuing the investigation in his own thesis by developing advanced mLSI systems and by optimizing the SMP valves and microfluidic chip designs.

## 5.3   Microfluidic valves design and operation

In this section, I detail the operating cycle of the SMP valves I have developed and their overall design. In particular, I discuss the actuation loop and timing to switch the valve state for both NC and NO valves. The main components present in the microfluidic platform are highlighted, with the microfluidic chip designed to match the shape of the SMP actuators implemented in the 4x4 rigid tactile tablet.

### 5.3.1   Normally closed (NC) and normally open (NO) valves design

To evaluate the potential and versatility of SMP actuators for microfluidic applications, the 4x4 microfluidic platform reported in Figure 5.3a has been manufactured. This proof-of-concept device is used to operate and compare many valve designs in parallel before implementing them in more complex mLSI systems. In particular, as illustrated in Figure 5.3b-c, NC valves with seat lengths ranging from $300\,\mu m$ to $600\,\mu m$ and NO valves with valve depths ranging from $150\,\mu m$ to $300\,\mu m$ have been fabricated and tested. The SMP actuator design and geometry is very similar to the 4x4 rigid tactile tablet, since only a SEBS impermeable fluid barrier is added on top. The active layer is first fabricated using blade-casting, with the heaters defined via either laser ablation or stencil printing through shadow mask. Its thickness is $112.5\,\mu m$; specifically $50\,\mu m$ for the SMP membrane, $25\,\mu m$ for the carbon-silicone heaters, and $37.5\,\mu m$ for the SEBS membrane. These actuators are then electrically interconnected plus mechanically bonded to the PCB. A polymethylmethacrylate (PMMA) pneumatic air chamber is sealed on the bottom of the PCB as pneumatic air input. This assembly is finally bonded to the micromachined polystyrene (PS) microfluidic chip in which NC or NO valves are designed. Because the type of valves is defined only by the shape of the microfluidic chip, both NC and NO valves could be implemented in the same device. In this thesis, to insure proper operation when applying the actuation pressure, two distinct microfluidic chips have been manufactured, with either only NC valves or only NO valves.
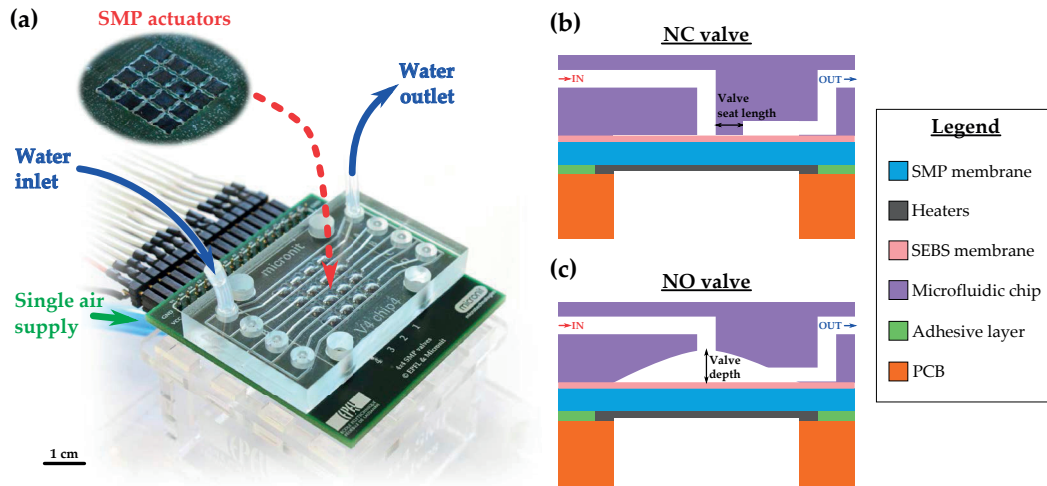
Figure 5.3 – Microfluidic platform with 16 SMP latching valves. (a) Picture of the microfluidic platform with 16 SMP latching valves of 3 mm in diameter on a 4 mm pitch. (b) Schematic illustration of the NC valve design highlighting the seat length dimension ranging from 300 μm to 600 μm. (c) Schematic illustration of the NO valve design highlighting the depth dimension ranging from 150 μm to 300 μm.

### 5.3.2 Operating cycle of SMP microfluidic valves

To implement the array of latching valves, the intrinsic bistability of SMPs and their hundred-fold change in stiffness with temperature are exploited. By synchronizing the common pneumatic air supply with the local Joule heating, only the heated SMP actuators are displaced and then latched in position. Figure 5.4 presents the working principle to open and close both types of valves, showing how they are repeatedly reshaped from their flat state to either their inflated or deflated state, respectively. Compared to conventional PDMS valves, both positions are stable with SMP valves and hence no power is required to latch in both states. De facto, the NC and NO valve terminology do not define well SMP valves, as it usually refers to the valve state requiring no power to be held.

The loop in Figure 5.4 is separated in two parts: the programming plus storing phase to define either the inflated or deflated shape and the recovering phase to restore the flat shape. The programming plus storing phase consists of applying an actuation air pressure of ±200 mbar for 5 s to all valves, while first locally Joule heating during 2 s only the activated valves and then letting them passively cool during 3 s for latching. The recovering phase consists of applying an opposite actuation air pressure of ±100 mbar for 2 s to all valves, while first locally Joule heating during 2 s only the activated valves and then letting them passively cool during 3 s for latching. Applying an opposite pressure strictly during the heating step of the recovering phase helps flattening back the SMP actuator, while preventing from deforming it in the opposite direction. In fact, the system also works without applying any opposite pressure during the recovering phase, but it is then less performing. Power consumption is restricted to the state switching phases, meaning that it is zero when latched in any array configuration.

**(a)**

<u>NC valve</u>



**(b)**
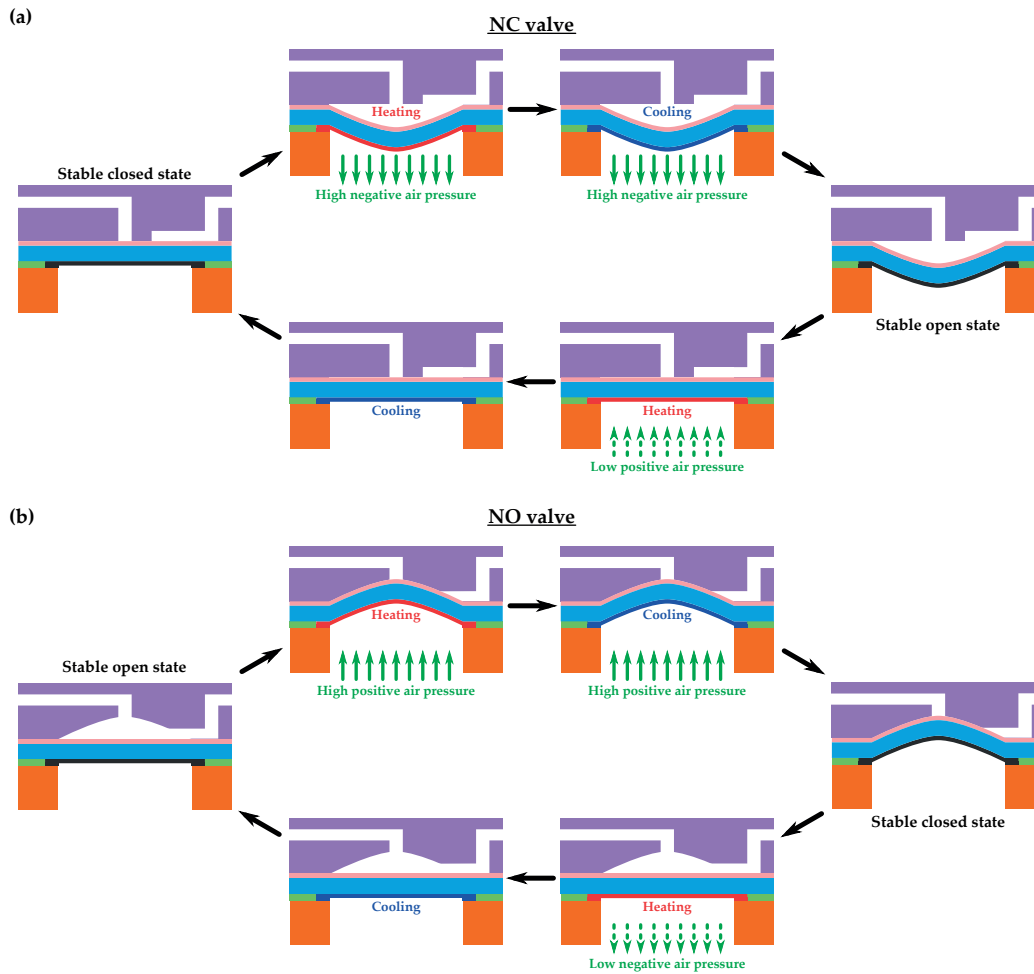
<u>NO valve</u>



Figure 5.4 – Operating principle of the SMP valves. (a) Schematic illustration of the operating cycle to change the state of the NC valve. (b) Schematic illustration of the operating cycle to change the state of the NO valve. To highlight the Joule heating timing, the heaters are red during the heating phase, blue during the passive cooling phase, and black during the latching (cold) phase. No power is required when latching in either the open or the closed positions.

## 5.4 Technology validation for microfluidic platforms

In this section, I present the results on valve performance in terms of conductance once opened, leakage once closed, and maximal pressure to drive fluid through the system before opening. The fluid used for the experiment is the deionized (DI) water from the laboratory. I also report on cyclic operation to evaluate the performance stability of the valves. The measurements have been performed with the help of my colleague Bekir Aksoy (EPFL-LMTS, Switzerland). *LabVIEW* is used to synchronize the different instruments and record the data. It enables for a detailed analysis of the valve behavior by comparing, as a function of time, the water flow rate to the Joule heating power, the actuation pressure to change state, and the drive pressure to flow water in the system.

### 5.4.1 NC and NO valves performance

Figure 5.5 demonstrate that SMP valves can successfully control water flow. The reported measurements are for a NC valve with 400 μm seat length and a NO valve with 250 μm depth, respectively. The SMP membrane is 50 μm thick in this experiment. Both valves remain closed up to 70 mbar of drive pressure before opening and present comparable conductance once opened. Similar performance has been measured for the other designs of NC and NO valves in which either the seat length or the depth dimension changes. The maximum drive pressure which a valve with a 50 μm thick SMP membrane can sustain has been experimentally measured to be in the range of 70 mbar to 80 mbar. Below this limit, the valve can safely operate for several cycles.

**(a)** **(b)**
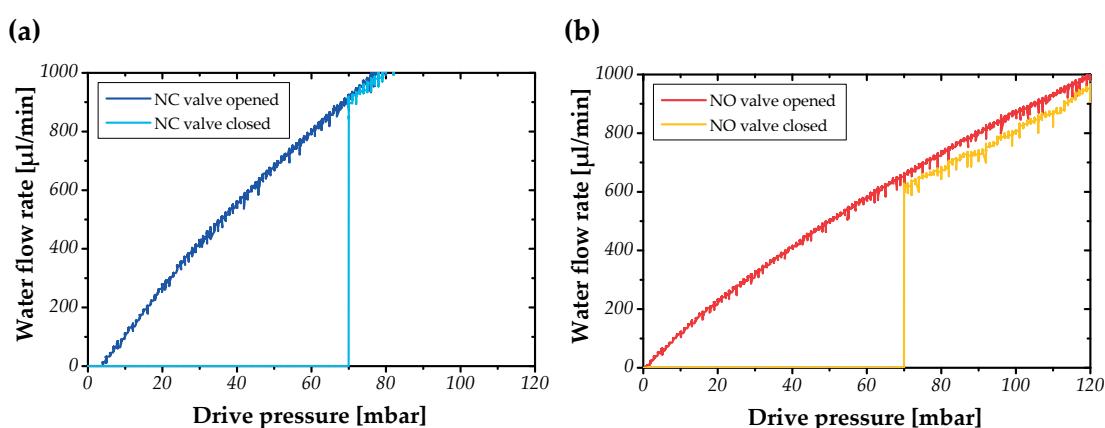


Figure 5.5 – Performance measurement of the SMP valves. (a) Measured water flow rate versus drive pressure for a NC valve with a seat length of 400 μm. (b) Measured water flow rate versus drive pressure for a NO valve with a depth of 250 μm. Both valves behave similarly.

The exact water pressure applied to the SMP actuator has not been directly measured. Because gravity variations along the setup are negligible, the water pressure on the SMP actuator is assumed to be equal in the steady-state to the drive pressure to flow water through the system. To measure it more accurately, a pressure sensor must be added to the setup, ideally close to the valve of interest.

In microfluidics, the holding force, the flow rate, and the switching speed requirements are broad and directly depend on the targeted real applications. By varying the SMP actuator geometry and the fluid channel size, the system can be optimized to reach specific goals. In particular, increasing the SMP membrane thickness will improve the holding force, but it comes at the price of more Joule heating power and slower switching speed. A study on the influence of the SMP membrane thickness on valve performance is currently on-going to find the optimal design for a 3 mm in diameter actuator.

The clear relationship between water flow rate and supplied drive pressure indicates that the overall fluidic resistance of the system is dominated by the microfluidic channels geometry. Hence, for a real application, the flow rate can be modulated by changing either the channel length or its cross-section area.

Since both types of valves are behaving similarly, it is preferable to operate with only NC valves in mLSI systems. Unlike NO valves, NC valves do not necessitate a good shape matching between the chip and the SMP actuator. Upon aging, the achieved displacement will likely decrease for both types of valves, implying that NO valves might stop operating.

## 5.4.2   Cyclic opening and closing of valves

To evaluate their stability over time, NC and NO valves have been cyclically operated. Figure 5.6 reports 10 opening + closing cycles of a NO valve with 150 µm depth and 50 µm thick SMP membrane. The drive pressure is set to 50 mbar during the entire measurement, a safe value permitting to continuously operate the NO valve. A constant voltage of 14 V is supplied to the actuator to locally Joule heat it. The Joule heating power is constant, indicating no heater degradation upon actuation. Because DI water continuously cools down the SMP actuator, the required Joule heating power in the microfluidic platform is slightly higher than for the haptic display. Indeed, 350 mW to 400 mW are required for the microfluidic plateform, while only 250 mW are used in the haptic display.

As reported in Figure 5.7, one opening + closing cycle can be analyzed more in depth by comparing, as a function of time, the water flow rate to the Joule heating power, the actuation pressure to switch state, and the drive pressure to flow water through the system. Each programming, storing, recovering, cooling, or latching phase is clearly distinguishable. Since DI water is an incompressible fluid, the overshoots in water flow rate are small fluid volumes expelled in and out from the valve location while switching state. By further adding an exhaust channel in the system, they might be avoided. Upon applying and removing the actuation pressure, small fluctuations in water flow rate are also generated.

Likewise, the valves can be cyclically operated while varying the drive pressure to adjust the water flow rate. As indicated in Figure 5.8, the obtained water flow rate is directly linked to the supplied drive pressure and is stable for a given drive pressure. During this experiment, a constant voltage of 15 V is supplied to the actuator to locally Joule heat it. Slightly increasing the Joule heating power with respect to the previous experiment enables to safely operate this NO valve up to 80 mbar.
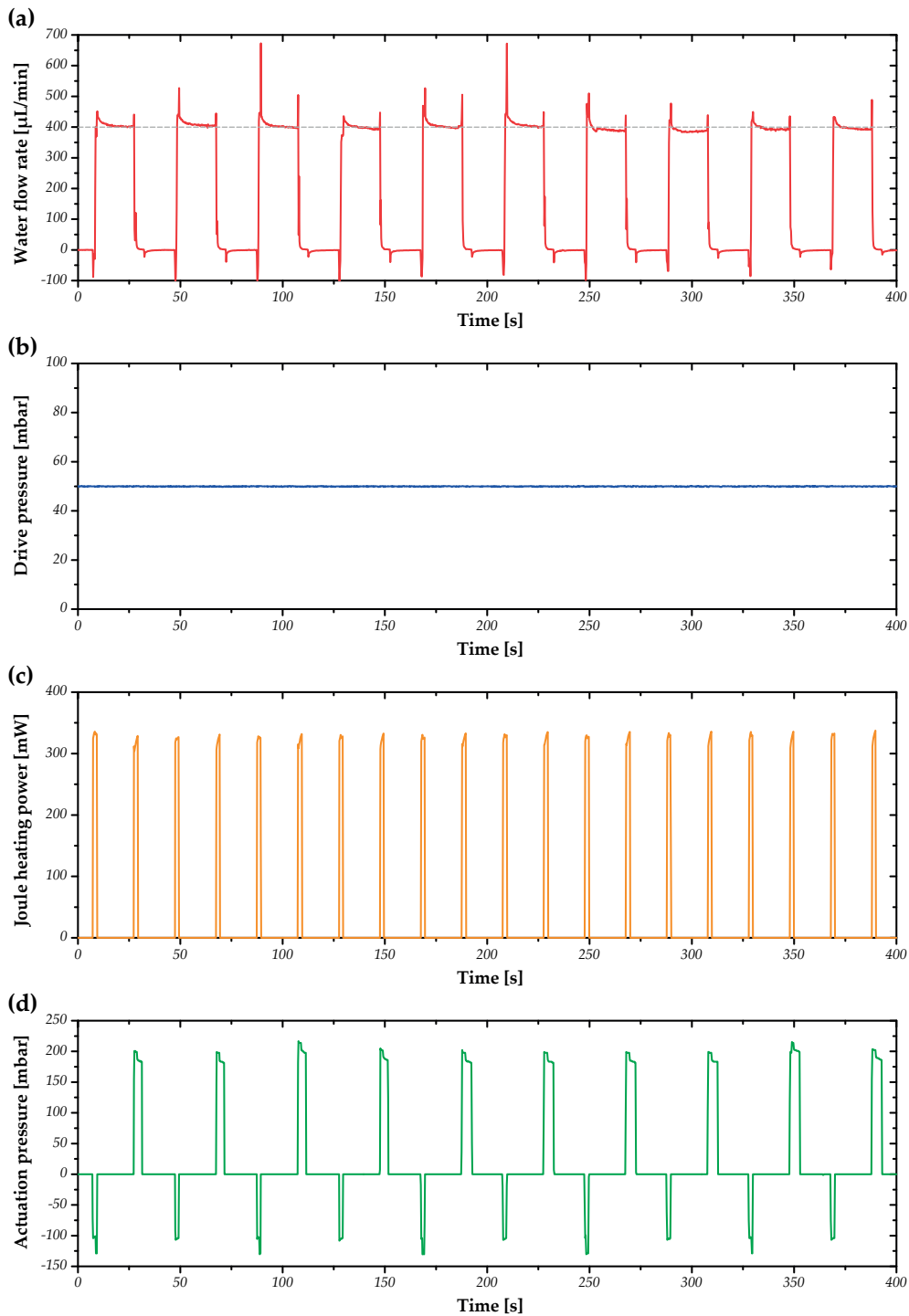
Figure 5.6 – Cyclic operation of a NO valve with constant drive pressure. (a) Measured water flow rate versus time. (b) Measured drive pressure versus time. (c) Measured Joule heating power versus time. (d) Measured actuation pressure versus time. The water flow rate is the output of the system while the drive pressure, Joule heating power, and actuation pressure are the inputs. The reported 10 cycles show stable performance over time.
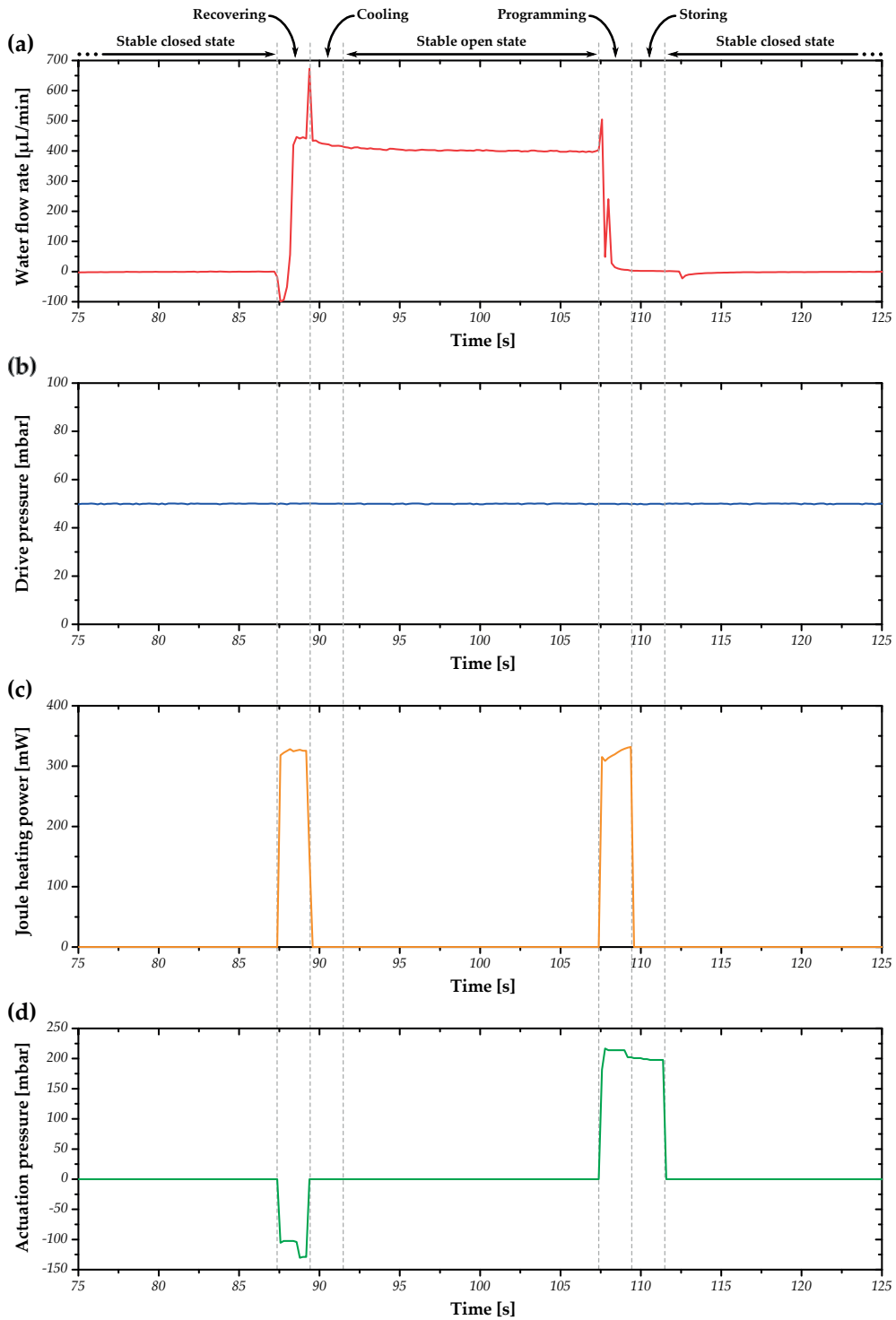
Figure 5.7 – Zoom on one opening + closing cycle of a NO valve highlighting the required steps to switch state. (a) Measured water flow rate versus time. (b) Measured drive pressure versus time. (c) Measured Joule heating power versus time. (d) Measured actuation pressure versus time. The water flow rate is the output of the system while the drive pressure, Joule heating power, and actuation pressure are the inputs.

**(a)**

**(b)**

**(c)**

**(d)**
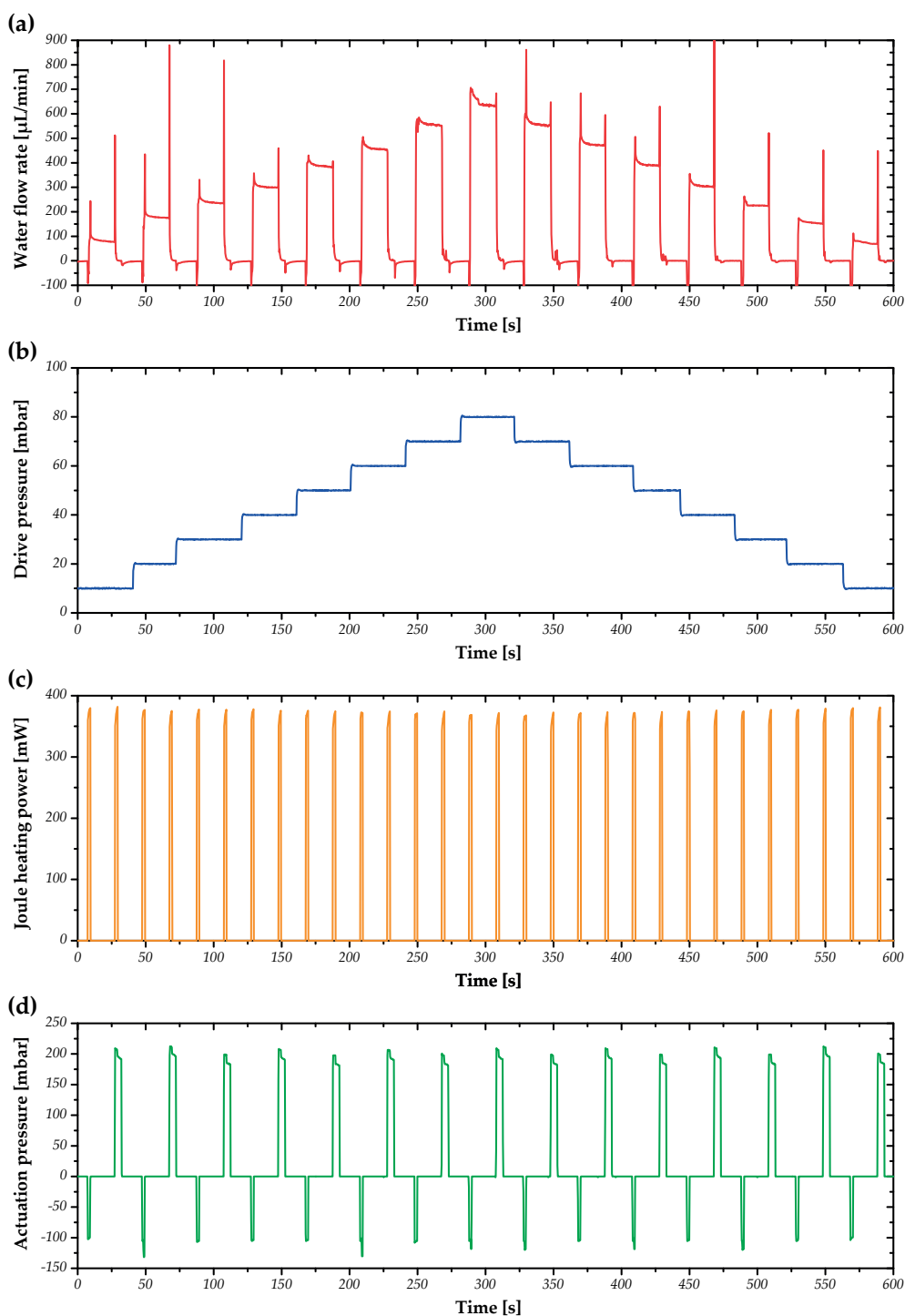
Figure 5.8 – Cyclic operation of a NO valve with ramped drive pressure. (a) Measured water flow rate versus time. (b) Measured drive pressure versus time. (c) Measured Joule heating power versus time. (d) Measured actuation pressure versus time. The water flow rate is the output of the system while the drive pressure, Joule heating power, and actuation pressure are the inputs. The reported cycles show direct stable correlation between water flow rate and drive pressure.

## 5.5   Conclusion

In this chapter, I described my 4x4 microfluidic platform and I reported on actuator performance to validate the use of SMP actuators as NC and NO valves.  This proof-of-concept device is used to evaluate and compare in parallel several valve designs, with the purpose of implementing the best one in the color mixer shown in Figure 5.9. The active layer consists in a 50 µm thick SMP membrane, on which a matrix of 25 µm thick CB/PDMS stretchable heaters on 4 mm pitch is integrated, with atop a 37.5 µm thick SEBS membrane acting as a impermeable fluid barrier. It is first mechanically bonded plus electrically interconnected to a 4-layers PCB, and then bonded plus sealed to a PMMA pneumatic air chamber. This assembly is finally bonded to a PS microfluidic chip, in which either the NC or the NO valve design are micromachined. Both NC and NO valves remain close up to 70 mbar of pressure to drive water through the system before opening and present similar conductance once opened. They show stable opening and closing behavior when operated cyclically at 50 mbar of drive pressure. Despite promising preliminary results, further design optimization of the SMP valves is still required prior to implement them in mLSI systems capable to perform advanced operations.

The working principle takes fully advantage of the intrinsic properties of SMPs to open and close the valves by repeatedly switching them between two stable states. The programming plus storing phase consists in applying an actuation pressure of ±200 mbar for 5 s to all valves, while first locally Joule heating during 2 s only the activated valves and then letting them passively cool during 3 s for latching.  And the recovering phase consists of applying an opposite actuation pressure of ±100 mbar for 2 s to all valves, while first locally Joule heating during 2 s only the activated valves and then letting them passively cool during 3 s for latching. Thanks to the drastic change in Young's modulus with temperature, only the Joule heated valves are moved, allowing for a simple and compact device form factor.
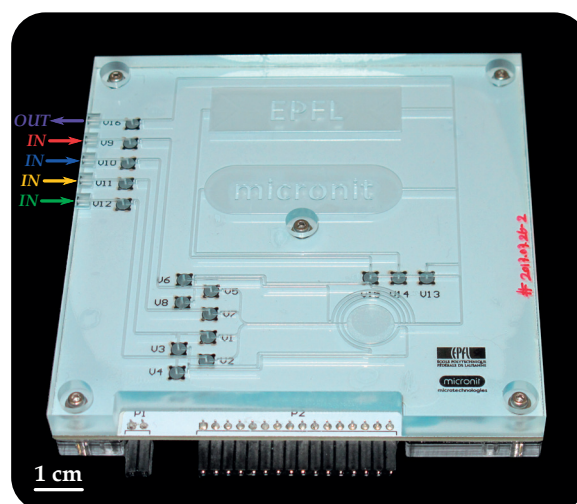


Figure 5.9 – Picture of the color mixer, which has 16 latching SMP valves with four separated color inlets and one global outlet. Upon improving the bonding of the SEBS membrane to the microfluidic chip at the large scale, this device will be tested and characterized.

# 6 Conclusion

## 6.1 Summary

My thesis contributes to the field of SMPs by providing an extremely versatile concept to arbitrarily control large arrays of SMP actuators. The key innovation consists in patterning compliant heaters on a thin SMP membrane and in synchronizing the local heating of each actuator with a global air pneumatic supply. By exploiting the large stiffness change with temperature of SMPs, the pneumatic air supply triggers motion of exclusively the Joule heated actuators. This enables to independently and reversibly reconfigure any array configuration with a simple, highly reproducible, and compact system architecture running at low voltage. The achieved actuator motion depends primarily on the air pressure applied during its reshaping phase. Moreover, benefiting from the intrinsic nature of SMPs, power consumption occurs only as the array is reconfigured.

My work demonstrates the relevance of this matrix of soft latching actuators for haptic displays and for microfluidic valves. In particular, the 32x24 flexible haptic display shows the full technology potential, the 4x4 rigid tactile tablet validates the actuator effectiveness, and the 4x4 microfluidic platform illustrates the concept versatility. To meet the specific requirements for both haptic and microfluidic applications, I optimized the actuator size, geometry and thickness using experimentally validated FEA models. The final actuator design is the best trade-off between force and displacement for a densely packed array of SMP actuators. I also specifically developed fabrication processes, and assembly tools which are compatible with large scale manufacturing, present high yield, and have good performance reproducibility.

### 6.1.1 Haptic displays using SMP actuators

**Main results**

In this thesis, I successfully developed haptic displays based on arrays of SMP actuators as taxels. The core of all devices is a 40 μm thick SMP membrane, on which a matrix of 25 μm thick CB/PDMS stretchable heaters on 4 mm pitch is integrated. This active layer is first mechanically bonded plus electrically interconnected to a 4-layers PCB, and then bonded plus sealed to a 3D-printed microchanneled pneumatic chamber. Each taxel can be individually controlled, requires in average 250 mW to heat up from 20 °C to 70 °C, and takes 2.5 s to latch to a different state. The 4x4 rigid tactile tablet demonstrates that SMP actuators are perceivable by any users and the 32x24 flexible haptic display illustrates the full technology potential. In the large array devices, each line (row or column) of taxels consumes at most 8 W, and the entire flexible haptic display is refreshed in under 1 min 30 s. The wearable sleeve weighs only 55 g and is 2 mm thick. More than 99 % of its 768 taxels are fully functional, with an actuator lifetime in excess of 20 000 cycles. Similar actuator fabrication yield was obtained with the 32x24 rigid tactile tablet. Hence, any high resolution pattern can be displayed on the device. The perception tests conducted with 15 blindfolded sighted users on a 4x4 rigid tactile tablet resulted in 98 % correct pattern recognition in less than 10 s exploration. Additional experiments with 24 blind and SVI participants proved that SMP-based tactile tablets are promising devices to help them understand graphics in full autonomy.

**Impact statement**

My work on haptic displays demonstrates that SMP actuators are a suitable taxel technology because they can provide simultaneously large displacement and significant holding force. As a proof-of-concept of a lightweight and fully reconfigurable soft system with over 750 individually addressable actuators, the 32x24 flexible haptic display has been reported; an important step towards wearable HMIs needed in VR and AR applications.

### 6.1.2 Microfluidic platforms using SMP actuators

**Main results**

In this thesis, I successfully developed a microfluidic platform based on arrays of NC or NO SMP valves. The core of the device is a 50 μm thick SMP membrane, on which a matrix of 25 μm thick CB/PDMS stretchable heaters on 4 mm pitch is integrated, with atop a 37.5 μm thick SEBS membrane acting as a impermeable fluid barrier. This active layer is first mechanically bonded plus electrically interconnected to a 4-layers PCB, and then bonded plus sealed to a PMMA pneumatic air chamber. This assembly is finally bonded to a PS microfluidic chip, in which either the NC or NO valve designs are micromachined. Both NC and NO valves remain close up to 70 mbar of drive pressure to flow water in the system before opening and present similar conductance once opened. They show stable opening and closing behavior when cyclically operated at 50 mbar of drive pressure. The valves are successfully and repeatedly switched between their open and closed latching states.

**Impact statement**

My work on microfluidic platforms demonstrates that SMP actuators are a promising microfluidic valve technology because they significantly simplify the overall system. As a proof-of-concept of cyclically operating NC and NO latching valves, the 4x4 microfluidic platform has been reported; an important step towards more complex mLSI systems.

## 6.2 Future work

In this section, I propose two research topics in the field of haptic displays which would broaden the application scope for large arrays of SMP actuators. First, I present a mean to amplify the actuator motion by adding a soft fluidic buffer atop the current active layer. This approach enables to significantly increase the apparent actuator displacement, without changing any of the actual fabrication and assembly steps. Moreover, by transforming *down + flat* states into apparent *flat + up* ones, it permits to drive the overall device with only negative air pressures, which additionally avoids parasitic buckling motion. Finally, I discuss transparent electrodes based on silver nanowires (AgNWs), because they would allow to couple optical and tactile information on any screen.

### 6.2.1 Fluidically coupled haptic displays

Adding a soft fluidic buffer atop the existing SMP actuators would permit for both amplifying the actuator motion and transferring dented + flat shapes into flat + raised ones. Fluidically coupled haptic displays have already been reported for enhancing the motion or the holding force of DEAs [106]. My idea, reported in Figure 6.1a, is to fill with an incompressible fluid each conic cavity. The cavity shape, specifically the top and bottom radii, is important because it directly defines the motion gain. Unlike the pneumatic chamber which is common to the entire array, the soft fluidic buffer has one individual cavity per actuator to independently and selectively amplify each taxel motion.

My plan to develop a fluidically coupled haptic display is presented in Figure 6.1b. First, the SMP haptic display is fabricate and assemble following the current manufacturing process, then the entire array is moved once down, and finally the soft fluidic buffer is placed on top. This latter component is composed of three SEBS layers thermally bonded together: the bottom thin membrane following the SMP actuator motion, the intermediate layer with individual conic cavities filled with DI water and the top thin membrane which the end-user would touch. The fabrication process for thin SEBS membranes was developed within my work on microfluidics and SEBS is preferable over PDMS due to its water impermeability. Because SEBS is an extremely soft elastomer, upon filling each cavity with fluid, the bottom thin membrane should deflate and map the SMP actuator shape.

**(a)**



**(b)**
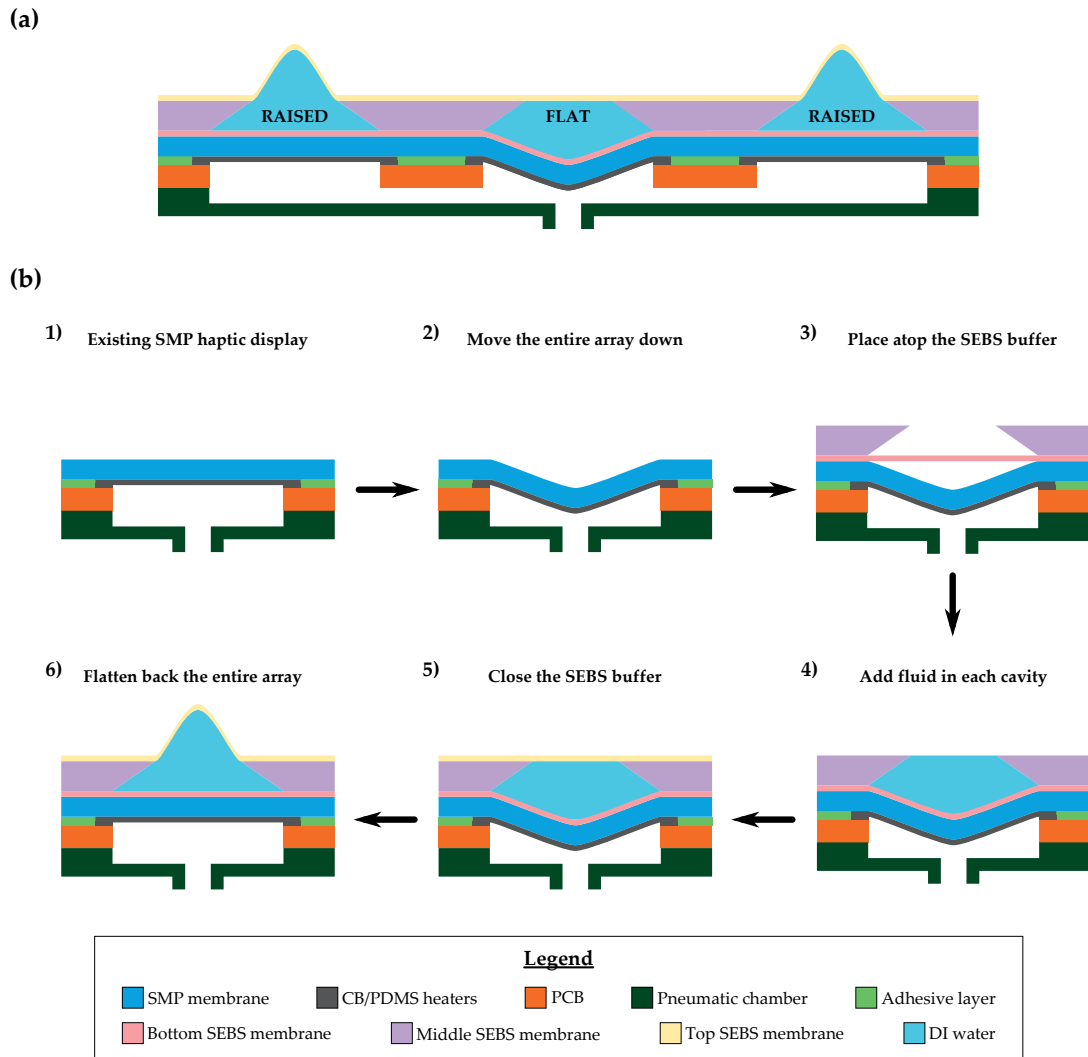


Figure 6.1 – Envisioned fluidically coupled haptic display. (a) Schematic cross-section of three actuators representing two raised and one flat taxels. Having one individual fluidic cavity per actuator allows for selective motion amplification. (b) Schematic illustration of the fabrication and assembly steps for the fluidically coupled haptic display. Starting with the existing SMP haptic display, first the entire array is moved down, then the SEBS buffer is placed atop the active layer, next each cavity is filled with fluid, and finally the SEBS buffer is closed. The soft fluidic buffer is made of SEBS because it is a water impermeable material.

Considering DI water as an incompressible fluid, the total volume trapped in each cavity remains constant. Using the shell method, the volume of revolution $V$ below a deformed membrane of radius $a$, of apex $h$, of deformed shape $f(r)$, and of normalized mode-shape $w(\xi)$ is given by Equation 6.1 [123].

$$V = 2\pi \int_0^a r f(r)\,dr = 2\pi a^2 h \int_0^1 \xi w(\xi)\,d\xi, \qquad f(r) = h w(\xi) \quad \text{and} \quad \xi = \frac{r}{a} \qquad (6.1)$$

With $w(\xi)$ given by Equation 6.2 for a tension parameter $k$ varying between 0 and $\infty$, depending on the amplitude of motion (for a pure plate $k \to 0$ and for a pure membrane $k \to \infty$) [124]. This tension parameter $k$ depends on the radial force $N$ at the center and on the actuator thickness $t$, Young's modulus $E$, radius $a$, and Poisson's ratio $v$.

$$w(\xi) = 1 - \frac{k\xi^2 I_1(k) - 2I_0(k\xi) + 2}{kI_1(k) - 2I_0(k) + 2}, \qquad k = \frac{a}{t}\sqrt{\frac{12(1-v^2)N}{Et}} \qquad (6.2)$$

Hence, as reported in Figure 6.2, the volume $V_1$ formed by the deflated bottom SEBS membrane is equal to the volume $V_2$ formed by the inflated top SEBS membrane. Assuming the same mode shape for both cases, as given by Equation 6.3, the motion gain $G$ defined as the apexes ratio is simply the inverse of the radii ratio to the square.

$$G = \frac{h_2}{h_1} = \left(\frac{a_1}{a_2}\right)^2 \qquad (6.3)$$
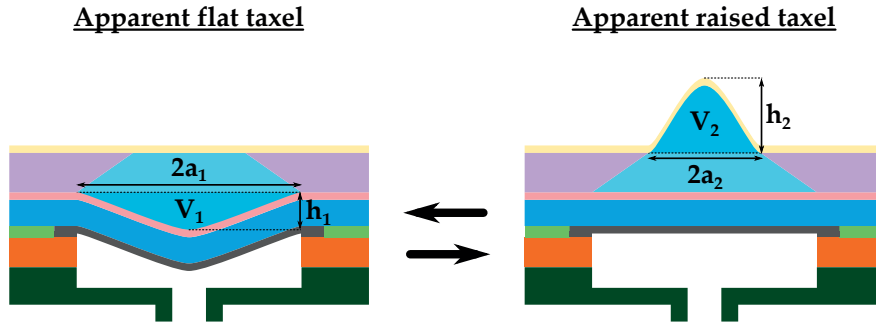


Figure 6.2 – Schematic illustration of the fluidic motion amplification. Considering DI water as an incompressible fluid, the volume $V_1$ and $V_2$ have to be equal.

Consequently, as reported in Table 6.1, displacements over $700\,\mu m$ could be reached without changing the existing SMP actuator design. Actually, even the Californian Braille standard might be fulfilled [125]. The main challenge remains to manufacture smaller and thinner SMP actuators to meet Braille standard, while keeping a high fabrication and assembly yield.

Table 6.1 – Expected motion amplification using a fluidically coupled haptic display. Examples of haptic displays based on the existing SMP actuator and aiming at the Braille standard are reported, with the SMP actuator displacement estimated from FEA simulations using *COMSOL Multiphysics*.

| Parameter | Haptic display based on existing SMP actuator | Haptic display aiming at Braille standard [125] |
|---|---|---|
| Radius $a_1$ | 1.5 mm | 1 mm |
| Displacement $h_1$ | 350 μm | 250 μm |
| Radius $a_2$ | 1 mm | 0.635 mm |
| Displacement $h_2$ | 790 μm | 620 μm |
| Motion gain $G$ | 2.25 | 2.48 |

## 6.2.2   Transparent heating electrodes

AgNWs are a promising material to fabricate transparent heating electrodes, which would allow for coupling haptic feedback with optical information on any screen. My laboratory recently purchased a dedicated desktop wax printer and filtration setup to develop in-house AgNW electrodes. Our setup is similar to Tybrandt et al. [66], who developed a fast and efficient method to obtain high resolution AgNW stretchable electrodes. Their fabrication steps are reported in Figure 6.3. My goal is to combine their process with hot press lamination to control temperature plus pressure during the transfer of the AgNW pattern from the polyvinylidene fluoride (PVDF) membrane to a thin sticky PDMS layer placed atop the SMP membrane.

My envisioned transfer method involves six main steps. First, a hydrophilic PVDF membrane is taped onto a carrier paper with the desired wax pattern printed on it using the desktop wax printer. Second, the patterned PVDF membrane is soaked in DI water and mounted into the filtration setup. Third, an aqueous dispersion of AgNWs is filtered through the parts of the PVDF membrane uncovered with wax, depositing the AgNWs on its surface. Forth, the PVDF membrane is dried out on a hot plate and put in contact with the thin sticky PDMS layer, which previously would have been blade-casted onto the SMP membrane. Fifth, the AgNW pattern is transferred from the PVDF membrane to the PDMS layer by hot press lamination. Finally, the PVDF membrane is peeled off, leaving the AgNW pattern on the PDMS layer placed atop the SMP membrane. Months of work are still required to develop and optimize this complete fabrication and assembly process.
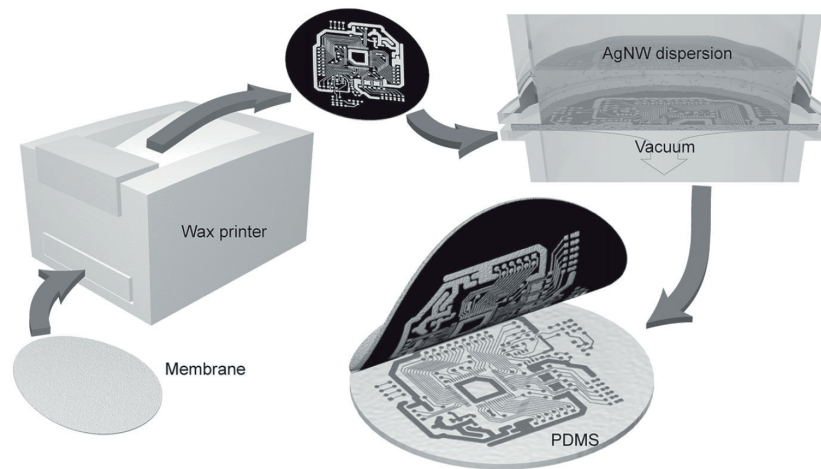
Figure 6.3 – Schematic illustration of AgNW electrodes patterning. The PVDF membrane is mounted on a paper carrier and the wax pattern is printed onto the membrane. The patterned membrane is mounted in a filtration setup and the AgNW dispersion is filtered through the uncovered areas of the membrane. The AgNW pattern is transferred to a semi-cured PDMS substrate under pressure and finally the membrane is peeled off (Reprinted from [66]).

To obtain transparent electrodes, the AgNWs need to be highly diluted in DI water. Tybrandt et al. [66] have reported AgNW area densities of $8000\,mg/m^2$, while Hong et al. [55] have obtained AgNW area densities of only $132\,mg/m^2$ for their transparent stretchable heaters. The target is to reproduce Hong et al. process following Tybrandt et al. method to manufacture an optically transparent active layer (SMP membrane + AgNW heaters), because it would allow for haptic feedback on any consumer electronic device containing a screen. As reported in Figure 6.4, one could imagine having buttons arbitrarily popping up on a smartphone screen when phoning, gaming, or searching.
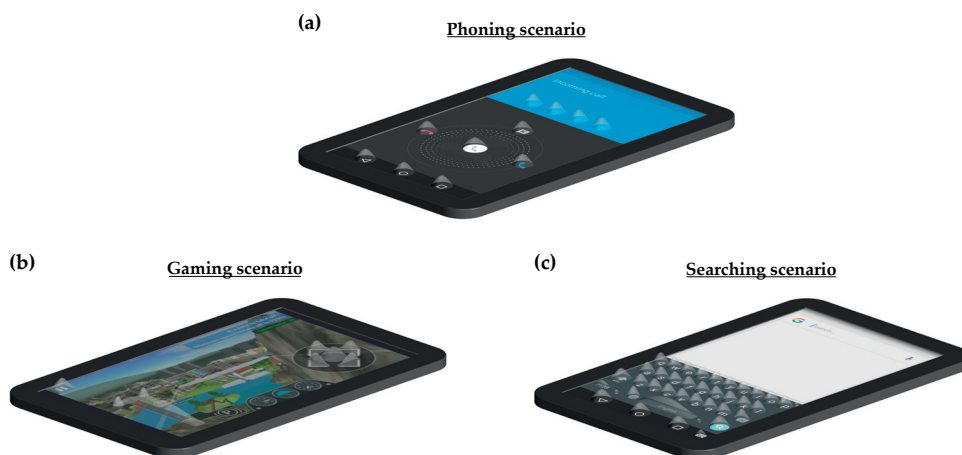


Figure 6.4 – Schematic illustration of buttons popping up on smartphones with reconfigurable screens notably for: (a) phoning, (b) gaming, or (c) searching scenarios.

## 6.3 Concluding remark

The recent advances in understanding the chemical and physical phenomena involved in SMPs have resulted in more material performance and reliability. Novel breakthrough devices implementing large arrays of SMP actuators will emerge from closer interdisciplinary collaboration among chemists and engineers. This soft technology present the unique feature of coupling drastic change in stiffness with intrisic multistability; both being attractive characteristics for haptic displays, soft robotics, mLSI systems, and adaptive optics. Hence, as a researcher, this is an exciting time for developing new SMP-based concepts and applications.

# Bibliography

[1] S. T. S. Holmström, U. Baran, and H. Urey, "Mems laser scanners: A review," *Journal of Microelectromechanical Systems*, vol. 23, no. 2, pp. 259–275, 2014.

[2] T.-W. Yeow, K. L. E. Law, and A. Goldenberg, "Mems optical switches," *IEEE Communications Magazine*, vol. 39, no. 11, pp. 158–163, 2001.

[3] S. Bauer, S. Bauer-Gogonea, I. Graz, M. Kaltenbrunner, C. Keplinger, and R. Schwödiauer, "A soft future: From robots and sensor skin to energy harvesters," *Advanced Materials*, vol. 26, no. 1, pp. 149–162, 2014.

[4] D. Rus and M. T. Tolley, "Design, fabrication and control of soft robots," *Nature*, vol. 521, no. 7553, pp. 467–475, 2015.

[5] R. F. Shepherd, F. Ilievski, W. Choi, S. A. Morin, A. A. Stokes, A. D. Mazzeo, X. Chen, M. Wang, and G. M. Whitesides, "Multigait soft robot," *Proceedings of the National Academy of Sciences*, vol. 108, no. 51, pp. 20 400–20 403, 2011.

[6] M. Wehner, R. L. Truby, D. J. Fitzgerald, B. Mosadegh, G. M. Whitesides, J. A. Lewis, and R. J. Wood, "An integrated design and fabrication strategy for entirely soft, autonomous robots," *Nature*, vol. 536, no. 7617, pp. 451–455, 2016.

[7] E. Brown, N. Rodenberg, J. Amend, A. Mozeika, E. Steltz, M. R. Zakin, H. Lipson, and H. M. Jaeger, "Universal robotic gripper based on the jamming of granular material," *Proceedings of the National Academy of Sciences*, vol. 107, no. 44, pp. 18 809–18 814, 2010.

[8] O. A. Araromi, I. Gavrilovich, J. Shintake, S. Rosset, M. Richard, V. Gass, and H. R. Shea, "Rollable multisegment dielectric elastomer minimum energy structures for a deployable microsatellite gripper," *IEEE/ASME Transactions on Mechatronics*, vol. 20, no. 1, pp. 438–446, 2015.

[9] G. Kofod, W. Wirges, M. Paajanen, and S. Bauer, "Energy minimization for self-organized structure formation and actuation," *Applied Physics Letters*, vol. 90, no. 8, p. 081916, 2007.

[10] J. Shintake, S. Rosset, B. Schubert, D. Floreano, and H. Shea, "Versatile soft grippers with intrinsic electroadhesion based on multifunctional polymer actuators," *Advanced Materials*, vol. 28, no. 2, pp. 231–238, 2016.

# Bibliography

[11] C. Laschi, M. Cianchetti, B. Mazzolai, L. Margheri, M. Follador, and P. Dario, "Soft robot arm inspired by the octopus," *Advanced Robotics*, vol. 26, no. 7, pp. 709–727, 2012.

[12] J. Hughes, U. Culha, F. Giardina, F. Guenther, A. Rosendo, and F. Iida, "Soft manipulators and grippers: A review," *Frontiers in Robotics and AI*, vol. 3, p. 69, 2016.

[13] T. Thorsen, S. J. Maerkl, and S. R. Quake, "Microfluidic large-scale integration," *Science*, vol. 298, no. 5593, pp. 580–584, 2002.

[14] A. Richter and G. Paschew, "Optoelectrothermic control of highly integrated polymer-based mems applied in an artificial skin," *Advanced Materials*, vol. 21, no. 9, pp. 979–983, 2009.

[15] I. M. Koo, K. Jung, J. C. Koo, J. D. Nam, Y. K. Lee, and H. R. Choi, "Development of soft-actuator-based wearable tactile display," *IEEE Transactions on Robotics*, vol. 24, no. 3, pp. 549–558, 2008.

[16] X. Niu, X. Yang, P. Brochu, H. Stoyanov, S. Yun, Z. Yu, and Q. Pei, "Bistable large-strain actuation of interpenetrating polymer networks," *Advanced Materials*, vol. 24, no. 48, pp. 6513–6519, 2012.

[17] H. Ishizuka and N. Miki, "Mems-based tactile displays," *Displays*, vol. 37, pp. 25 – 32, 2015.

[18] F. Vidal-Verdu and M. Hafez, "Graphical tactile displays for visually-impaired people," *IEEE Transactions on Neural Systems and Rehabilitation Engineering*, vol. 15, no. 1, pp. 119–130, 2007.

[19] M. Behl and A. Lendlein, "Shape-memory polymers," *Materials Today*, vol. 10, no. 4, pp. 20 – 28, 2007.

[20] P. T. Mather, X. Luo, and I. A. Rousseau, "Shape memory polymer research," *Annual Review of Materials Research*, vol. 39, no. 1, pp. 445–471, 2009.

[21] Q. Zhao, H. J. Qi, and T. Xie, "Recent progress in shape memory polymer: New behavior, enabling materials, and mechanistic understanding," *Progress in Polymer Science*, vol. 49, pp. 79 – 120, 2015.

[22] Z. Ren, W. Hu, C. Liu, S. Li, X. Niu, and Q. Pei, "Phase-changing bistable electroactive polymer exhibiting sharp rigid-to-rubbery transition," *Macromolecules*, vol. 49, no. 1, pp. 134–140, 2016.

[23] J. M. Ortega, W. Small, T. S. Wilson, W. J. Benett, J. M. Loge, and D. J. Maitland, "A shape memory polymer dialysis needle adapter for the reduction of hemodynamic stress within arteriovenous grafts," *IEEE Transactions on Biomedical Engineering*, vol. 54, no. 9, pp. 1722–1724, 2007.

74

[24] A. A. Sharp, H. V. Panchawagh, A. Ortega, R. Artale, S. Richardson-Burns, D. S. Finch, K. Gall, R. L. Mahajan, and D. Restrepo, "Toward a self-deploying shape memory polymer neuronal electrode," *Journal of Neural Engineering*, vol. 3, no. 4, p. L23, 2006.

[25] Y. Liu, H. Du, L. Liu, and J. Leng, "Shape memory polymers and their composites in aerospace applications: a review," *Smart Materials and Structures*, vol. 23, no. 2, p. 023001, 2014.

[26] H. Koerner, G. Price, N. A. Pearce, M. Alexander, and R. A. Vaia, "Remotely actuated polymer nanocomposites[mdash]stress-recovery of carbon-nanotube-filled thermoplastic elastomers," *Nat Mater*, vol. 3, no. 2, pp. 115–120, 2004.

[27] F. Li, L. Qi, J. Yang, M. Xu, X. Luo, and D. Ma, "Polyurethane/conducting carbon black composites: Structure, electric conductivity, strain recovery behavior, and their relationships," *Journal of Applied Polymer Science*, vol. 75, no. 1, pp. 68–77, 2000.

[28] R. Mohr, K. Kratz, T. Weigel, M. Lucka-Gabor, M. Moneke, and A. Lendlein, "Initiation of shape-memory effect by inductive heating of magnetic nanoparticles in thermoplastic polymers," *Proceedings of the National Academy of Sciences of the United States of America*, vol. 103, no. 10, pp. 3540–3545, 2006.

[29] M. Y. Razzaq, M. Anhalt, L. Frormann, and B. Weidenfeller, "Mechanical spectroscopy of magnetite filled polyurethane shape memory polymers," *Materials Science and Engineering: A*, vol. 471, no. 1, pp. 57 – 62, 2007.

[30] H. Zhang, H. Xia, and Y. Zhao, "Optically triggered and spatially controllable shape-memory polymer-gold nanoparticle composite materials," *J. Mater. Chem.*, vol. 22, pp. 845–849, 2012.

[31] BlindPAD, "BlindPAD: A Personal Assistive Device for BLIND and visually impaired people," accessed November 27, 2017. [Online]. Available: https://www.blindpad.eu

[32] F. Leo, E. Cocchi, and L. Brayda, "The effect of programmable tactile displays on spatial learning skills in children and adolescents of different visual disability," *IEEE Transactions on Neural Systems and Rehabilitation Engineering*, vol. 25, no. 7, pp. 861–872, 2017.

[33] C. M. Yakacki, R. Shandas, D. Safranski, A. M. Ortega, K. Sassaman, and K. Gall, "Strong, tailored, biocompatible shape-memory polymer networks," *Advanced Functional Materials*, vol. 18, no. 16, pp. 2428–2435, 2008.

[34] G. M. Baer, W. Small, T. S. Wilson, W. J. Benett, D. L. Matthews, J. Hartman, and D. J. Maitland, "Fabrication and in vitro deployment of a laser-activated shape memory polymer vascular stent," *BioMedical Engineering OnLine*, vol. 6, no. 1, p. 43, 2007.

[35] G. Vialle, M. D. Prima, E. Hocking, K. Gall, H. Garmestani, T. Sanderson, and S. C. Arzberger, "Remote activation of nanomagnetite reinforced shape memory polymer foam," *Smart Materials and Structures*, vol. 18, no. 11, p. 115014, 2009.

**Bibliography**

[36] X. Luo and P. T. Mather, "Conductive shape memory nanocomposites for high speed electrical actuation," *Soft Matter*, vol. 6, pp. 2146–2149, 2010.

[37] X. Gu and P. T. Mather, "Water-triggered shape memory of multiblock thermoplastic polyurethanes (tpus)," *RSC Adv.*, vol. 3, pp. 15 783–15 791, 2013.

[38] H. Jiang, S. Kelch, and A. Lendlein, "Polymers move in response to light," *Advanced Materials*, vol. 18, no. 11, pp. 1471–1475, 2006.

[39] C. M. Yakacki, T. D. Nguyen, R. Likos, R. Lamell, D. Guigou, and K. Gall, "Impact of shape-memory programming on mechanically-driven recovery in polymers," *Polymer*, vol. 52, no. 21, pp. 4947 – 4954, 2011.

[40] W. Huang, Z. Ding, C. Wang, J. Wei, Y. Zhao, and H. Purnawali, "Shape memory materials," *Materials Today*, vol. 13, no. 7, pp. 54 – 61, 2010.

[41] J. Rossiter, K. Takashima, F. Scarpa, P. Walters, and T. Mukai, "Shape memory polymer hexachiral auxetic structures with tunable stiffness," *Smart Materials and Structures*, vol. 23, no. 4, p. 045007, 2014.

[42] D. Ratna and J. Karger-Kocsis, "Recent advances in shape memory polymers and composites: a review," *Journal of Materials Science*, vol. 43, no. 1, pp. 254–269, 2008.

[43] A. Lendlein and S. Kelch, "Shape-memory polymers," *Angewandte Chemie International Edition*, vol. 41, no. 12, pp. 2034–2057, 2002.

[44] Q. Meng and J. Hu, "A review of shape memory polymer composites and blends," *Composites Part A: Applied Science and Manufacturing*, vol. 40, no. 11, pp. 1661 – 1672, 2009.

[45] H. Meng and G. Li, "A review of stimuli-responsive shape memory polymer composites," *Polymer*, vol. 54, no. 9, pp. 2199 – 2221, 2013.

[46] SMP Technologies Inc., "SMP Technologies," accessed November 27, 2017. [Online]. Available: http://www.smptechno.com/index_en.html

[47] Cornerstone Research Group Inc., "Cornerstone Research Group," accessed November 27, 2017. [Online]. Available: http://www.crgrp.com/

[48] Composite Technology Development Inc., "Composite Technology Development," accessed November 27, 2017. [Online]. Available: http://www.ctd-materials.com/

[49] W. Huang, B. Yang, and Y. Fu, *Polyurethane Shape Memory Polymers*. Taylor & Francis, 2011.

[50] C. Liang, C. A. Rogers, and E. Malafeew, "Investigation of shape memory polymers and their hybrid composites," *Journal of Intelligent Material Systems and Structures*, vol. 8, no. 4, pp. 380–386, 1997.

[51] G. Baer, T. S. Wilson, D. L. Matthews, and D. J. Maitland, "Shape-memory behavior of thermally stimulated polyurethane for medical applications," *Journal of Applied Polymer Science*, vol. 103, no. 6, pp. 3882–3892, 2007.

[52] M. Cabanlit, D. Maitland, T. Wilson, S. Simon, T. Wun, M. E. Gershwin, and J. Van de Water, "Polyurethane shape-memory polymers demonstrate functional biocompatibility in vitro," *Macromolecular Bioscience*, vol. 7, no. 1, pp. 48–55, 2007.

[53] L. R. Pahalagedara, I. Siriwardane, N. D. Tissera, R. N. Wijesena, and K. M. N. de Silva, "Carbon black functionalized stretchable conductive fabrics for wearable heating applications," *RSC Adv.*, vol. 7, pp. 19 174–19 180, 2017.

[54] D. McCoul, S. Rosset, N. Besse, and H. Shea, "Multifunctional shape memory electrodes for dielectric elastomer actuators enabling high holding force and low-voltage multisegment addressing," *Smart Materials and Structures*, vol. 26, no. 2, p. 025015, 2017.

[55] S. Hong, H. Lee, J. Lee, J. Kwon, S. Han, Y. D. Suh, H. Cho, J. Shin, J. Yeo, and S. H. Ko, "Highly stretchable and transparent metal nanowire heater for wearable electronics applications," *Advanced Materials*, vol. 27, no. 32, pp. 4744–4751, 2015.

[56] Y. Cheng, H. Zhang, R. Wang, X. Wang, H. Zhai, T. Wang, Q. Jin, and J. Sun, "Highly stretchable and conductive copper nanowire based fibers with hierarchical structure for wearable heaters," *ACS Applied Materials & Interfaces*, vol. 8, no. 48, pp. 32 925–32 933, 2016.

[57] S. Choi, J. Park, W. Hyun, J. Kim, J. Kim, Y. B. Lee, C. Song, H. J. Hwang, J. H. Kim, T. Hyeon, and D.-H. Kim, "Stretchable heater using ligand-exchanged silver nanowire nanocomposite for wearable articular thermotherapy," *ACS Nano*, vol. 9, no. 6, pp. 6626–6633, 2015.

[58] J. Je and J. Lee, "Design, fabrication, and characterization of liquid metal microheaters," *Journal of Microelectromechanical Systems*, vol. 23, no. 5, pp. 1156–1163, 2014.

[59] X. Gong and W. Wen, "Polydimethylsiloxane-based conducting composites and their applications in microfluidic chip fabrication," *Biomicrofluidics*, vol. 3, no. 1, p. 012007, 2009.

[60] L. Liu, S. Peng, X. Niu, and W. Wen, "Microheaters fabricated from a conducting composite," *Applied Physics Letters*, vol. 89, no. 22, p. 223521, 2006.

[61] O. A. Araromi, S. Rosset, and H. R. Shea, "High-resolution, large-area fabrication of compliant electrodes via laser ablation for robust, stretchable dielectric elastomer actuators and sensors," *ACS Applied Materials & Interfaces*, vol. 7, no. 32, pp. 18 046–18 053, 2015.

[62] S. Rosset, O. A. Araromi, S. Schlatter, and H. R. Shea, "Fabrication process of silicone-based dielectric elastomer actuators," *JoVE*, no. 108, p. e53423, 2016.

[63] S. Rosset and H. R. Shea, "Flexible and stretchable electrodes for dielectric elastomer actuators," *Applied Physics A*, vol. 110, no. 2, pp. 281–307, 2013.

[64] S. P. Lacour, S. Wagner, Z. Huang, and Z. Suo, "Stretchable gold conductors on elastomeric substrates," *Applied Physics Letters*, vol. 82, no. 15, pp. 2404–2406, 2003.

[65] O. Graudejus, P. Görrn, and S. Wagner, "Controlling the morphology of gold films on poly(dimethylsiloxane)," *ACS Applied Materials & Interfaces*, vol. 2, no. 7, pp. 1927–1933, 2010.

[66] K. Tybrandt and J. Vörös, "Fast and efficient fabrication of intrinsically stretchable multilayer circuit boards by wax pattern assisted filtration," *Small*, vol. 12, no. 2, pp. 180–184, 2016.

[67] M. Zarek, M. Layani, I. Cooperstein, E. Sachyani, D. Cohn, and S. Magdassi, "3d printing of shape memory polymers for flexible electronic devices," *Advanced Materials*, vol. 28, no. 22, pp. 4449–4454, 2016.

[68] Q. Ge, A. H. Sakhaei, H. Lee, C. K. Dunn, N. X. Fang, and M. L. Dunn, "Multimaterial 4d printing with tailorable shape memory polymers," vol. 6, p. 31110, 2016.

[69] H. Xu, C. Yu, S. Wang, V. Malyarchuk, T. Xie, and J. A. Rogers, "Deformable, programmable, and shape-memorizing micro-optics," *Advanced Functional Materials*, vol. 23, no. 26, pp. 3299–3306, 2013.

[70] Z. Wang, C. Hansen, Q. Ge, S. H. Maruf, D. U. Ahn, H. J. Qi, and Y. Ding, "Programmable, pattern-memorizing polymer surface," *Advanced Materials*, vol. 23, no. 32, pp. 3669–3673, 2011.

[71] J. Leng and S. Du, *Shape-Memory Polymers and Multifunctional Composites*. Taylor & Francis, 2010.

[72] K. Gall, P. Kreiner, D. Turner, and M. Hulse, "Shape-memory polymers for microelectromechanical systems," *Journal of Microelectromechanical Systems*, vol. 13, no. 3, pp. 472–483, 2004.

[73] H. Takehara, C. Jiang, K. Uto, M. Ebara, T. Aoyagi, and T. Ichiki, "Novel microfluidic valve technology based on shape memory effect of poly($\varepsilon$-caprolactone)," *Applied Physics Express*, vol. 6, no. 3, p. 037201, 2013.

[74] L. Hines, V. Arabagi, and M. Sitti, "Shape memory polymer-based flexure stiffness control in a miniature flapping-wing robot," *IEEE Transactions on Robotics*, vol. 28, no. 4, pp. 987–990, 2012.

[75] A. Firouzeh, M. Salerno, and J. Paik, "Stiffness control with shape memory polymer in underactuated robotic origamis," *IEEE Transactions on Robotics*, vol. 33, no. 4, pp. 765–777, 2017.

[76] A. Firouzeh and J. Paik, "Grasp mode and compliance control of an under-actuated origami gripper using adjustable stiffness joints," *IEEE/ASME Transactions on Mechatronics*, vol. PP, no. 99, pp. 1–1, 2017.

[77] S. Yun, X. Niu, Z. Yu, W. Hu, P. Brochu, and Q. Pei, "Compliant silver nanowire-polymer composite electrodes for bistable large strain actuation," *Advanced Materials*, vol. 24, no. 10, pp. 1321–1327, 2012.

[78] N. Besse, S. Rosset, J. J. Zarate, and H. Shea, "Flexible active skin: Large reconfigurable arrays of individually addressed shape memory polymer actuators," *Advanced Materials Technologies*, vol. 2, no. 10, p. 1700102, 2017.

[79] N. Besse, J. J. Zárate, S. Rosset, and H. R. Shea, "Flexible haptic display with 768 independently controllable shape memory polymers taxels," in *Proceedings of the International Conference on Solid-State Sensors, Actuators and Microsystems (TRANSDUCERS)*, June 2017, pp. 323–326.

[80] N. Besse, J. J. Zarate, S. Rosset, and H. Shea, "Device having a plurality of latching micro-actuators and method of operating the same," June 2017, US Patent App. 15/635,225.

[81] C. Holz and P. Baudisch, "The generalized perceived input point model and how to double touch accuracy by extracting fingerprints," in *Proceedings of the SIGCHI Conference on Human Factors in Computing Systems*, April 2010, pp. 581–590.

[82] T. Pretsch, "Review on the functional determinants and durability of shape memory polymers," *Polymers*, vol. 2, no. 3, pp. 120–158, 2010.

[83] X. Niu, S. Peng, L. Liu, W. Wen, and P. Sheng, "Characterizing and patterning of pdms-based conducting composites," *Advanced Materials*, vol. 19, no. 18, pp. 2682–2686, 2007.

[84] H. Chen, I. Botef, H. Zheng, M. Maaza, V. Rao, and V. Srinivasu, "Thermal conductivity and stability of nanosize carbon-black-filled pdms: fuel cell perspective," *International Journal of Nanotechnology*, vol. 8, no. 6-7, pp. 437–445, 2011.

[85] Chemours Company, "Chemours," accessed November 27, 2017. [Online]. Available: https://www.chemours.com/

[86] Akzo Nobel N.V., "Akzo Nobel," accessed November 27, 2017. [Online]. Available: https://www.akzonobel.com/

[87] Elkem Silicones, "Bluestar Silicones," accessed November 27, 2017. [Online]. Available: http://www.silbione.com/

[88] Hexpol TPE Ltd., "Hexpol TPE," accessed November 27, 2017. [Online]. Available: https://www.hexpoltpe.com/en/index.htm

[89] Adhesives Research Inc., "Adhesives Research," accessed November 27, 2017. [Online]. Available: http://www.adhesivesresearch.com/

[90] Henkel AG & Co., "Henkel," accessed November 27, 2017. [Online]. Available: http://www.henkel.com/

[91] 3M, "3M," accessed November 27, 2017. [Online]. Available: http://www.3mschweiz.ch/3M/fr_CH/unternehmen-alpine/

[92] N. Besse, S. Rosset, J. J. Zarate, E. Ferrari, L. Brayda, and H. Shea, "Understanding graphics on a scalable latching assistive haptic display using a shape memory polymer membrane," *IEEE Transactions on Haptics*, 2017.

[93] D. Leithinger, S. Follmer, A. Olwal, and H. Ishii, "Shape displays: Spatial interaction with dynamic physical form," *IEEE Computer Graphics and Applications*, vol. 35, no. 5, pp. 5–11, 2015.

[94] Metec AG, "Metec," accessed November 27, 2017. [Online]. Available: http://web.metec-ag.de/home%20english.html

[95] P. Smithmaitrie, J. Kanjantoe, and P. Tandayya, "Touching force response of the piezoelectric braille cell," *Disability and Rehabilitation: Assistive Technology*, vol. 3, no. 6, pp. 360–365, 2008.

[96] R. Velázquez, H. Hernández, and E. Preza, "A portable piezoelectric tactile terminal for braille readers," *Applied Bionics and Biomechanics*, vol. 9, no. 1, pp. 45–60, 2012.

[97] K.-U. Kyung, J.-Y. Lee, and J. Park, "Haptic stylus and empirical studies on braille, button, and texture display," *BioMed Research International*, vol. 2008, p. 369651, 2008.

[98] S. Gallo, C. Son, H. J. Lee, H. Bleuler, and I.-J. Cho, "A flexible multimodal tactile display for delivering shape and material information," *Sensors and Actuators A: Physical*, vol. 236, pp. 180 – 189, 2015.

[99] M. Benali-Khoudja, M. Hafez, and A. Kheddar, "VITAL: An electromagnetic integrated tactile display," *Displays*, vol. 28, no. 3, pp. 133 – 144, 2007.

[100] E. Strasnick and S. Follmer, "Applications of switchable permanent magnetic actuators in shape change and tactile display," in *Proceedings of the Annual Symposium on User Interface Software and Technology*, October 2016, pp. 123–125.

[101] J. J. Zarate, O. Gudozhnik, A. S. Ruch, and H. Shea, "Keep in touch: Portable haptic display with 192 high speed taxels," in *Proceedings of the CHI Conference Extended Abstracts on Human Factors in Computing Systems*, May 2017, pp. 349–352.

[102] X. Wu, S.-H. Kim, H. Zhu, C.-H. Ji, and M. G. Allen, "A refreshable braille cell based on pneumatic microbubble actuators," *Journal of Microelectromechanical Systems*, vol. 21, no. 4, pp. 908–916, 2012.

[103] R. Velãzquez, E. E. Pissaloux, M. Hafez, and J. Szewczyk, "Tactile rendering with shape-memory-alloy pin-matrix," *IEEE Transactions on Instrumentation and Measurement*, vol. 57, no. 5, pp. 1051–1057, 2008.

[104] R. Vitushinsky, S. Schmitz, and A. Ludwig, "Bistable thin-film shape memory actuators for applications in tactile displays," *Journal of Microelectromechanical Systems*, vol. 18, no. 1, pp. 186–194, 2009.

[105] E. Wilhelm, T. Schwarz, G. Jaworek, A. Voigt, and B. E. Rapp, "Towards displaying graphics on a cheap, large-scale braille display," in *Proceedings of the International Conference on Computers for Handicapped Persons*, July 2014, pp. 662–669.

[106] H. S. Lee, H. Phung, D.-H. Lee, U. K. Kim, C. T. Nguyen, H. Moon, J. C. Koo, J. do Nam, and H. R. Choi, "Design analysis and fabrication of arrayed tactile display based on dielectric elastomer actuator," *Sensors and Actuators A: Physical*, vol. 205, pp. 191 – 198, 2014.

[107] N. Besse, S. Rosset, J. J. Zárate, and H. Shea, "BlindPAD Tactile Display: 4x4 SMP Demo," accessed November 27, 2017. [Online]. Available: https://youtu.be/TMegjjbYLPA

[108] N. Besse, S. Rosset, J. J. Zarate, and H. Shea, "Flexible 32x24 SMP Active Skin," accessed November 27, 2017. [Online]. Available: https://youtu.be/pY2-7OiYDeI

[109] N. Besse, S. Rosset, J. J. Zárate, C. Lorini, G. Zini, F. Bertora, D. Torazza, L. Brayda, and H. Shea, "32x24 SMP prototype," accessed November 27, 2017. [Online]. Available: https://youtu.be/AOnj-4xYA6s

[110] I. Rousseau, "Challenges of shape memory polymers: A review of the progress toward overcoming smp's limitations," vol. 48, pp. 2075 – 2089, 2008.

[111] R. Velãzquez, O. Bazán, and M. Magaña, "A shoe-integrated tactile display for directional navigation," in *Proceedings of the IEEE/RSJ International Conference on Intelligent Robots and Systems*, October 2009, pp. 1235–1240.

[112] Z. Cattaneo, M. Fantino, J. Silvanto, C. Tinti, A. Pascual-Leone, and T. Vecchi, "Symmetry perception in the blind," *Acta Psychologica*, vol. 134, no. 3, pp. 398 – 402, 2010.

[113] K. Sathian, "Practice makes perfect: Sharper tactile perception in the blind," *Neurology*, vol. 54, no. 12, pp. 2203–2204, 2000.

[114] N. Besse, R. Boom, B. Hoogenberg, B. Aksoy, M. Blom, and H. Shea, "Array of independent microfluidic valves driven by shape memory polymer actuators using a single pneumatic supply," in *Proceedings of the Miniaturized Systems for Chemistry and Life Sciences (MicroTAS) Conference*, October 2017, pp. 651–652.

**Bibliography**

[115] S. Haeberle and R. Zengerle, "Microfluidic platforms for lab-on-a-chip applications," *Lab Chip*, vol. 7, pp. 1094–1110, 2007.

[116] D. Mark, S. Haeberle, G. Roth, F. von Stetten, and R. Zengerle, "Microfluidic lab-on-a-chip platforms: requirements, characteristics and applications," *Chemical Society Reviews*, vol. 39, pp. 1153–1182, 2010.

[117] W. H. Grover, R. H. C. Ivester, E. C. Jensen, and R. A. Mathies, "Development and multi-plexed control of latching pneumatic valves using microfluidic logical structures," *Lab Chip*, vol. 6, pp. 623–631, 2006.

[118] R. H. Liu, J. Bonanno, J. Yang, R. Lenigk, and P. Grodzinski, "Single-use, thermally actu-ated paraffin valves for microfluidic applications," *Sensors and Actuators B: Chemical*, vol. 98, no. 2, pp. 328 – 336, 2004.

[119] R. Pal, M. Yang, B. N. Johnson, D. T. Burke, and M. A. Burns, "Phase change microvalve for integrated devices," *Analytical Chemistry*, vol. 76, no. 13, pp. 3740–3748, 2004.

[120] K. W. Oh, K. Namkoong, and P. Chinsung, "A phase change microvalve using a meltable magnetic material: ferro-wax," *Micro Total Anal. Syst*, vol. 1, pp. 554–556, 2005.

[121] B. Yang and Q. Lin, "A latchable phase-change microvalve with integrated heaters," *Journal of Microelectromechanical Systems*, vol. 18, no. 4, pp. 860–867, 2009.

[122] Z. Hua, R. Pal, O. Srivannavit, M. A. Burns, and E. Gulari, "A light writable microflu-idic "flash memory": Optically addressed actuator array with latched operation for microfluidic applications," *Lab Chip*, vol. 8, pp. 488–491, 2008.

[123] J. Stewart, *Single variable calculus: Concepts and contexts.* Cengage Learning, 2009.

[124] M. Sheplak and J. Dugundji, "Large deflections of clamped circular plates under initial tension and transitions to membrane behavior," *Journal of Applied Mechanics*, vol. 65, no. 1, pp. 107–115, 1998.

[125] State of California, "Braille Tactile Signage," accessed November 27, 2017. [Online]. Available: http://www.dgs.ca.gov/dsa/Programs/progAccess/braille.aspx

# List of Abbreviations

| | |
|---|---|
| 3D | three-dimensional |
| | |
| AgNW | silver nanowire |
| AR | augmented reality |
| | |
| CB | carbon black |
| CMOS | conventional metal-oxide-semiconductor |
| | |
| DEA | dielectric elastomer actuator |
| DEMES | dielectric elastomer minimum energy structure |
| DI | deionized |
| DMA | dynamic mechanical analysis |
| DMF | dimethylformamide |
| DoF | degree of freedom |
| DSC | differential scanning calorimetry |
| | |
| EM | electromagnetic |
| | |
| FEA | finite element analysis |
| | |
| HMI | human-machine interface |
| | |
| ITO | indium tin oxide |
| | |
| MEMS | microelectromechanical system |
| mLSI | microfluidic large scale integration |
| | |
| NC | normally closed |
| NO | normally open |
| | |
| PCB | printed circuit board |
| PCM | phase-change material |

| | |
|---|---|
| PDMS | polydimethylsiloxane |
| PET | polyethylene terephthalate |
| PMMA | polymethylmethacrylate |
| PS | polystyrene |
| PVDF | polyvinylidene fluoride |
| | |
| RF | radio-frequency |
| | |
| SEBS | styrene ethylene butylene styrene |
| SEM | scanning electron microscope |
| SMA | shape memory alloy |
| SME | shape memory effect |
| SMP | shape memory polymer |
| SMPU | shape memory polyurethane |
| SVI | severely visually impaired |
| | |
| taxel | tactile pixel |
| TCR | thermal coefficient of resistance |
| TE-NIL | thermal exposure nanoimprint lithography |
| | |
| USB | universal serial bus |
| | |
| VR | virtual reality |

# List of publications

## Journal articles

- **N. Besse**, S. Rosset, J. J. Zárate, and H. Shea, "Flexible Active Skin: Large Reconfigurable Arrays of Individually Addressed Shape Memory Polymer Actuators", *Advanced Materials Technologies*, vol. 2, no. 10, pp. 1700102, 2017 (Cover Picture).

- **N. Besse**, S. Rosset, J. J. Zárate, E. Ferrari, L. Brayda, and H. Shea, "Understanding Graphics on a Scalable Latching Assistive Haptic Display using a Shape Memory Polymer Membrane", *IEEE Transactions on Haptics*, 2017.

- A. Marette, A. Poulin, **N. Besse**, S. Rosset, D. Briand, and H. Shea, "Flexible Zinc–Tin Oxide Thin Film Transistors Operating at 1 kV for Integrated Switching of Dielectric Elastomer Actuators Arrays", *Advanced Materials*, vol. 29, no. 30, pp. 1700880, 2017 (Frontispiece).

- D. McCoul, S. Rosset, **N. Besse**, and H. Shea, "Multifunctional Shape Memory Electrodes for Dielectric Elastomer Actuators Enabling High Holding Force and Low-Voltage Multisegment Addressing", *Smart Materials and Structures*, vol. 26, no. 2, pp. 025015, 2017.

## In preparation

- **N. Besse**, R. J. Boom, B. Hoogenberg, B. Aksoy, M. Blom, and H. Shea, "Large Array of Independent Microfluidic Latching Valves Driven by Shape Memory Polymer Actuators using a Single Pneumatic Supply", manuscript in preparation.

- J. J. Zárate, **N. Besse**, O. Gudozhnik, A. S. Ruch, and H. Shea, "Array of Bistable Latching Electromagnetic Actuators", manuscript in preparation.

## Conference proceedings

- **N. Besse**, R. J. Boom, B. Hoogenberg, B. Aksoy, M. Blom, and H. Shea, "Array of Independent Microfluidic Valves Driven by Shape Memory Polymer Actuators using a Single Pneumatic Supply", in *Proceedings of the MicroTAS 2017 Conference*, Savannah (Georgia, United States), October 22-26, 2017, pp. 651-652.

- F. Pece, J. J. Zárate, V. Vechev, **N. Besse**, O. Gudozhnik, H. Shea, and O. Hilliges, "MagTics: Flexible and Thin Form Factor Magnetic Actuators for Dynamic and Wearable Haptic Feedback", in *Proceedings of the UIST 2017 Conference*, Quebec City (Canada), October 22-25, 2017, pp. 143-154 (Honorable Mention Award).

- **N. Besse**, J. J. Zárate, S. Rosset, and H. R. Shea, "Flexible Haptic Display with 768 Independently Controllable Shape Memory Polymers Taxels", in *Proceedings of the Transducers 2017 Conference*, Kaohsiung (Taiwan), June 18-22, 2017, pp. 323–326.

## Oral presentations

- **N. Besse**, S. Rosset, and H. Shea, "Tactile Display Enabled by Selective Patterning of Integrated Stretchable Heaters on Shape Memory Polymer Membranes", presented at *the SPIE-EAPAD 2016 Conference*, Las Vegas (Nevada, United States), March 21-24, 2016.

### Submitted

- D. McCoul, S. Rosset, **N. Besse**, and H. Shea, "Dielectric Elastomer Minimum Energy Structures with High Holding Force", submitted to *the SPIE-EAPAD 2018 Conference*.

## Poster presentations

- A. Marette, A. Poulin, **N. Besse**, S. Schlatter, S. Rosset, D. Briand and H. Shea, "A Flexible 4x4 Array of 1 kV Dielectric Elastomer Actuators Driven by an Integrated Matrix of High-Voltage Thin-Film Transistors", presented at *the EuroEAP 2017 Conference*, Cartagena (Spain), June 6-7, 2017.

- D. McCoul, **N. Besse**, S. Rosset and H. Shea, "Multifunctional Shape Memory Electrodes for Dielectric Elastomer Actuators Enabling High Holding Force and Low-Voltage Multi-segment Addressing", presented at *the EuroEAP 2016 Conference*, Helsingør (Denmark), June 14-15, 2016.

# Live demonstrations

- J. J. Zárate, F. Pece, V. Vechev, **N. Besse**, O. Gudozhnik, R. Hinchet, H. Shea, and O. Hilliges, "MagTics: Flexible and Thin Form Factor Magnetic Actuators for Dynamic and Wearable Haptic Feedback", presented at *the UIST 2017 Conference*, Quebec City (Canada), October 22-25, 2017.

- J. J. Zárate, **N. Besse**, O. Gudozhnik, A. S. Ruch, and H. Shea, "Portable Haptic Display with 12x16 Tactile Pins", presented at *the IEEE World Haptics 2017 Conference*, Fürstenfeldbruck (Germany), June 6-9, 2017.

- J. J. Zárate, O. Gudozhnik, A. S. Ruch, **N. Besse**, and H. Shea, "Keep in Touch: Portable Haptic Display with 192 High Speed Taxels", presented at *the CHI 2017 Conference*, Denver (Colorado, United States), May 6-11, 2017.

- **N. Besse**, J. J. Zárate, S. Rosset, L. Brayda, and H. Shea, "A Scalable 4x4 Graphical Tablet Based on Shape Memory Polymers", presented at *the IEEE Haptics Symposium 2016 Conference*, Philadelphia (Pennsylvania, United States), April 8-11, 2016 (Best Demonstration Finalist).

- **N. Besse**, S. Rosset, A. Poulin and H. Shea, "4x4 Tactile Display Based on Shape Memory Polymers", presented at *the SPIE-EAPAD 2016 Conference*, Las Vegas (Nevada, United States), March 21-24, 2016.

# Patent application

- **N. Besse**, J. J. Zárate, S. Rosset, and H. Shea, "Device Having a Plurality of Latching Microactuators and Method of Operating the Same", *US Patent Application*, no. 15/635,225, filed on June 28, 2017.

# Curriculum Vitae

Nadine Besse
Rue de la Dîme 41
2000 Neuchâtel
Switzerland

Phone: +41 21 695 4372
Mobile: +41 79 811 1092
Email: nadine.besse@epfl.ch
Nationality: Swiss citizen

## Eductation

2013 – 2017    **PhD in Microsystems and Microelectronics**
École Polytechnique Fédérale de Lausanne - Soft Transducers Laboratory (EPFL-LMTS), Switzerland.

2011 – 2013    **MSc in Microengineering** (GPA: 5.78/6.00)
École Polytechnique Fédérale de Lausanne (EPFL), Switzerland.
Specialization in Micro- and Nano-Systems and Minor in Space Technologies.
Master Project Abroad at the University of California Berkeley, United States.

2008 – 2011    **BSc in Microengineering** (GPA: 5.33/6.00, Rank: 3/71)
École Polytechnique Fédérale de Lausanne, Switzerland.
3$^{rd}$ Year Exchange Program at the McGill University, Canada.

## Professional experience

Nov. 2013
–
Nov. 2017    **Research assistant and PhD student at the EPFL-LMTS** (Prof. H. Shea)
Development of reconfigurable flexible haptic displays and microfluidic platforms combining integrated stretchable heaters on shape memory polymer membrane with a single pneumatic supply.
Main teaching assistant for Static and Dynamic (1$^{st}$ Year Bachelor).
Mentor for High School and Master students.

Jun. 2011
–
Feb. 2012    **Internship at Lemoptix SA** (N. Abélé)
Development of an automatic analysis software, implementation of reliability tests, and characterization of optical MEMS mirrors in the cleanroom.

# Selected publications

## Journal articles

**N. Besse**, S. Rosset, J. J. Zárate, and H. Shea, "Flexible Active Skin: Large Reconfigurable Arrays of Individually Addressed Shape Memory Polymer Actuators", *Advanced Materials Technologies*, vol. 2, no. 10, pp. 1700102, 2017.

**N. Besse**, S. Rosset, J. J. Zárate, E. Ferrari, L. Brayda, and H. Shea, "Understanding Graphics on a Scalable Latching Assistive Haptic Display using a Shape Memory Polymer Membrane", *IEEE Transactions on Haptics*, 2017.

A. Marette, A. Poulin, **N. Besse**, S. Rosset, D. Briand, and H. Shea, "Flexible Zinc–Tin Oxide Thin Film Transistors Operating at 1 kV for Integrated Switching of Dielectric Elastomer Actuators Arrays", *Advanced Materials*, vol. 29, no. 30, pp. 1700880, 2017.

D. McCoul, S. Rosset, **N. Besse**, and H. Shea, "Multifunctional Shape Memory Electrodes for Dielectric Elastomer Actuators Enabling High Holding Force and Low-Voltage Multi-segment Addressing", *Smart Materials and Structures*, vol. 26, no. 2, pp. 025015, 2017.

A. Vásquez Quintero, **N. Besse**, P. Janphuang, R. Lockhart, D. Briand, and N. F. de Rooij, "Design Optimization of Vibration Energy Harvesters Fabricated by Lamination of Thinned Bulk-PZT on Polymeric Substrates", *Smart Materials and Structures*, vol. 23, no. 4, pp. 045041, 2014.

## Conference proceedings

**N. Besse**, R. J. Boom, B. Hoogenberg, B. Aksoy, M. Blom, and H. Shea, "Array of Independent Microfluidic Valves Driven by Shape Memory Polymer Actuators using a Single Pneumatic Supply", in *Proceedings of the MicroTAS 2017 Conference*, Savannah (Georgia, United States), October 22-26, 2017, pp. 651-652.

F. Pece, J. J. Zárate, V. Vechev, **N. Besse**, O. Gudozhnik, H. Shea, and O. Hilliges, "MagTics: Flexible and Thin Form Factor Magnetic Actuators for Dynamic and Wearable Haptic Feedback", in *Proceedings of the UIST 2017 Conference*, Quebec City (Canada), October 22-25, 2017, pp. 143-154.

**N. Besse**, J. J. Zárate, S. Rosset, and H. R. Shea, "Flexible Haptic Display with 768 Independently Controllable Shape Memory Polymers Taxels", in *Proceedings of the Transducers 2017 Conference*, Kaohsiung (Taiwan), June 18-22, 2017, pp. 323–326.

**N. Besse**, A. Vásquez Quintero, D. Briand, P. Janphuang, R. Lockhart, J. J. Ruan and N. F. de Rooij, "PZT-Based Energy Harvesters on Plastic Foil Optimized Through Theoretical Modeling and Fabrication Improvements", in *Proceedings of the PowerMEMS 2012 Conference*, Atlanta (Georgia, United States), December 2-5, 2012, pp. 42-45.

## Awards and distinctions

- Cover Picture of Advanced Materials Technologies with the 32x24 flexible SMP active skin (2017).

- Honorable Mention Award at the UIST Conference for the MagTics paper (2017).

- Frontispiece of Advanced Materials with the flexible ZTO-TFTs (2017).

- Best Demonstration Finalist at the IEEE Haptics Symposium Conference for the 4x4 SMP graphical tablet (2016).

- Omega Prize Award for the Best Master Project in Microengineering (2013).

- EPFL WISH-Foundation Scholarship for the Master Project Abroad (2013).

## Technical skills

| | |
|---|---|
| Engineering | SolidWorks, COMSOL, MATLAB, LabVIEW, Altium |
| Programming | C, C++, Python |
| Office | Microsoft Office Suite, LaTeX, Origin, The Gimp, Inkscape |

## Language skills

| | | | |
|---|---|---|---|
| French | Native | Italian | Conversant |
| English | Fluent | German | Basic knowledge |

## Hobby

| | |
|---|---|
| Basketball | Active player from 2000 to 2017. Played the last 10 years in $1^{st}$ and $2^{nd}$ Swiss Woman Division. |
| Waterpolo | Active player from 1996 to 2002 and again since 2017. Play now in $1^{st}$ Swiss Woman Division and $3^{rd}$ Swiss Men Division. |